THE DEVELOPMENT OF SURFACE BASED MEASUREMENTS FOR MONITORING SELF HEATING OF SOLID FUEL STOCKPILES

Paul Anderson

A thesis submitted to the Faculty of Engineering University of the Witwatersrand, Johannesburg, in fulfilment of the requirements for the degree of Doctor of Philosophy

Johannesburg 1991

DECLARATION

I declare that this thesis, except where acknowledged, is my own, unaided work. It is being submitted for the Degree of Doctor of Philosophy in the University of the Witwatersrand, Johannesburg. It has not been submitted before for any degree or examination in any other University.

17th day of September 1991 17/09/91

ABSTRACT

Analysis of temperatures measured in an experimental coal bed (using the classical conductive-convective approach) confirm previously published permeabilities of similar beds, and furthermore validate the use of heat-transfer coefficients at exposed surfaces of coal stockpiles. The range of the estimated heat transfer coefficients is similar to natural convective coefficients at flat horizontal surfaces, which is expected.

An attempt is made to analyse the dependence of surface heat transfer coefficient on particle size, but unacceptably large confidence intervals for the estimated coefficients prevent any meaningful conclusions from being reached. Recommendations are made for experimental design which would solve this problem.

In follow-up studies on the abovementioned experimental temperatures, the relation between the surface temperature profile and the power input to the bed is investigated, resulting in a simple, fundamentally sound model expressing the relation between the surface temperature and power input to a simple one dimensional bed. It is demonstrated that the model is essentially a single parameter model, that parameter being the surface heat transfer coefficient.

By simple extension the model is applied to the estimation of energy release in experimental beds, and shown to be highly effective. Application to full-scale stockpiles, where surface temperatures variations are not radial, is discussed, and it is explained how the model can be effectively applied as a comparative tool in the absence of heat transfer coefficients, provided case histories are maintained.

It is believed that this technique is novel, and can immediately be put to effective use in the coal stockpiling industry by providing practitioners with consistent estimates of combustion rates and rates of pollutant production.

As discussed throughout this thesis, and elsewhere, the

permeability of a stockpile has a drastic effect on its behaviour, particularly the tendency to combustion. The effect of localised flows of air in stockpiles (caused by inhomogeneity within) on tendency to combustion is also well known.

A technique has therefore been developed which gives indications of permeability and inhomogeneity in beds of particulates. The technique is based on measurement of pressure at the surface of a bed, in the region of a series of pneumatic pulses. Trends in the amplitude-frequency behaviour allow conclusions regarding the interior of the bed to be drawn; the amplitude-frequency curve can in principle be analysed to give quantitative information regarding the bed.

Experimental results on small scale inhomogeneous beds show distinctly different behaviour compared to those for simple homogeneous beds. A simple model of the system demonstrates the factors which affect the measurements; further development of the technique is, however, required before it can be directly applied in the field.

To Helen, my wife

For her continued support and enthusiasm

Acknowledgements

I would like to express my gratitude to the following people:

Michael Anderson - for his lively assistance with the pneumatic experimental work

Christopher Anderson - for assistance with the mechanical design of the pneumatic testing apparatus

Messrs. Peter Cockroft and Sandy Harris (in particular) and all workshop staff for the excellent standard of workmanship in the design, construction, maintenance, and modification of the pneumatic experimental apparatus.

Prof. D. Glasser and Prof. A. Bryson, my supervisors, for assistance with the development of the ideas and models contained in this thesis, and assistance with the preparation of the thesis.

Prof D. Glasser who, through his research grants, funded this work.

SYMBOLS

A	area	m^2
Bi	Biot number = hL/k	-
C_n	constant in general solutions	varies
d_p	particle diameter	m
D	diameter	m
g	gravitational accelleration	$m.s^{-2}$
h	heat-transfer coefficient	$W.m^{-1}.K^{-1}$
H	height of source above reference	m
K	permeability	m^2
L	length scale	m
M	molecular mass	$kg.mol^{-1}$
P	pressure	Pa
Q	power	W
Q'	power per unit length	$W.m^{-1}$
Q''	power per unit area	$W.m^{-2}$
r	radial coordinate	m
R	gas constant	$J.mol^{-1}.K^{-1}$
Ra	Rayleigh number=$KgR\rho^o\beta T_o/(\mu\alpha)$	-
Ra_1	modified Rayleigh number=$KgL\rho^o/(\mu\alpha)$	
T	temperature	K, °C
u	radial or horizontal velocity	$m.s^{-1}$
v	vertical velocity	$m.s^{-1}$
V	volume	m^2
x	horizontal cartesian coordinate	m
y	vertical cartesian coordinate	m
z	vertical cylindrical coordinate	m

Subscripts

o	value at time zero
a, amb	ambient value
b	refers to average quantity for the bed
L	lumped value
max	maximum value
m	molar quantity
g	refers to gas

Superscripts

*	dimensionless quantity	
o	refers to base value	

Greek symbols

α	thermal diffusivity $= k_b/(\rho_g C_{p,g})$	$m^2.s^{-1}$
β	coefficient of thermal expansion	K^{-1}
Δ	deviation from avg., ambient or steady value	
ϵ	void fraction	-
μ	viscosity	$[kg.m^{-1}.s^{-1}]$
φ_s	sphericity of particle	-
κ	effective permeability of orifice	
θ	dimensionless temperature	-
ρ	density	$kg.m^{-3}$ $mol.m^{-3}$
ξ	dimensionless horizontal coordinate	-
ζ	dimensionless vertical coordinate	-
ω	angular frequency	$rad.s^{-1}$

THE DEVELOPMENT OF SURFACE BASED MEASUREMENTS FOR MONITORING SELF HEATING OF SOLID FUEL STOCKPILES

Contents

1 INTRODUCTION
1.1 Porous Media in Nature and Technology 1
1.2 Previous Studies of Relevance to this Thesis 3
1.3 Aims of this Study 6
1.4 Summary 7

2 THEORY OF TRANSFER PROCESSES IN POROUS MEDIA
2.1 Characteristics and Description of Porous Media 8
2.2 Momentum Transfer in Porous Media 12
2.2.1 The empirical theory of Darcy
2.2.2 Limitations of Darcy's law
2.2.3 Empirical theory of Brinkman
2.2.4 Conclusions
2.3 Heat Transfer in Porous Media 15
2.3.1 Mechanisms of heat transfer in porous media
2.3.2 Summary
2.4 Simultaneous Energy and Momentum Transfer in Natural Convection in Porous Media 20
2.5 Conclusion 21

3 Experimental Methods and Equipment
3.1 Heat transfer experiments 22
3.1.1 Bed fitted with a rod-shaped heater
3.1.2 Bed fitted with a cylindrical heater
3.2 Momentum transfer experiments 24
3.2.1 Measurement of the frequency response of a porous medium to pneumatic pulses
3.2.2 Measurement of the permeability of a porous medium

4 Experimental Results
4.1 Momentum transfer experimental results 33
4.1.1 Frequency-response results
4.1.2 Steady behaviour - permeability measurements
4.2 Discussion 50
4.3 Summary 52

5 Development of Some Surface-based Measurement Techniques
5.1 Modelling Natural thermal convection in porous media 53
5.1.1 Two-dimensional conductive-convective modelling
5.1.2 Development of a simplified one-dimensional model
5.2 Transient Momentum Transfer in porous media 78
5.2.1 Development of a surface-based method for characterising porous media
5.2.2 Application of the model
5.2.3 Discussion
5.3 Conclusions

6 A Systematic Approach to Monitoring Solid Fuel Stockpiles
6.1 Identification of Developing Combustion Hazards 101
6.2 Corrective Action 103
6.3 Construction of New Stockpiles 106
6.4 Conclusion 108

7 Conclusions 109

REFERENCES 114

Appendix A Experimental methods and equipment
A.1 Heat transfer experimental equipment A1

A.2 Momentum transfer experimental equipment A2
A.2.1 Pressure measurement
A.2.2 Signal conditioning
A.2.3 Data acquisition

Appendix B Experimental results
B.1 Heat-transfer experimental results - detailed results of Benson-Armer & Leibowitz B2
B.2 Momentum-transfer experimental results

Appendix C Heat transfer modelling
C.1 Two-dimensional modelling C1
C.1.1 'PDFELM' - a finite element code for the solution of steady or unsteady nonlinear partial differential equations.

C.2 One dimensional modelling C1
C.2.1 Derivation of model equation
C.2.2 'LAYER', a FORTRAN 77 program to solve the one-dimensional model

C.3 Application of the layer model to realistic situations C7
C.3.1 'SURFACE', a FORTRAN 77 program to calculate dissipation of energy within porous bodies from surface temperatures

Appendix D Momentum transfer modelling
D.1 Derivation of unsteady model equations D1
D.1.1 Derivation for a compressible fluid
D.1.2 Simplification for incompressible fluids
D.1.2.1 Development of a discrete analog of a inhomogeneous (layered) bed
D.2 'PERIODIC', a FORTRAN 77 program which rigorously simulates unsteady pressure distribution in a one-dimensional body. D18

List of Figures

Fig. No.	Page
3.1.1 Thermistor positioning used by Young et al (1986)	23
3.1.2 Schematic diagram of Benson-Armer & Leibowitz's experimental apparatus	23
3.1.3 Thermistor positioning used by Benson-Armer & Leibowitz	25
3.2.1 Mechanical diagram of pneumatic test apparatus	27
3.2.2 Diagram of pneumatic test measurement apparatus	28
3.2.3 Sketch of apparatus used to measure permeability	31
4.1a through 4.15a - plots of measured pressure amplitude offset vs. frequency	
4.1b through 4.15b - plots of measured phase lag vs. frequency	
5.1.1 Sketch of idealised bed with cylindrical heater	61
5.1.2 Plot of experimental and best-fit temperature contours (Q=10W, d_p=20mm)	62
5.1.3 Plot of calculated streamlines (Q=10W, d_p=20mm)	63
5.1.4 Alternative comparison of measured and calculated temperatures (Q=10W, d_p=10mm)	63
5.1.5 Plot of sum-of-squared errors contours (Q=18W, d_p=10mm)	64
5.1.6 Plot of surface temperature (Q=7.5W, d_p=20mm)	64
5.1.7 Plot of streamlines showing effect of solid heater (Q=10W, d_p=20mm)	
5.1.8 Comparison of calculated surface temperature profiles for porous and solid heater (Q=10W, d_p=20mm)	70
5.1.9 Sketch of theoretical one-dimensional layer	70a
5.1.10 Variation of energy dissipation with surface temperature difference and heat transfer coefficient	70a
5.2.1 Schematic sketch of layered bed	85
5.2.2 Plot of pressure amplitude offset vs. frequency effect of bed composition	85

5.2.3 Plot of lag vs. frequency - effect of bed composition 88
5.2.4 Plot of pressure profile - effect of bed composition 88
5.2.5 Plot of pressure profile - effect or frequency 90
5.2.6 Plot of pressure amplitude offset vs. frequency affect of layer of different voidage 90
5.2.7 Plot of normalised pressure amplitude offset vs. frequency-effect of layer of different voidage 92
5.2.8 Plot of lag vs. frequency - effect of layer of different voidage. 92
5.2.9 Sketch of multi-chamber model 95
5.2.10 Plot of pressure amplitude offset vs. frequency for multi chamber model - effect of permeability 'profile' 96
5.2.11 Plot of lag vs. frequency for multi chamber model 97

List of Tables

Table No. Page

4.1 Pneumatic test experimental beds 34

5.1 Fitted parameters - rod heater experiments 59
5.2 Fitted parameters - cylindrical heater experiments 60
5.3 Fitted heat transfer coefficients - rod heater 67
5.4 Fitted heat transfer coefficients - cylindrical heater 67
5.5 Energy estimated from measured surface temperarature 73
5.6 Energy estimated from simulated surface temperatures 74
5.7 Base-case paremters for pneumatic test simulations 86
5.8 Parameters for discrete resistance model 94

1 INTRODUCTION

This thesis deals with the detection and prevention of combustion within coal stockpiles, using fundamentally based models to develop scientific methods for this purpose. The study of heat and momentum transfer is directly relevant to this aim, but is also important in many other applications, both natural and technological. This chapter introduces the main theme of the thesis, and outlines some related applications which could benefit from a similar approach, if not some of the actual results of this thesis.

1.1 Porous Media in Nature and Technology

The frequency with which porous media occur in nature and applications in technology has resulted in a need to understand the processes by which mass, momentum and energy are transferred within such media. A vast body of published literature has therefore been built up in a collective effort to understand and quantify these processes. In the early 1800's, Darcy published a treatise which explored the variation of water flowrate with pressure-drop across sand beds, resulting in the so-called Darcy law, which expresses velocity as a function of pressure-drop per unit length, fluid viscosity μ, and permeability, K of the medium.

$$v = -\frac{K}{\mu}\frac{dP}{dx} \tag{1.1}$$

Since Darcy's work, the need for fundamental understanding of tranport in porous media has grown, as engineering design, technology, geophysics, and related fields demand increased levels of sophistication. The application of models to prediction and design requires confidence in the models themselves, as well as in the parameters which apply. It is therefore important to examine the applicability of models on a fundamental basis and to develop means of reliably and accurately determining the necessary parameters. Some possible applications are introduced below:

- predicting the transport of contaminants (pollutants, radioactive wastes etc.) in soils and porous rocks, as an aid to planning the prevention of, or limiting the contamination of precious groundwaters. This is of particular relevance in the South African context, considering the shortage of freshwater resources.

- Prediction of the transport of energy within sandstone strata or other porous media assists in the optimal usage of geothermal resources and artificial thermal reservoirs.

- Models of transient depressurisation behaviour of gas-pockets in sandstone strata are useful to plan draw-off rates of natural gas resources.

- Insulation relies on pockets of stagnant gas, held in place by fibrous or granular materials, to reduce rates of heat transfer. The efficiency of insulation is drastically reduced by internal convection, the onset of which is dependent on a number of factors, most notably permeability. Mathematical models of insulation materials have been and will continue to be used to determine optimal configurations and orientations.

- The dissipation of heat and pollutants within granular radioactive materials has been a topic of many studies, with applications to disposal of radioactive waste, and strategies for dealing with nuclear power-station disasters. In such applications, it is critically important to produce estimates with high degrees of confidence; reliable models and parameters are of utmost importance here.

- The transient behaviour of pressure in porous media can be used to obtain estimates of permeability or of the volume of a porous body which is imbedded in rock, such as is the case with sandstone pockets. (This concept is developed and tested in subsequent chapters.

- The behaviour of stockpiles of granular materials is better understood if mass, energy and momentum transfer within these piles is properly characterised. Large stockpiles of coal represent substantial investments, and must therefore be adequately protected. Coal, a material often stockpiled in megaton quantities, has a tendency to spontaneously ignite under certain circumstances. Improved understanding of these circumstances would make a substantial contribution to protection of a valuable resource; subsequent chapters discuss this aspect in detail, and develop procedures for monitoring coal stockpiles.

The above cases constitute a minor portion of existing and potential applications, and serve only to indicate the variety of fields which rely on an understanding of processes occurring within porous media. In particular, the last three items may be used to advantage in the field of stockpile monitoring, the objective of this thesis. It has been demonstrated that porous media and their behaviour are vitally important to many aspects of technology and the natural environment. It follows that fundamental work in the field makes a positive contribution to our efforts to protect the environment, and to improvement of technology through understanding of the processes involved.

1.2 Previous studies of relevance to this thesis

Two particular studies are highly relevant to this thesis, and large amounts of data from these sources were made available by the authors, to whom I am indebted. A brief outline of these studies is presented below; for further details, the reader is referred to subsequent chapters where they are discussed in detail. The work of Young, Williams and Bryson (1986) is available in the literature for reference. The work by Benson-Armer and Leibowitz has not been previously published, so all of the relevant details have been included.

Young et al used the classical conductive-convective model to describe energy and momentum transfer in coal stockpiles, and find optimum parameters by fitting model predictions to temperatures measured within an experimental coal bed artificially heated by a thin rod. The internal temperature profile was measured with and array of thermistors supported on a grid of thin nylon string. The parameters considered by Young et al are permeability and effective thermal conductivity of the bed; this study assumed the temperature of the upper surface of the coal bed to be ambient, which in their case gave reasonable results. Due to this assumption, their study could not reach any conclusions regarding mechanisms of heat transfer at the exposed surface of coal stockpiles, mechanisms which are of course essential to the understanding of the so-called 'hot spots' observed on combusting stockpiles.

Their study produced three main results of particular importance to this work:

- they produced a reliable estimate of the effective thermal conductivity of coal beds in the temperature range of interest to studies on spontaneous combustion.

- the correspondence of their model results with experimental measurements showed that the simplified conductive-convective modelling approach is adequate for this type of work

- their results confirmed that natural thermal convection is the mechanism which maintains the flow of air to combusting regions in coal stockpiles.

Benson-Armer and Leibowitz (unpublished) used Young et al's apparatus, modified (see below) in a manner designed to shed light on two factors:

- the mechanisms of heat transfer at the surface of coal stockpiles

- the effect of particle size on convective heat transfer within coal stockpiles, including heat transfer at the surface

Young et al's apparatus was modified by replacing the thin rod heater with a small centrally located cylindrical heater, intended to simulate a concentrated region of combustion, and by slightly rearranging the array of thermistors in anticipation of small changes in temperature profile. The measurements were repeated for beds composed of three different characteristic particle sizes.

As expected, the profiles measured in these beds were significantly different to those measured by Young et al. In particular, higher surface temperatures were encountered as a result of the concentrated heat source; this enabled some investigation into the mechanisms of heat transfer at exposed surfaces of coal stockpiles. Unfortunately, their numerical method of solving the equations was inadequate to deal with the numerical behaviour of the solution, and they could not reach any conclusions.

This thesis has therefore analysed the measurements of Benson-Armer and Leibowitz's, and Young et al, fitting surface heat transfer coefficient and permeability as parameters. The results show that temperatures at the surface of coal stockpiles may be adequately modelled using simple heat transfer coefficients, though no conclusions could be reached regarding the effect of particle size on this parameter. This work is discussed extensively is Chapter 5.

Although their results have not been applied in this thesis, the article by Glasser, Williams, Brooks, Burch and Humphries (1991) has shed some light on the nature of the heat transfer coefficient on the exposed surfaces of porous media. They used a simple model (based on the summation of natural and forced convection flows) which explains variations in the heat transfer coefficient with flowrates. Any further developments in this area will further understanding of the mechanisms involved at the surface, as well as improving accuracy of the approximate monitoring techniques developed here. No studies in existence could be found regarding the in-situ determination of permeability of large-scale stockpiles of coal or any other granular materials.

1.3 Aims of this study

Spontaneous combustion within coal stockpiles is always preceded by the appearance of hot spots on the surface. Due to the complexity and cost of rigorous multidimensional models, an approximate but fundamentally based technique is required in order to grade and assess the hot spots, since not all hot spots mark regions of active combustion.

It has been shown that the permeability of coal stockpiles is a parameter of much significance (see particularly Brooks, 1986, and the discussion in 2.1). Little attention, however, has been given in the literature to the in situ measurement of this parameter, by any means whatsoever, let alone practical and easily applied methods. The difficulty of determining this parameter is enhanced by inhomogeneity and by the fact that laboratory analysis of extracted samples can not give reliable estimates of the properties of the stockpile itself. Furthermore, it is impractical to apply the rigorous methods used by Young et al and others each time any indication of permeability is required.

A need therefore exists for a simple non-intrusive method to estimate permeability, one which does not necessarily require the medium to be contained inside solid, impermeable walls of finite extent.

The aims of this thesis may therefore be summarised as follows:

- to investigate the mechanisms of heat transfer at exposed surfaces of coal stockpiles, thereby developing techniques which allow early detection of combustion hazards via scientific monitoring of surface temperatures.

- to develop and verify a surface-based method of measuring permeability of large-scale stockpiles.

These aims are achieved by the systematic application of theoretically sound yet simple models to the analysis of experimental data, both existing and new. The models are shown to indicate internal characteristics and behaviour of coal stockpiles by interpretation of measurements taken only at the surface. This is considered to be a significant contribution to both the general state of knowledge in the field of conductive-convective energy transfer in porous media, and the field of scientific coal stockpile management.

1.4 Summary

The cumbersome nature of complex, rigorous models for heat and momentum transfer in porous media has resulted in a search for simplified, yet theoretically sound models of these phenomena. Since practical application of these models requires reliable parameters, some reliable estimates of these parameters have been determined. These investigations have yielded insight into the phenomena under consideration, and some approximate methods for practical, scientific management of coal stockpiles.

2 THEORY OF TRANSFER PROCESSES IN POROUS MEDIA

Since the aim of the thesis is to develop methods of monitoring porous media (in particular stockpiles of coal), the characterisation of porous media is of relevance; a brief introduction of the terminology and important parameters is presented below.

The remainder of this chapter introduces the relevant theory of transfer in porous media

2.1 *Characteristics and Description of Porous Media*

The permeability of a porous medium depends on the shape, size, and distribution of the pores, and on the void fraction of the medium. Strictly speaking, models of flow in a porous medium should account for the multitude of different paths by which the fluid could flow through the medium, as well as the continual mixing and splitting the fluid would undergo. The model should account for the drag the fluid experiences as as it flows through the pores.

Since such models would clearly be impractical for everyday use, and the quality and applicability of the results unlikely to justify the enormous effort involved, porous media are generally described in terms of a number of basic parameters. These are permeability, porosity or voidage, nature of the solid material, nature of the fluid filling the voids, pore shapes and tortuosities (affected by granule shape, if applicable), and the directional nature, or anisotropy, of the medium. These quantities, clearly dependent on each other to a large degree, are discussed briefly below.

2.1.1 Permeability

Except in cases where particle shape and packing are regular (single-sized spheres packed in body-centred cube arrangements for example) permeability must generally be determined experimentally, since it is intimately affected by pore-shape and tortuosity, etc.. Various generalised expressions for permeability are possible in certain cases, yet accuracy and reliability usually dictate experimental measurement of sorts. The voidage, particle size and shape-factor all have marked effects on the permeability, and unfortunately accurate independent determination of those parameters is very difficult. Excepting cases where particle geometry and packing are regular, permeability of the medium is usually measured as a single parameter, and this measurement is of no use if the medium is physically disturbed.

In an attempt to fundamentally understand the effects of scale, geometry and packing on this parameter, some workers have modelled flow in computer-simulated random media and have calculated permeability and other transport properties directly (Vrettos, Imakoma & Okazaki 1989a & 1989b). The results of this work are encouraging, though substantial amounts of computer time are required to generate results.

2.1.2 Voidage, or void fraction

A complicating factor in the study of porous media is the tendency of beds of particles to have significant local variations in voidage (and thus permeability) particularly near walls and other solid intrusions. Several workers have addressed these aspects, for example Haughey and Beveridge (1966) examined local voidage variation in beds, using measurements of coordination number and actuan voidage to verify their coordination-number based theory. Robles, Baird & Tierney (1958), and Benenati and Brosilow (1962) examined variations in voidage at vessel walls; since void fraction is unity at the walls of packed vessels, this effect is of much importance below certain particle-diameter to bed-dimension ratios. A further complicating factor is that it is difficult to measure even average voidage in randomly packed beds without using intrusive methods; in uncontained media, direct measurement of any sort is usually impossible. Local voidage variation is difficult and tedious to measure in situ, and in general, destructive methods of measurement (see Roblee *et al*, 1958) are required.

Thus, void fraction of porous media, although a simple concept in principle, is a topic worthy of study all on its own. In the case of coal stockpiles, inhomogeneity is of special significance, since local variations in particle size cause local variations in permeability, resulting in localised flows of oxygen, which in turn promote the formation of hot spots and combustion. This aspect is discussed in more detail in subsequent chapters

2.1.3 Properties of the solid material

Thermal energy transfer is the process most likely to be affected by properties of the solid portion of the bed. Although measurement of thermal conductivity of a solid is not trivial by any standards, the technology and techniques are well developed by comparison to measurements on heterogeneous materials such porous media; in dealing with energy transfer in porous media, thermal conductivity of the solid-phase is generally considered to be known.

Mass transfer in porous media is not affected by the nature of the solid (surface roughness excepted), unless the solid itself is porous (e.g. activated carbon), or otherwise accessible to the migrating species in question (e.g. ion-exchange resins). The behaviour of such systems is extremely complex and is a field of research in its own; such systems are not considered in this work at all; Gunn (1970) gives a concise, clear analysis of various situations involving intra-particle transfer.

2.1.4 Properties of the fluid

Mass, energy, and momentum transfer are clearly all affected very strongly by the physical and transport properties of the fluid which fills the voids of the medium. Since knowledge in this field is comparatively well advanced, these parameters present no difficulties to a study such as this. There are in fact several published studies which explicitly examine the effect of varying fluid properties, for example, Bertin & Ozoe (1986) examine the effect of Prandtl number on natural convection patterns; Horne & O'Sullivan (1978) examine the effect of temperature dependent viscosity and thermal expansion coefficient, to mention only two.

Fluid properties, therefore, although exceptionally important to work in this field, are sufficiently well understood for the purposes of studying transfer processes in porous media.

2.1.5 Isotropy and anisotropy

Transport properties in isotropic media do not vary with the direction of transport, while variation with direction in anisotropic materials can be marked. Anisotropy can be either macroscopic or microscopic. A medium consisting of parallel layers of different materials possesses macroscopic anisotropy (see McKibbin & Tyvand 1982). A medium consisting of fibres with nonrandom orientation will also have anisotropic transport properties, as shown by Koch & Brady (1986).

The anisotropic behaviour of layered media can be used to great advantage in the design of systems to protect groundwaters from pollution, as shown by Yeh, Gelhar & Gutjahr (1985) in a three-part study of unsaturated flow in porous media. Kvernvold & Tyvand (1979) show how insulation orientation can be used to optimise performance of insulation material, by taking advantage of anisotropy.

Isotropy and anisotropy therefore, represent far more than theoretical abstractions. However, the aims of this study are to develop a means for monitoring coal stockpiles using only surface measurements, and theory is not yet sufficiently developed to cope with the consequences of anisotropy in general. Regarding the pneumatic pulse-testing of artificially constituted anisotropic porous media (see subsequent chapters), preliminary indications are that inhomogeneity can be detected to some degree, though not yet quantitatively. Further discussion of theories of transport in anisotropic porous media would therefore not contribute positively to the thesis in any way, and the reader is referred to the literature for details of this aspect.

2.2 Momentum Transfer in Porous Media

As discussed in 2.1, due to the complex nature of most porous media, approximations are used to model transfer processes. In many applications local spatial averages of transfer variables are acceptable for the purpose; in such cases, macroscopic laws describing the averages are adequate. The scope of this work is adequately served by such approximate laws, and the purpose of this chapter is to outline existing theories, and refer the reader to the literature for further, detailed information, and supporting proof of the models or theories.

2.2.1 Empirical theory of Darcy

As discussed briefly in 1.2, the earliest known formal theory for momentum transfer in porous media is that of Darcy. Following observation and experiment, Darcy proposed a relation in the form of equation 2.1.

$$v = \frac{-K}{\mu}\frac{dP}{dx} \qquad (2.1)$$

v is the superficial velocity of the fluid	$[m.s^{-1}]$
K is the permeability of the medium	$[m^2]$
P is the pressure	$[Pa]$
x is the spatial coordinate	$[m]$
μ is the viscosity of the fluid	$[kg.m^{-1}.s^{-1}]$

This equation models the porous medium as an array of infinitely small point-particles which resist flow to a degree quantified by K, so that v, the velocity, is equal to the flowrate divided by the total area.

The laminar portion of the Ergun equation can be reduced to the form of (2.1) to give an expression for permeability of media composed of particles:

$$\frac{\Delta P}{L} = \frac{150(1-\epsilon)^2 \mu v}{\epsilon^3 \varphi_s^2 d_p^2} \quad \text{(laminar portion of Ergun equation)}$$

where ΔP is the pressure difference [Pa]
L is the distance over which ΔP is measured [m]
d_p is the diameter of the particles [m]
φ_s is the shape factor [-]
ϵ is the voidage [-]

Bird, Stewart and Lightfoot (1960) define the shape factor φ_s.

The above equation may be rearranged and compared to (1.1) to give:

$$K = \frac{\epsilon^3 \left[\varphi_s d_p\right]^2}{150(1-\epsilon)^2} \tag{2.2}$$

Note that for nonspherical particles the quantities φ_s and d_p are not uniquely defined, and that voidage of the medium has a marked effect. It is therefore not possible to calculate permeability of particulate media by analysis of a loose sample and application of (2.1). Doi (1976) proposes a variational method of calculating permeability of media based on spatial correlation functions, the measurement of which requires undisturbed portions of the medium with the particles 'frozen' in place with wax or resin. This method is time-consuming, expensive, and highly complex, and requires the use of expensive image-analysis machines, and as such cannot be easily applied.

Since the proposition of the above empirically derived equations, many studies have been devoted to rigorous derivations of models for momentum transfer in porous media. Among these studies are Whitaker (1966), Slattery (1969), and Lebon & Cloot (1986). In all of these studies, it is shown that Darcy's law may be applied in creeping-flow situations, with small or negligible spatial variations in permeability of the medium, among other restrictions not of relevance here. The import of these and other studies goes far beyond mere verification of Darcy's law under restrictive assumptions; however, for the purposes of this work, it is adequate that Darcy's law has been shown to be applicable under suitable circumstances. The reader is referred to these works for deeper insight into the problem.

2.2.2 Limitations of Darcy's law

It is clear that the second-order spatial derivatives of velocity are not present in (2.1), as they are in the Navier-Stokes equations for flow of free-fluids. As a result, boundary conditions for zero-slip at solid, confining boundaries (if any) cannot be applied. It happens that this is of little consequence to the aims of the thesis, since solid container walls are generally absent or have little effect.

In cases where flow at impermeable boundaries is of prime interest, the Darcy law is totally inadequate. Cases in which flow at walls is of critical importance include heat and mass transfer at the walls containing porous media, and where bypassing of flow along the walls is significantly large. Hsu & Cheng (1985) discuss the inadequacy of the Darcy law in cases such as these, and use the Brinkman law (see 2.2.3) to model flow in a porous medium in which a vertical plate is submerged.

A further, less serious limitation of Darcy's law is that it applies only to laminar flow.

2.2.3 Empirical theory of Brinkman

Brinkman (1947) added second spatial derivatives of velocity to the Darcy law, arguing that momentum transfer equations for flow in porous media should display consistent limiting behaviour. Although this modification was not rigorously motivated at the time, it has since been justified in the works by Whitaker (1966), Slattery (1969), and Lebon & Cloot (1986). In these works, it is shown to be a special case of rigorous equations, as is Darcy's law. Brinkman's law is adequate for a wider class of situations than Darcy's law; since it is not used in this work due to the absence of any wall-effects of importance, it is not reproduced here, or discussed any further.

2.2.4 Conclusions

Although Darcy's law is not justifiable for all conditions, a vast body of natural convection literature leaning heavily on it is in existance. The reason for this is that in many cases, the flows are small enough to be well within the laminar flow-regime, and impermeable boundaries are nonexistent or of limited significance. This work deals with such cases, and as a result Darcy's law is used exclusively to describe momentum transfer.

Whichever momentum transfer equation is used, the dependence of pressure on spatial variables must be properly allowed for. Consider the case where there are vertical temperature variations; in such a case, the spatial pressure derivative depends on the temperature gradient as well. Under these circumstances, momentum and heat transfer become linked, an important phenomenon which is discussed in 2.3 below.

2.3 Heat Transfer in Porous Media

There is extensive literature dealing with this topic, much of it concerned with natural convection. Naturally, in such cases heat and momentum transfer are intimately linked and must be considered simultaneously. This section outlines current theory of heat transfer; simultaneous heat and momentum transfer is discussed at a later stage. Balakrishnan & Pei (1979), and Brooks (1986) report on extensive literature surveys on thermal energy transfer in porous media, and the reader is referred to those for details of work not referenced here.

Note that in this work as well as in the majority of published work in this field, local thermal equilibrium between fluid and solid is assumed. Obvious exceptions to this are studies which focus on the dynamics of solid-fluid heat-exchange, see Gunn (1970), Hughes, Klein & Close (1976), and Martin (1978), to name only a few examples of such studies.

2.3.1 Mechanisms of heat transfer in porous media

radiation

Radiation occurs between solid and solid, gas and solid and vice-versa, and gas absorbs radiation in between. Even in cases where geometry is regular and well-defined, analysis of radiative heat-exchange is not a simple matter; in this work, as well as the vast majority of work in the field, pore geometry is irregular and very much ill-defined, and rigorous analysis of radiation is highly complex, if not impossible. Whitaker (1980) has performed a detailed analysis of radiation in porous media for cases in which the fluid is stagnant. Due to the complexity of the resulting transport equation, and the fact that it holds only for stagnant systems, Whitaker's result is not applicable to this work.

Young (1975) has shown that the role played by radiation is important in beds of 1mm particles at around 400°C, and that as particles become smaller the temperature at which radiation effects become significant *increases*. Since this work concentrates on temperatures well below 400°C and particle diameters between 1mm and 20mm, it is not necessary to account for radiation effects. Furthermore, if temperature gradients are small, linearisation of the radiation equations is possible (Brooks 1986), and the radiation effect may be incorporated into the effective conductivity of the medium, meaning that the medium is considered to be a continuum. (See also *conduction* below.)

Clearly, the approach of radiation as a contribution to effective conductivity of the medium is only of use when this effective conductivity is experimentally measured, since *a priori* calculation is difficult and unreliable. Beveridge and Haughey (1971) present a detailed discussion of radiation models; however, since radiation is not significant here, the reader is referred to that work for details *conduction*

Conduction occurs in parallel, through both the solid and fluid; only in sintered media (partially fused particulate media) is there little or no resistance to conduction at the contact-point between particles. In particulate media in general, direct contact between particles is very scarce, so conduction across gaps between particles constitutes a large portion of the conductive resistance. The marked effect of contact-point area on the ability of a medium to conduct heat is clearly demonstrated by Beveridge & Haughey (1971).

The nature of conduction in porous media is best conceived if the medium is visualised as a series of 'rods' of solid surrounded by gas, or simply as a single lump of solid in contact with a body of gas. There is also exchange of heat between solid and fluid of course, so that neither the series nor parallel conduction sufficiently explains experimental results. Actual heat transfer in porous media is very complex, so complex geometric models are required to obtain approximations of this. Beveridge & Haughey demonstrate several types of geometric approximations, but as these models are not not applicable to this work, they are not discussed any further.

Whatever approximation is used to describe conduction, the result is that the medium is modelled as a homogeneous, continuous solid with a thermal conductivity equal to the effective overall conductivity. Effective thermal conductivity obtained from reliable experimental work and theoretical analysis are used in this work.

convection

Convection in porous media is a complex phenomenon, as are the other modes of heat transfer. However, as in describing radiation and conduction, recourse is made to a continuum description of the fluid. The convecting fluid, as for momentum transfer models, is considered to be flowing through an array of infinitely small point-particles, which resist flow as discussed in 2.1. Thus, the usual equations describing convective heat transfer are used, with suitable interpretation being given to the thermal conductivity variable.

2.3.2 Summary

Although several elaborate theories for a priori calculation of radiation, conduction, and momentum transfer properties of porous media are referred to above, these are not used due to their approximate nature and complexity. This work uses Darcy's law to describe momentum transfer, the concept of effective thermal conductivity of porous media to describe conduction heat transfer in porous media, and the classical equations for convective heat transfer. The result of this is that the overall equations describing heat transfer in the bed take the usual convective-conductive form (Bird, Stewart & Lightfoot 1960).

$$\rho_g C_{pg} \underset{\sim}{v} \cdot \nabla T - k_b \nabla^2 T = Q \qquad (2.3)$$

where ρ_g is the density of the gas [$kg.m^{-3}$]
C_{pg} is the constant pressure heat capacity of the gas [$J.kg^{-1}K^{-1}$]
$\underset{\sim}{v}$ velocity vector [$m.s^{-1}$]
T is temperature [K]
∇ is the gradient operator [-]
Q is power input per unit volume [$W.m^{-3}$]
k_b is the thermal conductivity of the bed [$W.m^{-1}.K^{-1}$]

The terms in the velocity vector $\underset{\sim}{v}$, obtained by application of Darcy's law, must satisfy the equation of continuity so that mass balance is maintained.

2.4 Simultaneous Momentum and Energy Transfer in Natural Convection

In this case the effects of energy and momentum transfer on each other are best modelled using stream-functions, and application of the *Boussinesq* assumption (which is that density is considered constant everywhere except in the body-force term of the momentum equation). Pressure is eliminated by application of stream functions, and the resultant equations, for vertical cylindrical geometry in dimensionless form, are :

$$\frac{\partial^2\psi}{\partial\xi^2} - \frac{1}{\xi}\frac{\partial\psi}{\partial\xi} + \frac{\partial^2\psi}{\partial\zeta^2} = \xi\cdot \mathrm{Ra}\,\frac{\partial\theta}{\partial\xi} \qquad (2.4)$$

$$\left(\frac{1}{\xi}\frac{\partial\psi}{\partial\zeta}\right)\frac{\partial\theta}{\partial\xi} - \left(\frac{1}{\xi}\frac{\partial\psi}{\partial\xi}\right)\frac{\partial\theta}{\partial\zeta} - \frac{1}{\xi}\frac{\partial\theta}{\partial\xi} - \frac{\partial^2\theta}{\partial\xi^2} - \frac{\partial^2\theta}{\partial\zeta^2} = \frac{QL^2}{k_b T_o} \qquad (2.5)$$

The following quantities have been used in the nondimensionalisation of the above equations:

u	lateral velocity	[m/s]
v	vertical velocity	[m/s]
u^*	dimensionless radial velocity	$= u\alpha/L$
v^*	dimensionless vertical velocity	$= v\alpha/L$
L	a characteristic length scale	[m]
α	thermal diffusivity	$= k_b/(\rho_g C_{pg})$
ψ	dimensionless stream function	
ξ	dimensionless radial coordinate	$= r/L$
ζ	dimensionless vertical coordinate	$= z/L$
θ	dimensionless temperature	$= (T-T_o)/T_o$
T_o	reference temperature	K
ρ_o	fluid density at T_o	$kg.m^{-3}$
Q	input power (see below)	$W.m^{-3}$
β	coefficient of thermal expansion of the fluid	K^{-1}
μ	viscosity of the fluid	$kg.m^{-1}.s^{-1}$
Ra	Rayleigh number	$= KgL\rho_o\beta T_o/(\mu\alpha)$

Note that Q, the input power, may be a function of position or temperature.

Boundary conditions are as follows:

$$\psi(0,\zeta) = \psi(1,\zeta) = 0 \qquad 0 \le \zeta \le 1$$
$$\psi(\xi,0) = 0 \qquad 0 \le \xi \le 1$$
$$\left.\frac{\partial\psi}{\partial\zeta}\right|_{\zeta=1} = 0 \qquad 0 \le \xi \le 1$$
$$\left.\frac{\partial\psi}{\partial\xi}\right|_{\xi=0} = 0 \qquad 0 \le \zeta \le 1$$
$$\left.\frac{\partial\theta}{\partial\zeta}\right|_{\zeta=1} = -Bi\cdot\theta \qquad 0 \le \xi \le 1$$
$$\theta(\xi,0) = 0 \qquad 0 \le \xi \le 1$$
$$\theta(1,\zeta) = 0 \qquad 0 \le \zeta \le 1$$

Equations (2.3) and (2.4), with boundary conditions are used to model natural convection in vertical cylinders filled with porous media. Havstad & Burns (1982) present a complete derivation of these equations in dimensional form.

2.5 Conclusion

The basics of the theory of transport in porous media have been described above, and the roles of the major parameters introduced. It is not the intention of the thesis to introduce any new theories regarding the fundamentals of transfer processes, so the theories as discussed above are adequate for the purpose of this work. There is a considerable amount of contention regarding the validity of the above theories, particularly in the case of inhomogeneous media. Slattery (1969) and Whittaker (1966) have investigated in great detail, and at the most fundamental level, some of the more subtle aspects, and the reader is referred to these publications for details.

Despite the approximate nature of the theories discussed above, it will be seen that in general, adequate results may be obtained over the range of relevance to coal stockpile monitoring.

3 EXPERIMENTAL METHODS AND EQUIPMENT

3.1 Heat Transfer Experiments

All of the heat-transfer measurements used here are from previous work. The experimental methods and equipment used in the unpublished studies will be discussed briefly.

3.1.1 Bed fitted with a rod-shaped heater

Young *et al* (1986) measured the steady-state temperatures on a cross-section normal to the centrally located horizontal rod-heater (intended to approximate a line heater) in the bed. The objective of the study was to experimentally verify the conductive-convective model described in 2.3, and to estimate both the effective thermal conductivity and permeability of the bed by minimising the sum-of-squared temperature prediction errors. 45 thermistors were placed on a plane perpindicular to the horizontally-placed heater. Young *et al's* bed was 1m square and 0.5m deep, and packed with coal particles nominally 10mm in diameter. Fig. 3.1.1 shows placement of the thermistors and heater in the bed.

These measurements were repeated for various power inputs, and the bed was not disturbed in any way between successive runs, so as to ensure identical permeability of the bed at all times. See Young et al's publication (1986) for further discussion of methods and equipment.

3.1.2 Bed fitted with a cylindrical heater

Benson-Armer & Leibowitz (unpublished) used Young *et al's* bed, but placed a small cylindrical heater (30mm diameter by 60mm long) vertically, at the centre of the bed, 0.3m from the bottom. Furthermore, they also performed the measurements on three different coal-beds, each comprised of different nominal particle sizes (under 5mm, 10mm, and 20mm respectively). Fig. 3.1.2 shows a schematic diagram of the bed and heater, and

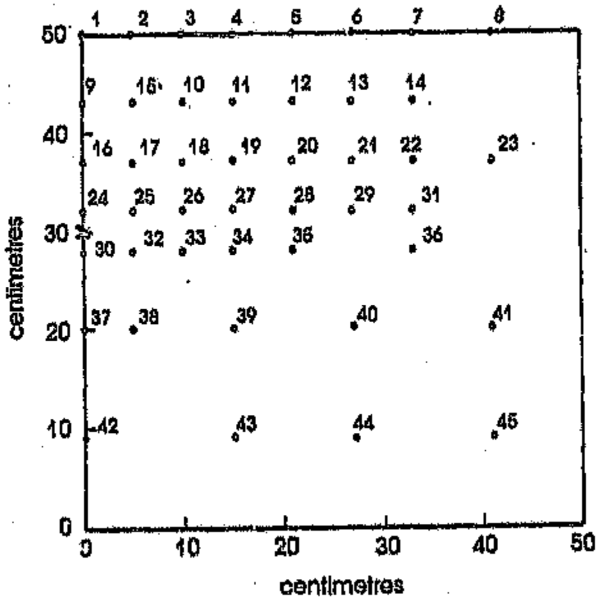

3.1.1 Thermistor positioning used by Young et al

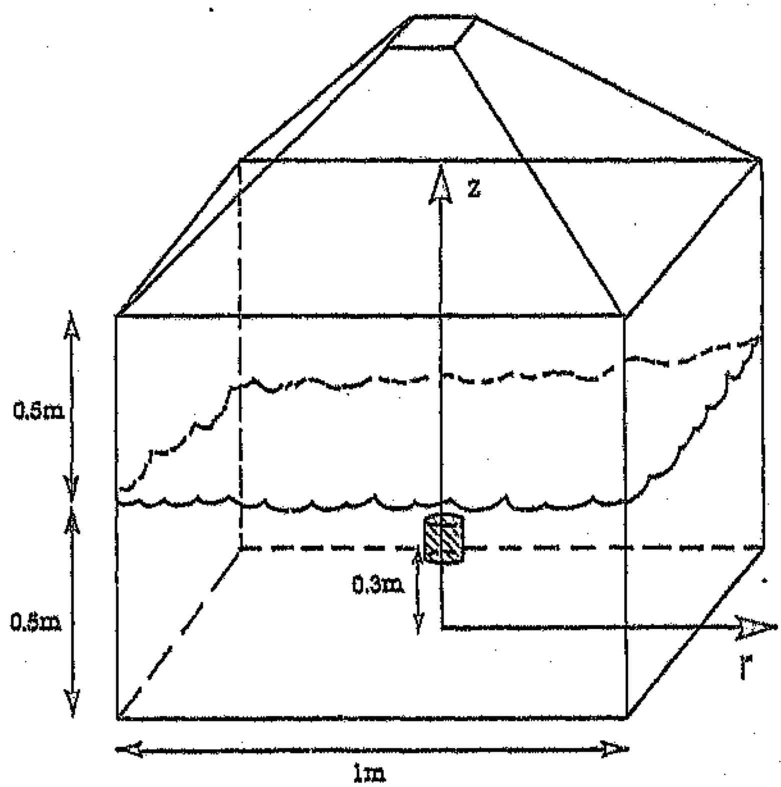

3.1.2 Schematic diagram of Benson-Armer & Leibowitz's experimental apparatus

Fig.3.1.3 shows thermistor and heater position in the bed.

Note that thermistor positioning, due to anticipated differences in measured results, was slightly different from that in Young *et al's* study. The motivation for repeating Young *et al's* measurements and analysis with a localised source was two-fold:

- to more accurately reproduce and simulate a localised energy source in a packed bed, since so-called 'hot-spots' tend to be localised, not stretched out in a line. Also, due to the concentrated nature of the source, higher temperatures are to be expected both in the bed and on the surface. This allows some investigation into mechanisms of heat transfer on the surface of the bed.

- to obtain results which would allow the effects of particle size on the heat- and momentum transfer parameters to be determined.

As Benson-Armer & Leibowitz's report is unpublished, their experimental procedure is described below:

The procedure for each bed type began with packing the bed, taking special care in the vicinity of the array of thermistors. Once packed, the bed was purged with nitrogen to prevent spontaneous combustion of the coal, and the heater was turned on. It was found that five days were required for the temperatures to reach steady state, at which time the temperature readings were stored on tape. Thereafter, power input to the heater was increased in preparation for the next run. The temperature measurements made by Benson-Armer & Leibowitz are contained in Appendix B, in their entirety, since these results have not been published before.

3.2 Momentum Transfer Experiments

A method to qualitatively investigate the interior of a porous medium without using intrusive or destructive methods is

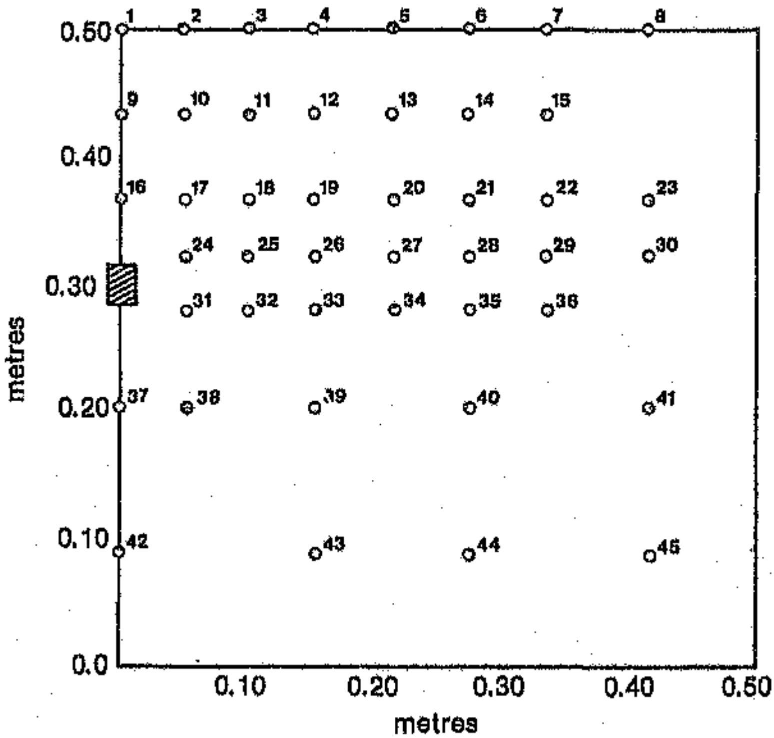

3.1.3 Thermistor positioning used by Benson-Armer & Leibowitz proposed here. The method was originally conceived as a means of probing porous media in a manner which would elucidate the internal structure, an objective which cannot be achieved by the usual steady-flow methods. In the case where the medium is freely constituted (i.e. not contained within impermeable walls) the usual steady-flow methods are in any case not applicable, as pressure 'drop' and area for flow are both ill-defined. The procedure consists of varying the volume of a cylinder, the open end of which is placed on the surface of the medium, and measuring the time varying pressure at the surface of the medium. Application of the procedure and results may be found in 5.2.1; the equipment and procedure used is discussed in detail below.

3.2.1 Measurement of the frequency response of a porous medium

mechanical design of the eq· .ment

The equipment designed to make these measurements consists of a piston inside a cylinder connected to a flat plate, which is held in place on the surface of a bed of granular material contained inside a larger cylinder. The flat plate made a seal with the inside of the larger cylinder, preventing the fluid (air) from leaking out. A pressure transducer was placed at the base of the smaller cylinder to sense the pressure at the surface of the bed. The piston was reciprocated approximately sinusoidally, using a variable-speed motor. A sketch of the apparatus is shown in Fig. 3.2.1.

measurement system and electronics

Fig. 3.2.2 shows a simplified diagram of the measurement system. A Data Instruments High Performance pressure transducer (data-sheet in APPENDIX A) was used. The transducer uses strain-gauges connected to a Wheatstone bridge, which produces a voltage proportional to the pressure. The power to drive the Wheatstone bridge was taken from a PC-68 strain-gauge amplifier (see APPENDIX A for details), and the Wheatstone output was fed

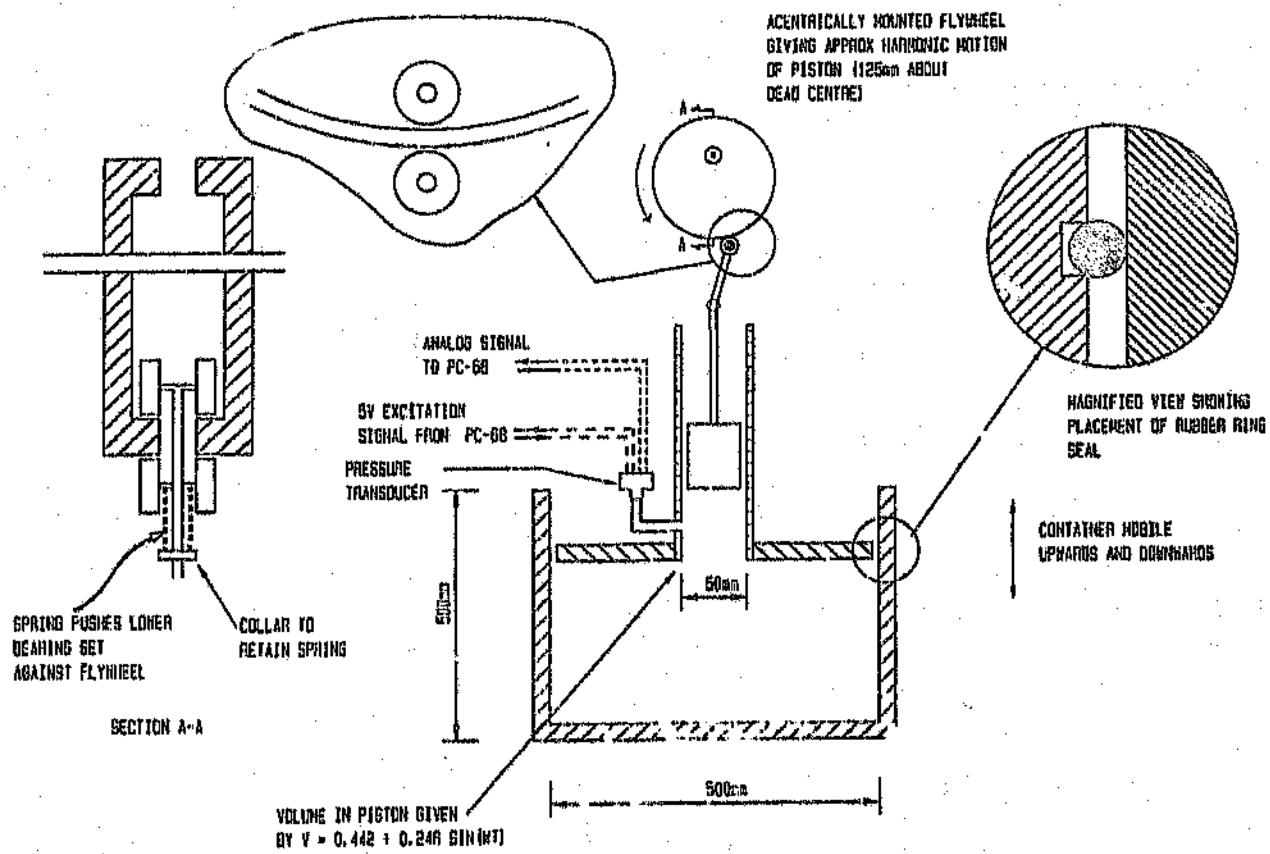

3.2.1 Mechanical diagram of pneumatic test apparatus

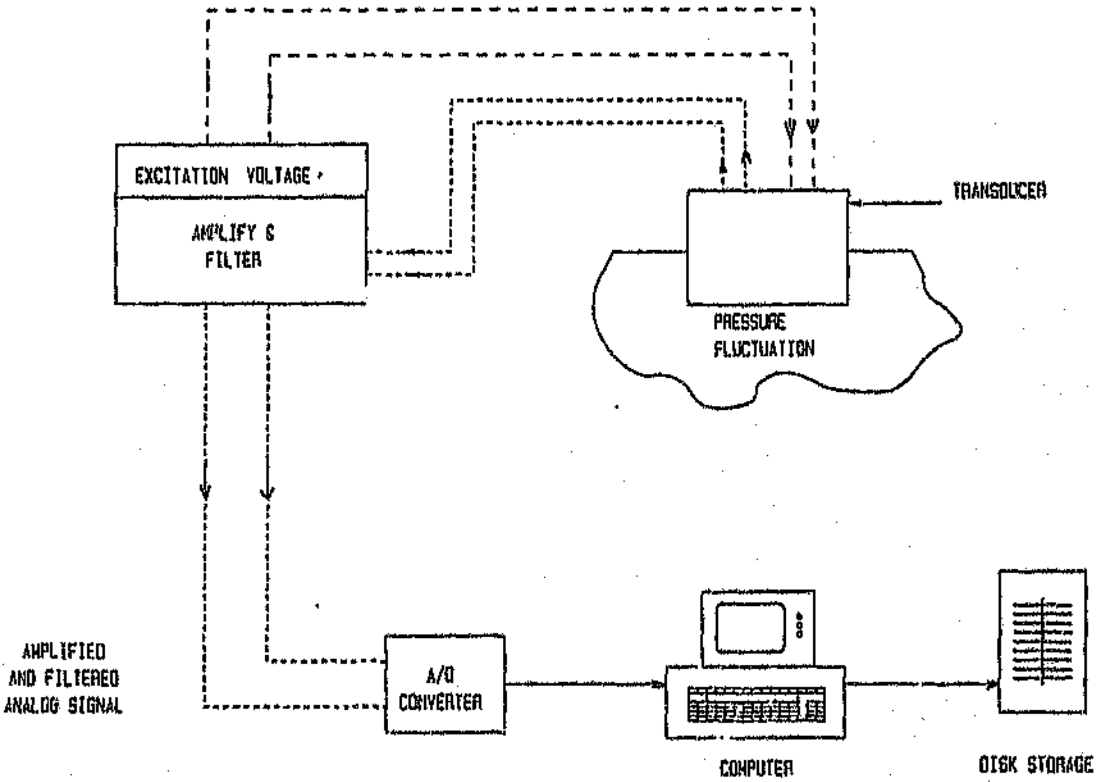

3.2.2 Diagram of pneumatic-test measurement apparatus back into the PC-68, which filtered and amplified the signal. The filter removed any components of the signal with frequencies higher than 100 Hz, considerably higher than any signal actually expected from the transducer, and the gain was set at 100. The conditioned, amplified analog signal was fed into a high-speed analog-to-digital converter, which was in turn connected to an IBM-compatible XT computer. The computer was used to set up and control the sampling procedure, and to store and view the results. The AD card controlling software allowed selection of desired sampling frequency and length of data collection.

To ensure that all measurements commenced at a predetermined point in the cycle of the piston, a limit-switch circuit was connected to the trigger-bit of the AD converter. A small arm was attached to the piston, and positioned so that it just closed the limit-switch at the bottom of the piston's cycle.

method

A bed was prepared in the container by loading the desired granular material or combination thereof: the bed was raised to ensure that the piston and sealing disk made contact with the surface of the medium, and the piston was raised to the centre of its travel before sealing the system by shutting valve 2. The motor was run, at a slow pace to begin with, and the pressure was sampled at a suitable rate.

In all cases, the sampling frequency was equal to or greater than 100 per second. The reason for such high sampling rates is that maximum pressure had to be measured as accurately as possible, and since the pressure-time trace is likely to be approximately sinusoidal, high sampling rates are required to achieve this. Note that a sampling frequency of 100 per second is well above the minimum required to guard against aliasing, since the frequency of the reciprocating piston was less than 5 Hz in all cases.

Since sampling frequency was very accurately known, it was not necessary to measure reciprocation frequency independently. This could be determined from the period of the measured trace. After the samples were stored on disk, the speed control on the motor was adjusted slightly upward, and the procedure repeated. Attainment of steady-state, for the beds and volumes used here, was seen to be rapid enough that waiting was not necessary.

The amplitude of the trace, and its phase (compared to the pressure trace expected for a blocked piston outlet) position of the piston) were determined for each run, numerically as well as by inspection. Inspection was used to ensure that random spikes (if any) did not spoil the results, though no unacceptable features (spikes or irregularities) were found in any of the traces. Repeatability of maximum pressure was 10 Pa for any given run and the period of the trace (calculated from peak-to-peak) was repeatable within the limits of sampling frequency (i.e. within 0.01 seconds for a sampling frequency of 100 per second).

3.2.2 Measurement of the permeability of a porous medium

In order to have independent measurements of the bed permeabilities, it was arranged to have a measured flow of air at low, measured pressure drop passed through the entire bed. Since total bed area, and depth could be measured, this allowed calculation of permeability using Darcy's law. The equipment associated with these measurements is shown in Fig. 3.2.3.

It was necessary to prevent the granular material from falling out through the exit-hole at the bottom, as well as to ensure uniform flow-distribution throughout the length of the bed. The only way to achieve the former was to have the bottom exit hole covered with material impervious to the granules, and the only way to achieve the latter was to have a small air-space across the entire cross-section of the bed, both at top and bottom. Achieving the air-space at the top was simple: the disc at the top was kept a small distance off the bed-surface during these measurements. It was necessary, however, to support the bed at

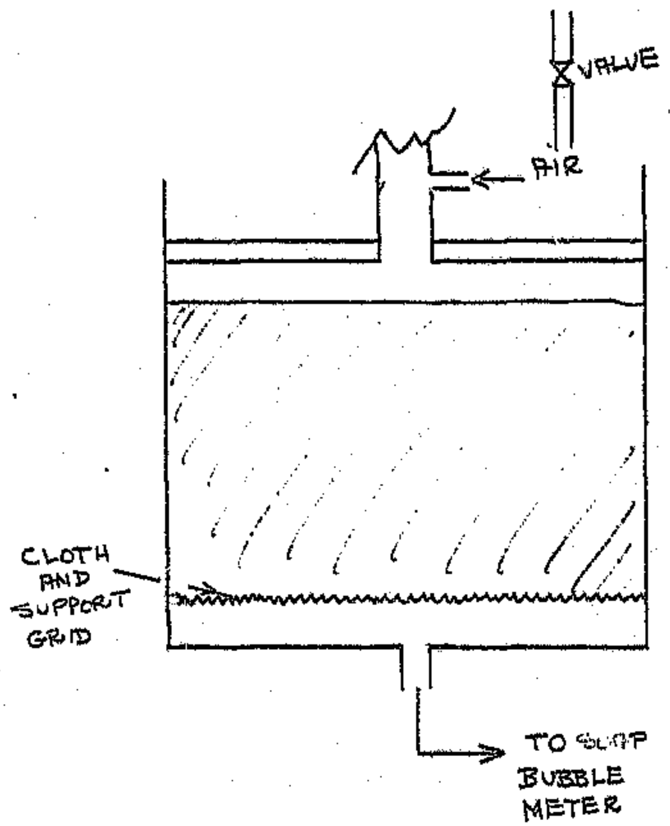

3.2.3 Sketch of apparatus used to measure permeability the bottom with a cloth, stretched over a very coarse mesh which was in turn supported on 10mm studs on the bottom of the container. Granules were thus prevented from falling out, and uniform flow distribution was ensured by the air-gaps at top and bottom.

The presence of the retaining cloth, however, presented a problem when measuring the permeability of the coarser material, since cloth resistance was found to contribute significantly to pressure drop. Thus, for the coarser material, pressure-drop/flow characteristics were measured for two different bed depths, allowing the resistance of the cloth-mesh combination to be determined. When subsequent measurements were made, the cloth resistance as previously determined was used to arrive at the correct permeability of the bed.

Note that during the frequency-response measurements discussed in 3.2.1, the presence of the cloth presented no problem, as pressure pulses did not have sufficient time to propagate to the bottom of the bed; this was especially true for runs in which the bed contained any reasonable depth of fine granules.

4 EXPERIMENTAL RESULTS

The results of the momentum transfer experiments (described in the preceding chapter) are presented in this chapter. The measurements of Leibowitz and Benson-Armer (unpublished), are reproduced in their entirety in Appendix B; all other heat transfer experimental results have been published elsewhere.

4.1 Momentum Transfer Experimental Results

4.1.1 Steady momentum transfer results

The permeability of two beds (composed of the 0.5mm nominal particles and the 2mm nominal particles were measured as:

$K \approx 3 \times 10^{-11}\ m^2$ 2mm particles
$K \approx 2 \times 10^{-12}\ m^2$ 0.5 mm particles

Permeability was measured over a pressure-drop range of 400 Pa/m to 4000 Pa/m. The permeability calculated at the highest pressure drop was approximately 75% of that calculated at the lowest measurable pressure drop. The reason for this was not investigated at all, since only an approximate permeability was required for the purposes of general comparison with model results; no further attention is paid to these results.

4.1.2 Unsteady momentum transfer results

Measurements as described in 3.2 were made on a number of different bed types (summarised in Table 4.1 below). As described in 3.2, pressure was logged with sufficient frequency to get accurate representation of its maximum value, and to prevent aliasing. For each run the amplitude of the pressure trace, and its phase with respect to piston position were calculated. It is the amplitude and phase of the pressure trace that are presented and used in this work, and all of these results appear in the graphs presented in this chapter.

Table 4.1 - Pneumatic Test Experimental Beds

Bed	Description	
1	230 mm of 2 mm	
2	340 mm of 2 mm	
3	455 mm of 2 mm	
4	350 mm of 0.5mm	
5	70 mm of 2 mm on top of 350 mm of 0.5mm	
6	130 mm of 2 mm on top of 240 mm of 0.5mm	
7	200 mm of 2 mm on top of 240 mm of 0.5mm	
8	200 mm of 2 mm on top of 240mm of 0.5mm (repeat run 7)	repeat of run 7 after 2 weeks
S	3 mm diam. orifice	
M	6 mm diam. orifice	
L	10 mm diam. orifice	

The graphs presented in Fig.'s 4.1a through 4.11a, and 4.1b through 4.11b show the dependence of pressure amplitude offset (P_{max}-$P_{\omega o}$, where P_{max} is the amplitude of the pressure and $P_{\omega o}$ is the pressure amplitude at low frequency), and time lag on reciprocation frequency for each of the above bed configurations and orifice sizes. Fig. 4.14a and 4.14b show overlays of P_{max}-$P_{\omega o}$ and lag respectively for runs 1 through 8. The pressure amplitude offset results in 4.14a clearly display sufficient resolution to distinguish one bed from another, but the lag results in Fig. 4.14b are not resolved to the same extent. Note that $P_{\omega o}$ is the pressure measured low frequency, is and corresponds to the case where pressure is evenly distributed throughout the entire system. $P_{\omega o}$ approaches ambient pressure for piston volume variations small in comparison to bed volume

The general trend present in the results, as expected, is that amplitude increases with frequency. The explanation for this is that as frequency increases, gas velocities inside the bed (through the orifice) increase, requiring larger pressure gradients. This is discussed in detail in Chapter 5, with regard to interpretation of model results. Also, as expected, as frequency increases, time lag decreases. This is satisfying, since as frequency increases, one would expect the system to behave more and more like a blocked piston, which would display no lag at all (by definition of lag used here, which is referenced to a blocked piston).

Measurements similar to those on the packed beds were made on a system in which the resistance of the bed was replaced with an orifice, placed right at the mouth of the reciprocator. The motivation for this was to see if there was any correspondence between the distributed resistance case (packed beds) and the point resistance of the orifice, and to see if there were consistently identifiable trends. Furthermore, the resistance of the orifice plates could be very tightly controlled, since they were precision machined with square edged holes. There could therefore be no room for doubt about which had the most or least resistance. The measured amplitude offsets are shown in Fig.'s

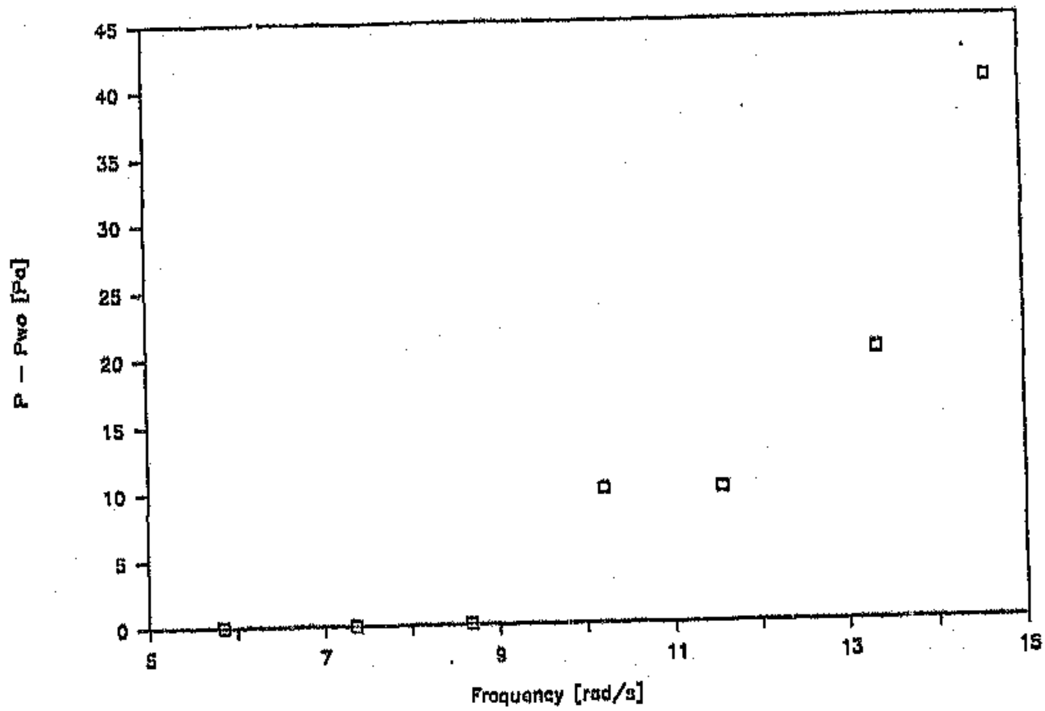

Fig. 4.1a Plot of pressure amplitude offset vs. frequency for run 1

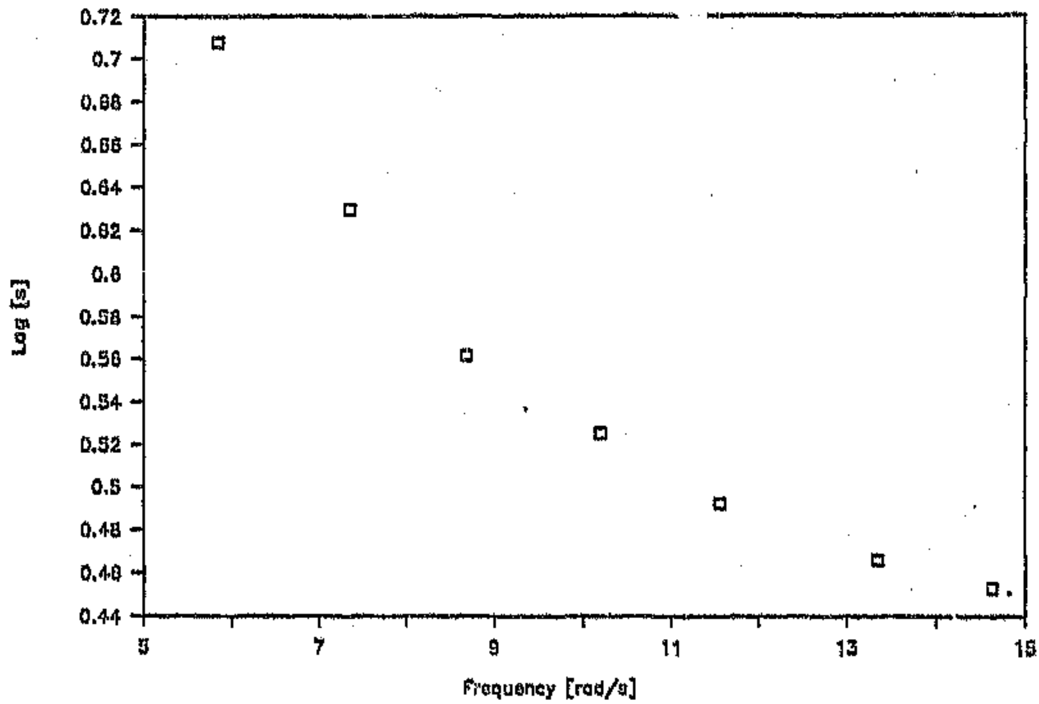

Fig. 4.1b Plot of lag vs. frequency for run 1

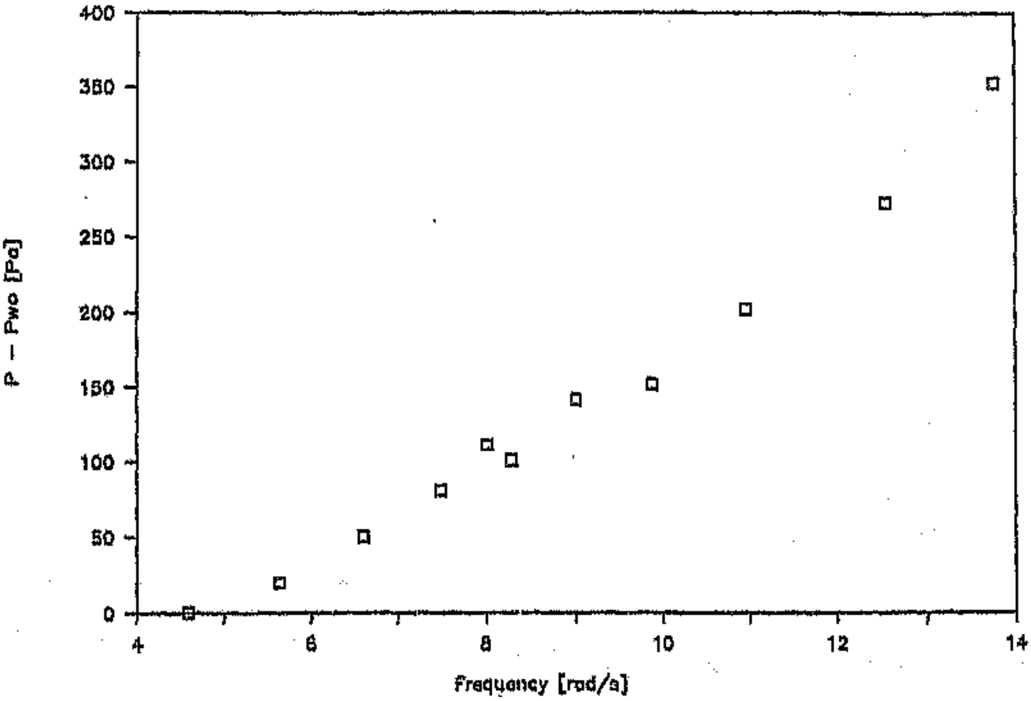

Fig. 4.2a Plot of pressure amplitude offset vs. frequency for run 2

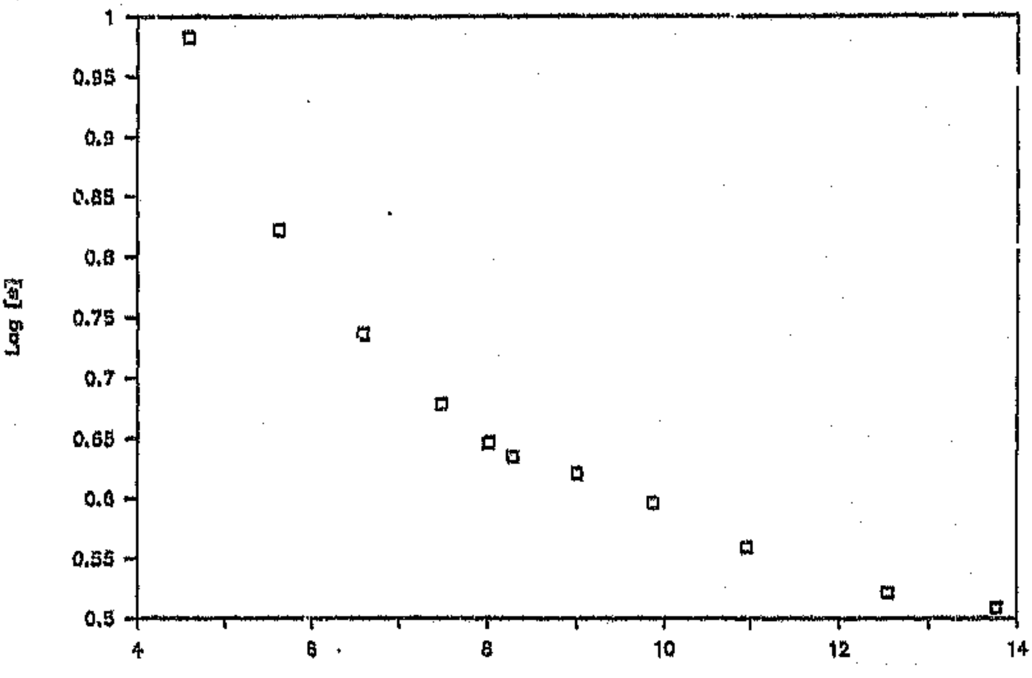

Fig. 4.2b Plot of lag vs. frequency for run 2

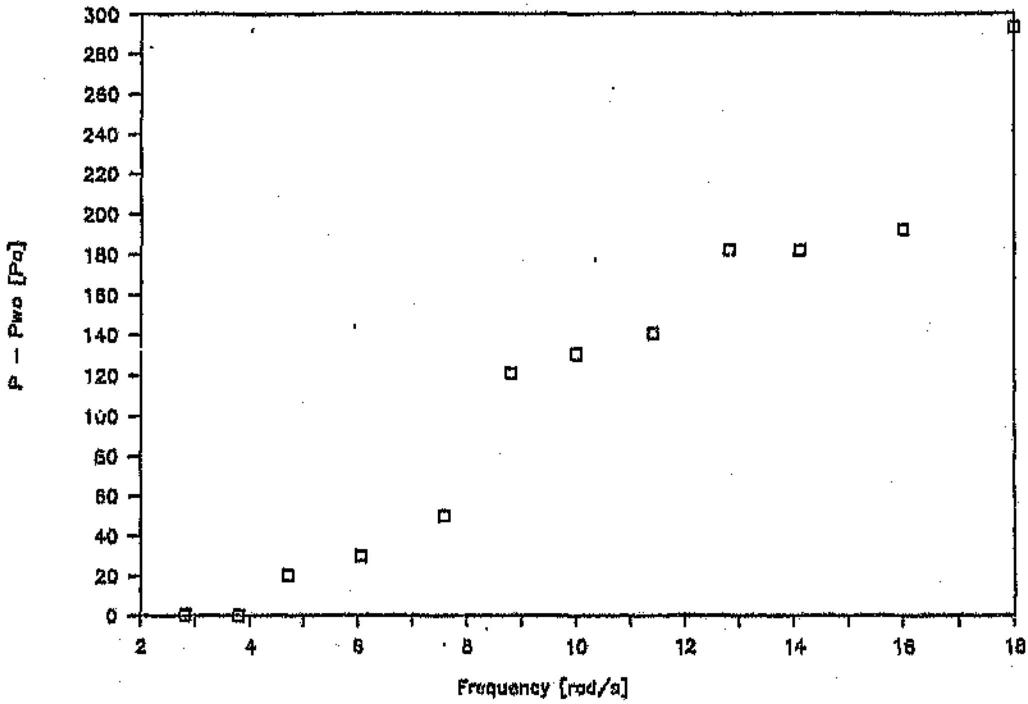

Fig. 4.3a Plot of pressure amplitude offset vs. frequency for run 3

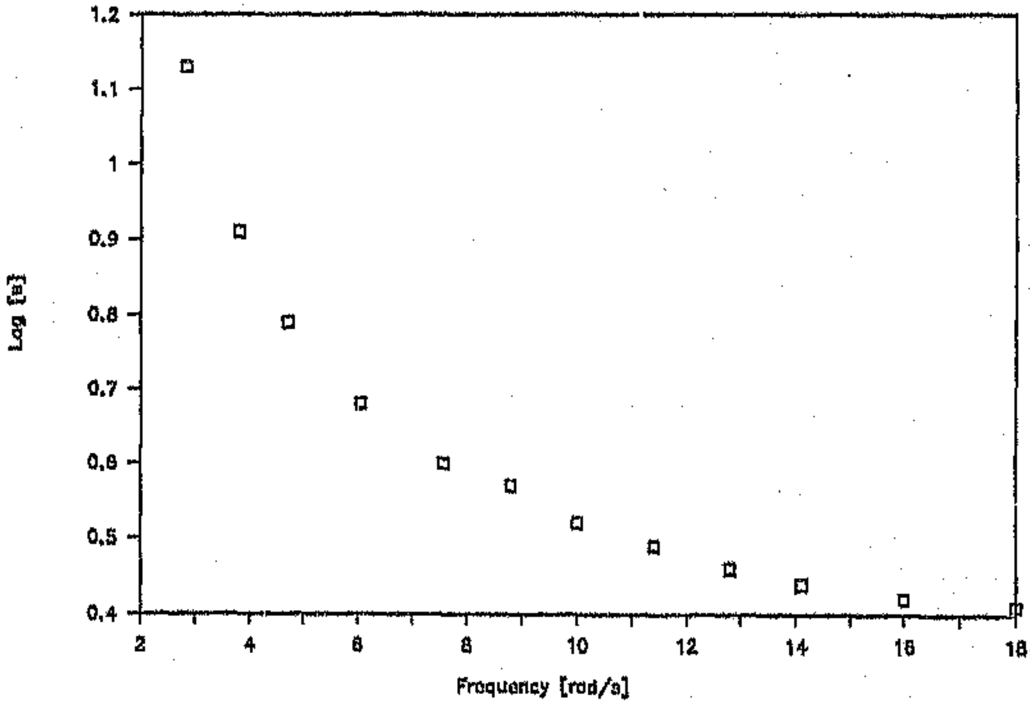

Fig. 4.3b Plot of lag vs. frequency for run 3

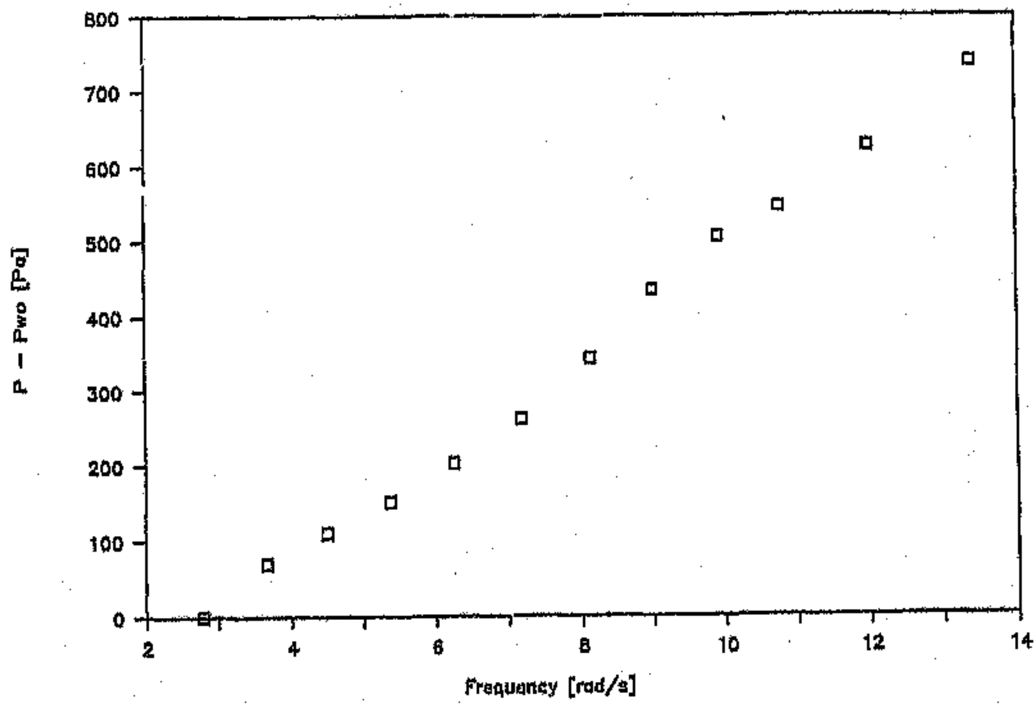

Fig. 4.4a Plot of pressure amplitude offset vs. frequency for run 4

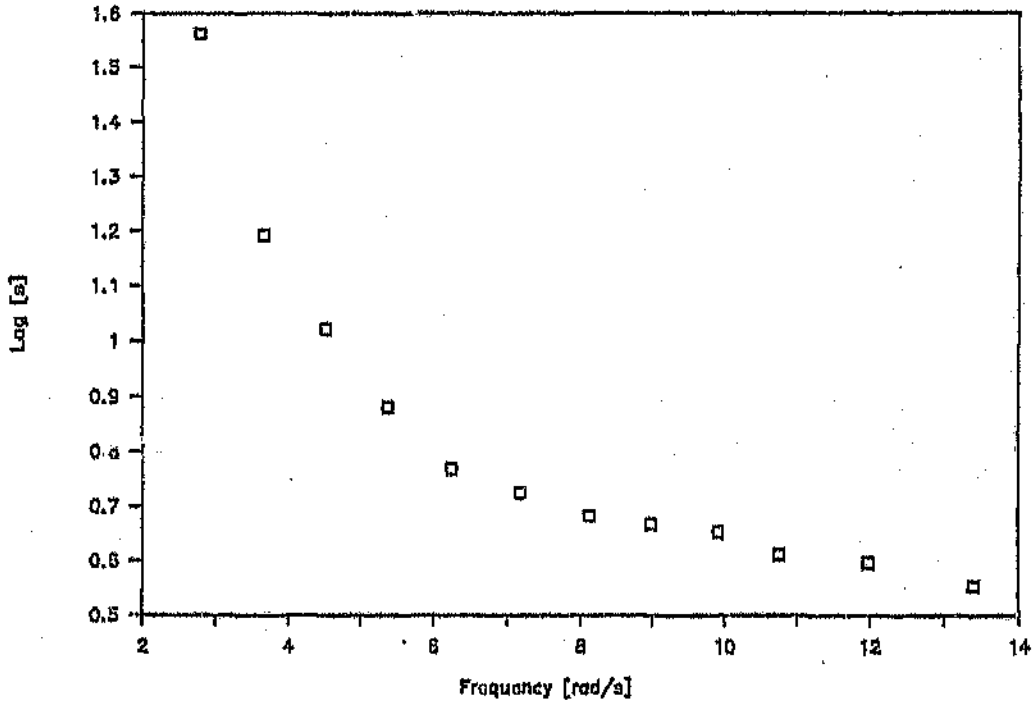

Fig. 4.4b Plot of lag vs. frequency for run 4

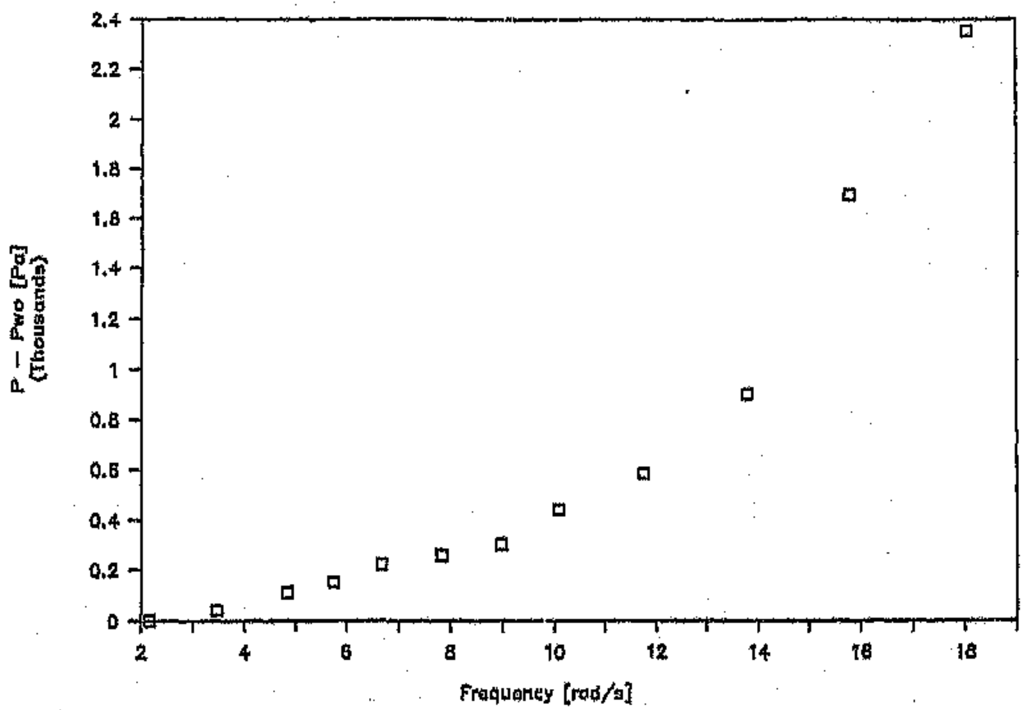

Fig. 4.5a Plot of pressure amplitude offset vs. frequency for run 5

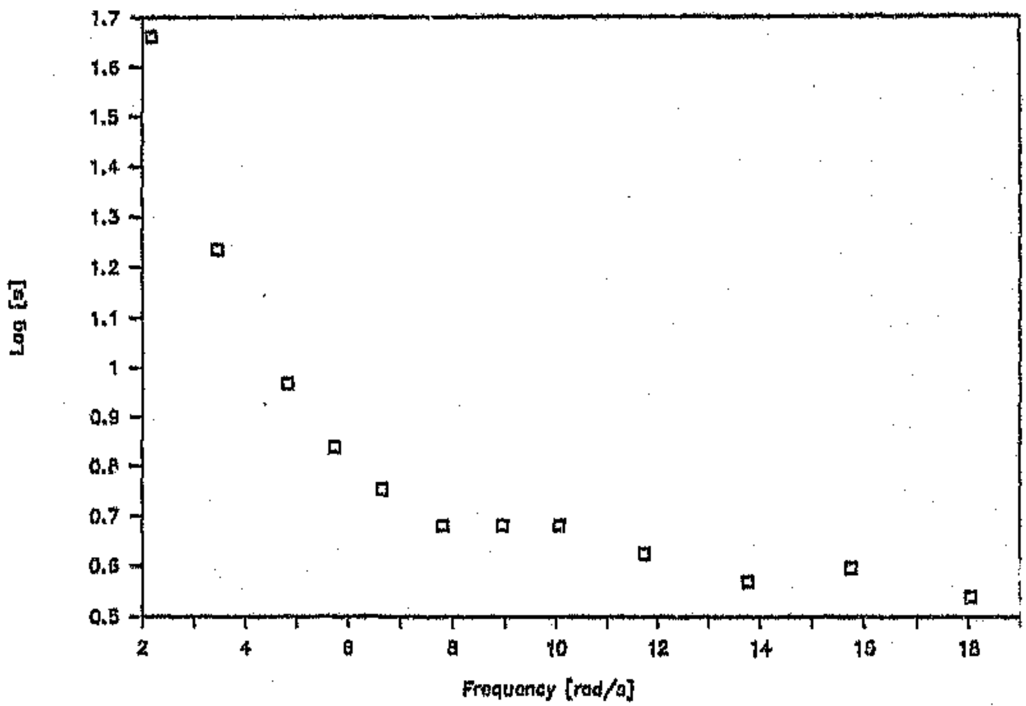

Fig. 4.5b Plot of lag vs. frequency for run 5

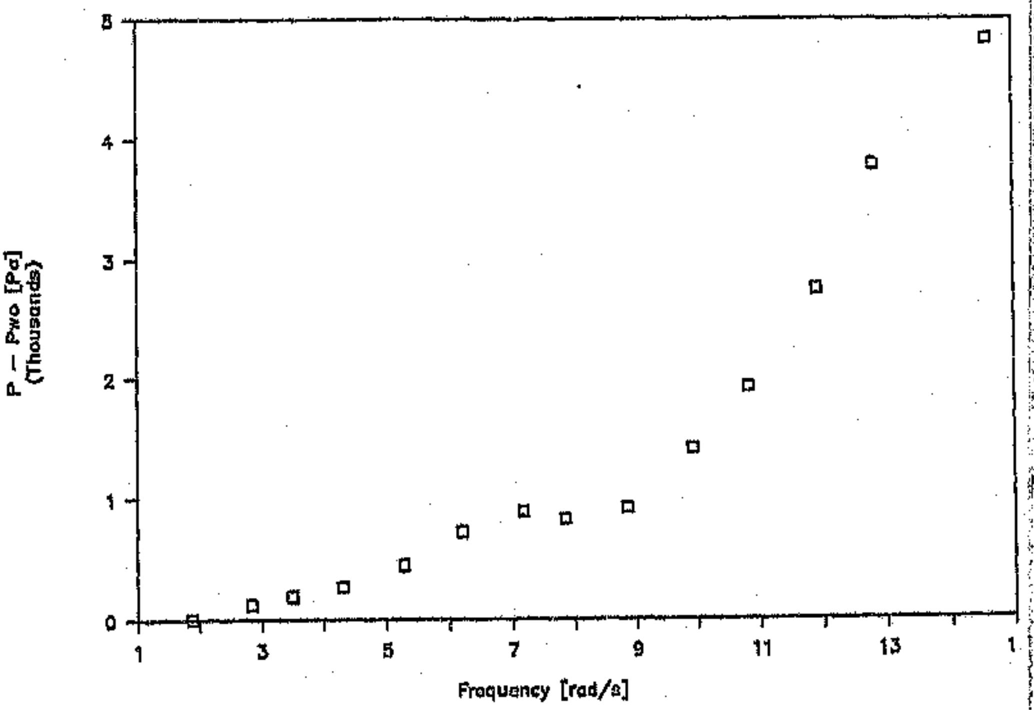

Fig. 4.6a Plot of pressure amplitude offset vs. frequency for run 6

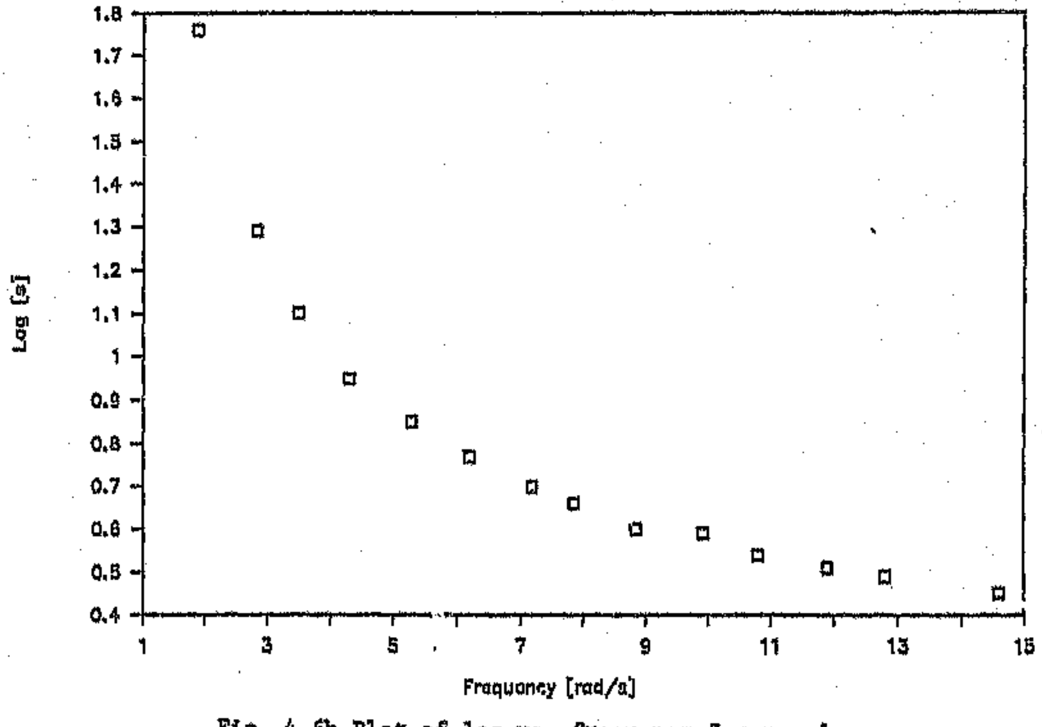

Fig. 4.6b Plot of lag vs. frequency for run 6

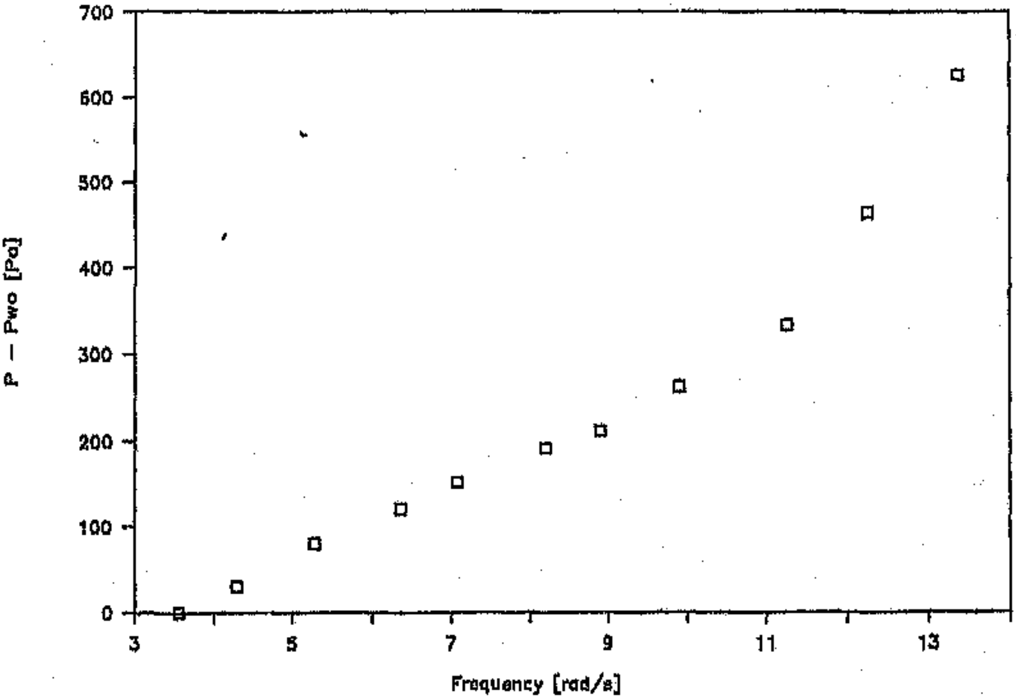

Fig. 4.7a Plot of pressure amplitude offset vs. frequency for run 7

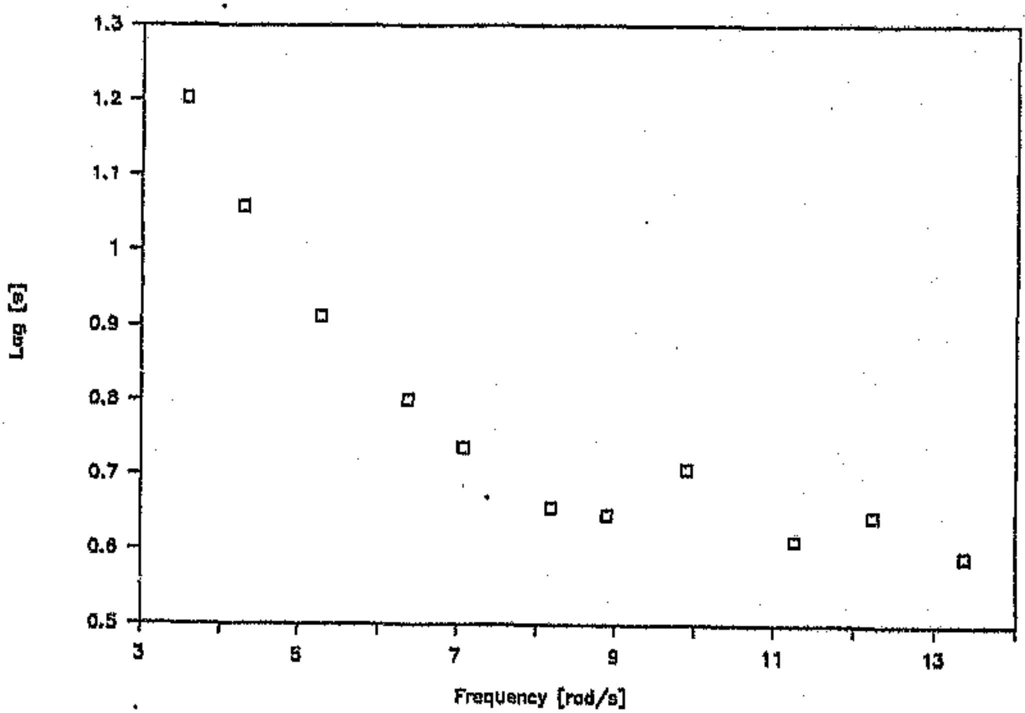

Fig. 4.7b Plot of lag vs. frequency for run 7

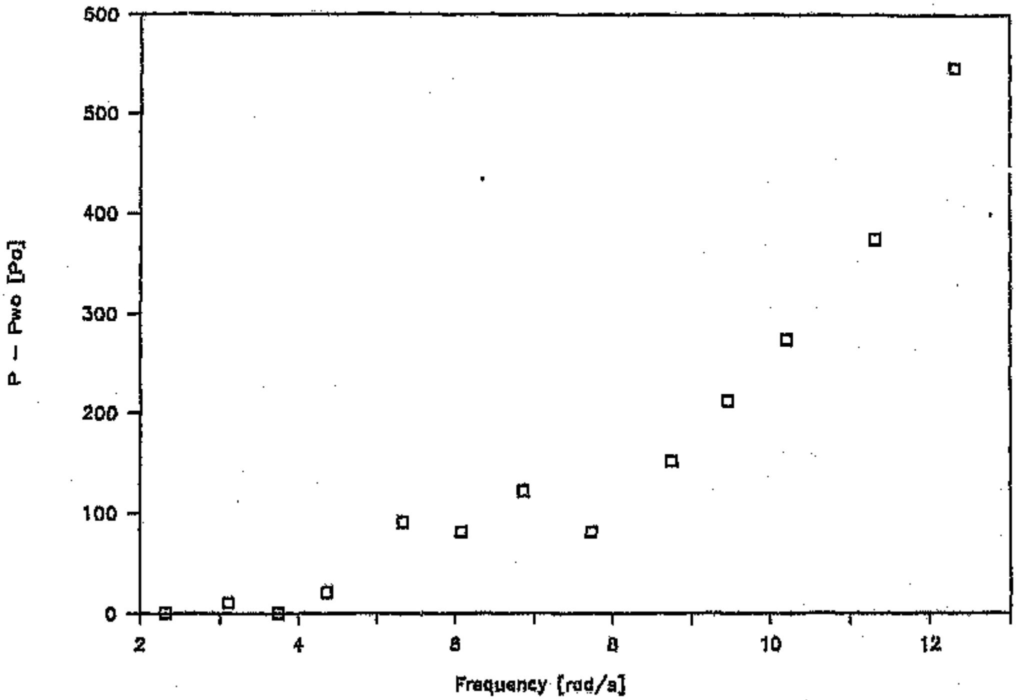

Fig. 4.8a Plot of pressure amplitude offset vs. frequency for run 8

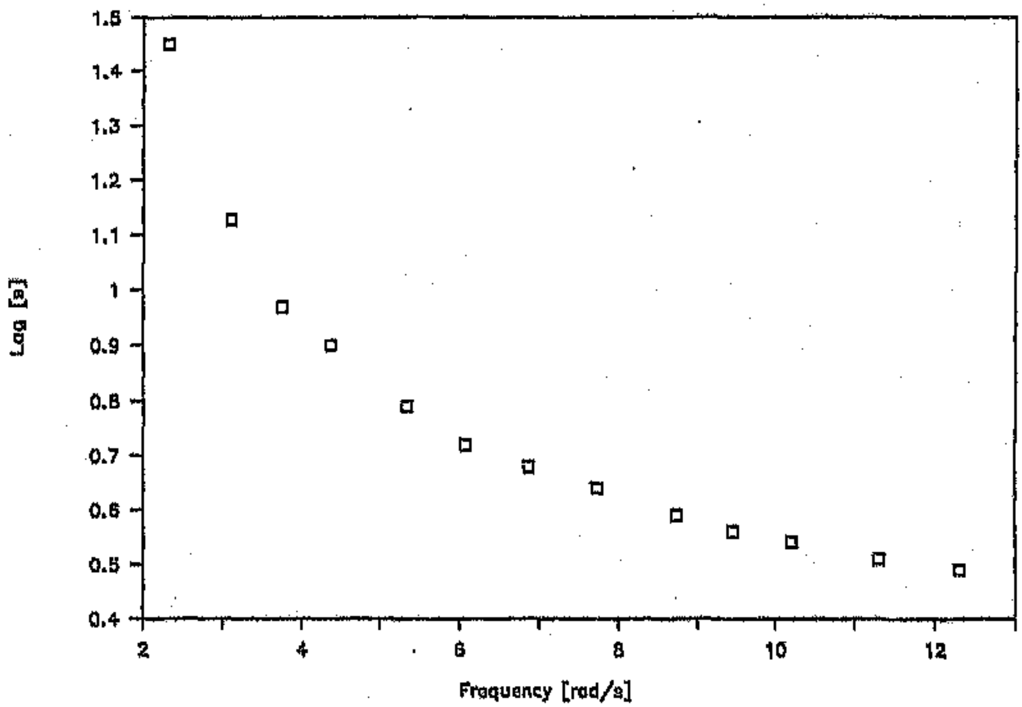

Fig. 4.8b Plot of lag vs. frequency for run 8

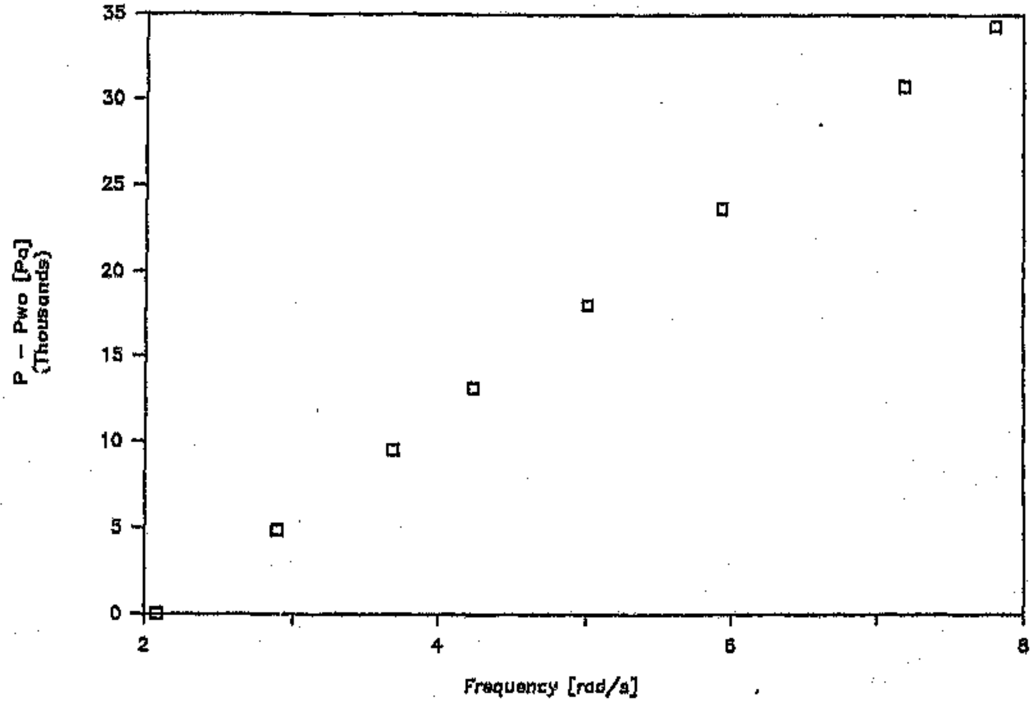

Fig. 4.9a Plot of pressure amplitude offset vs. frequency for 3mm hole

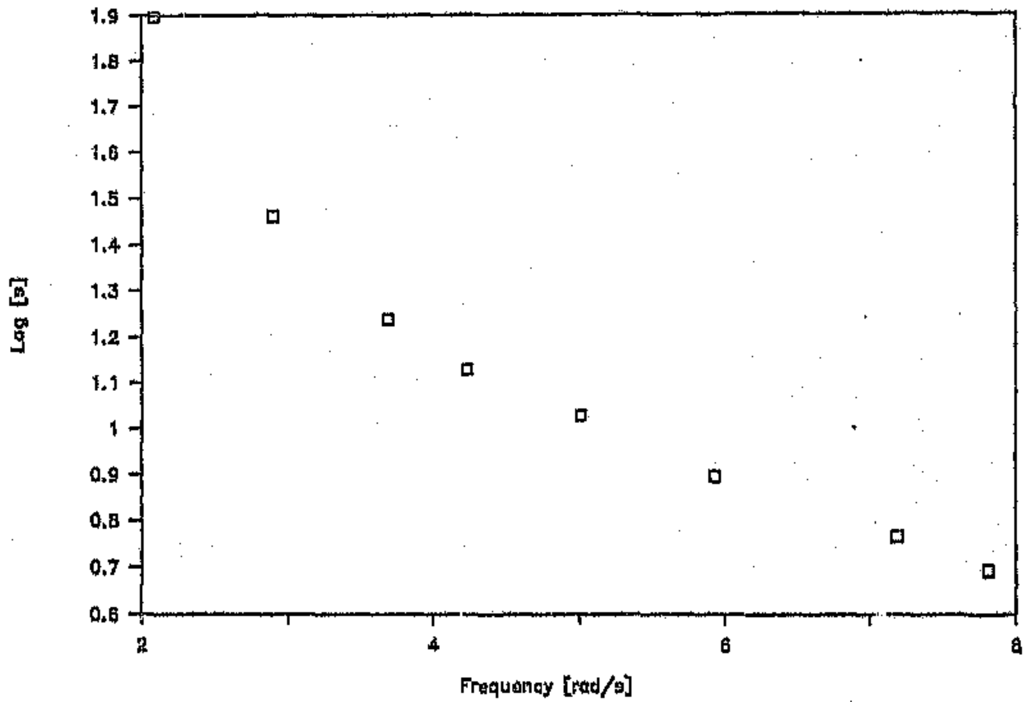

Fig. 4.9b Plot of lag vs. frequency for 3mm hole

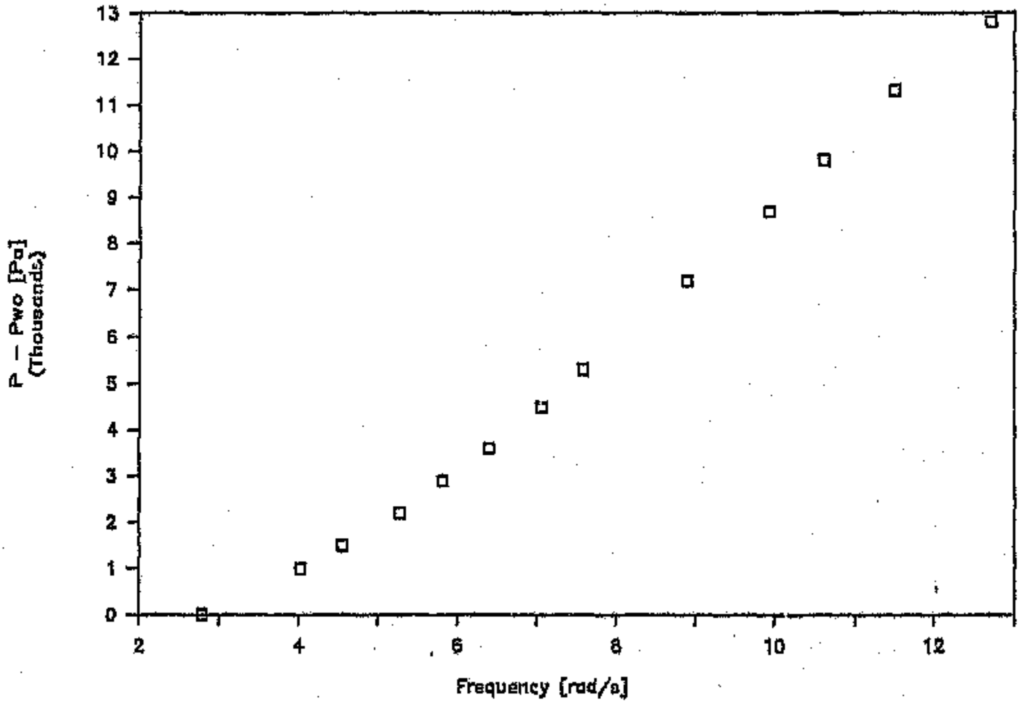

Fig. 4.10a Plot of pressure amplitude offset vs. frequency for 6mm hole

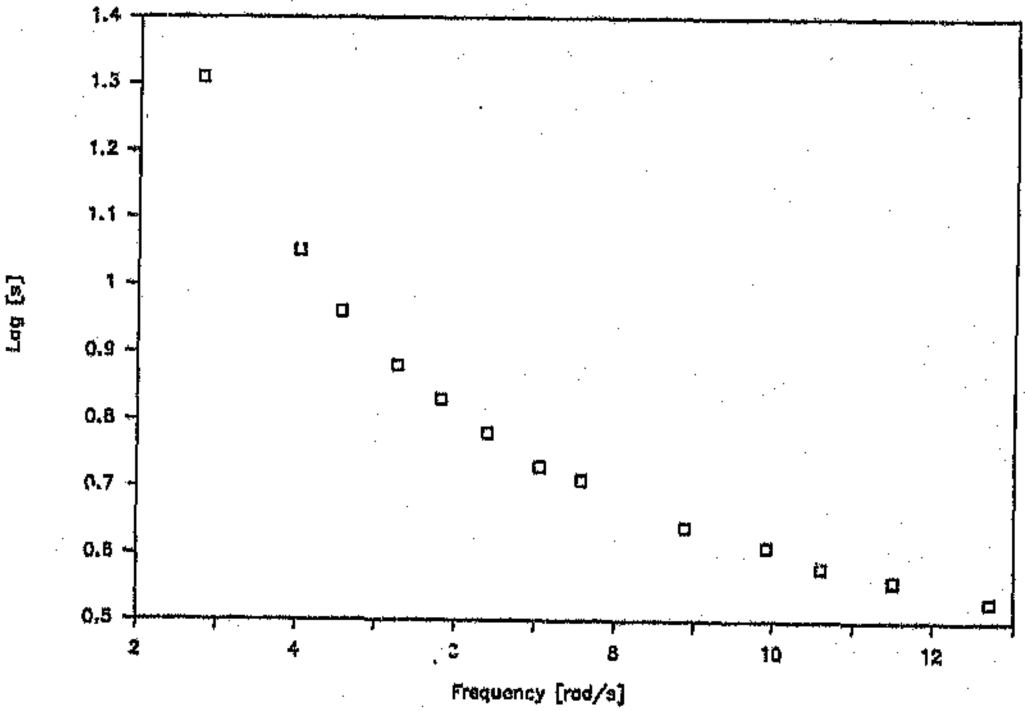

Fig. 4.10b Plot of lag vs. frequency for 6mm hole

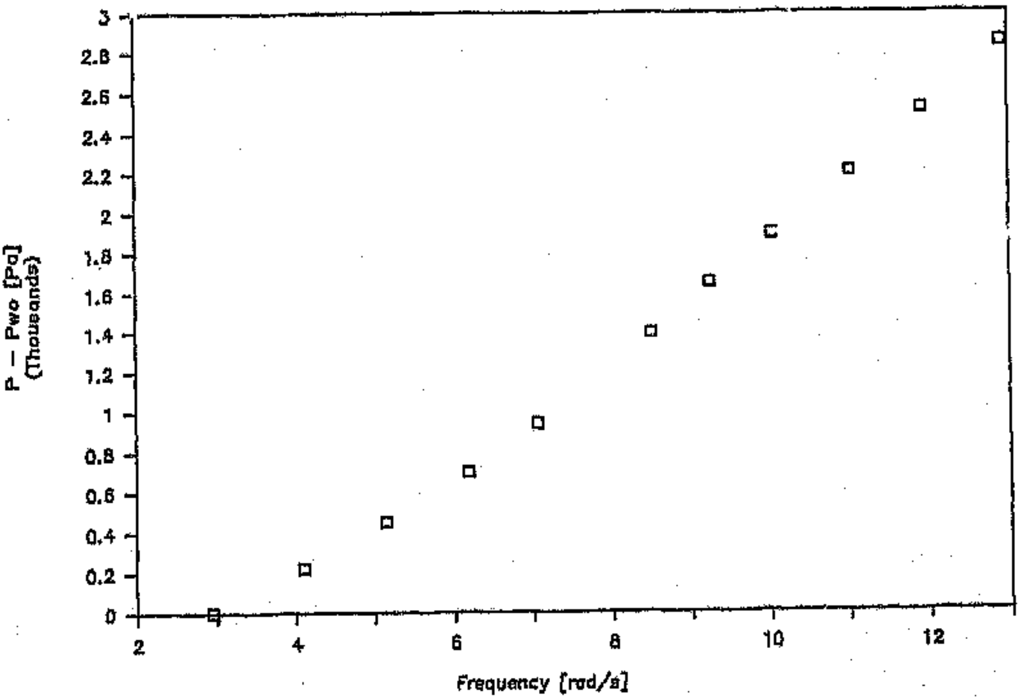

Fig. 4.11a Plot of pressure amplitude offset vs. frequency for 10mm hole

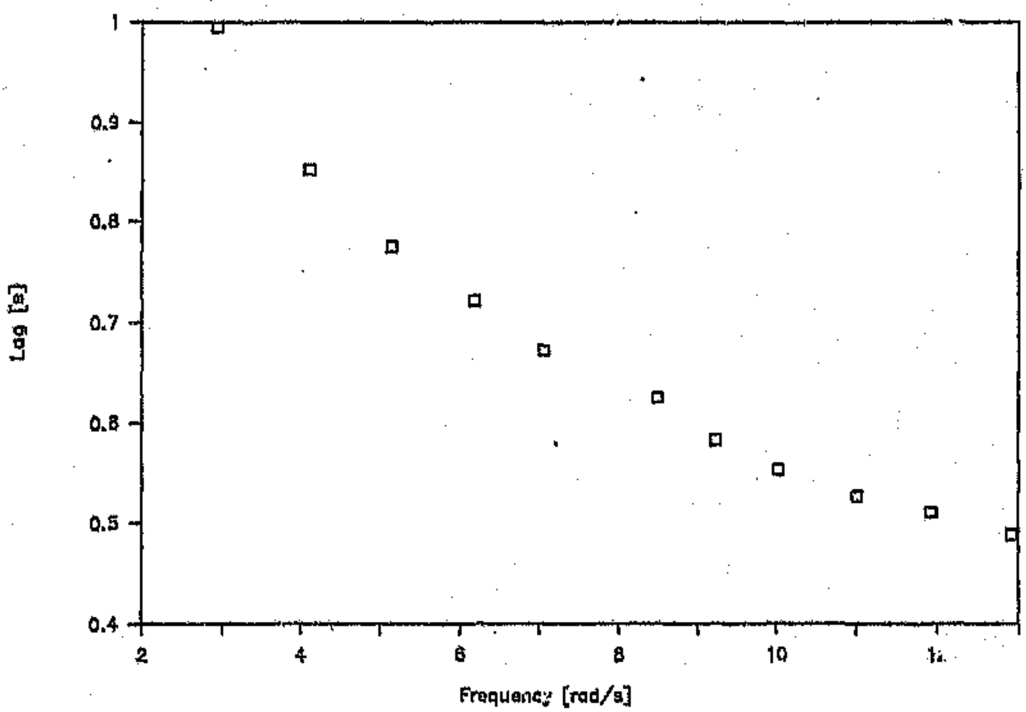

Fig. 4.11b Plot of lag vs. frequency for 10mm hole

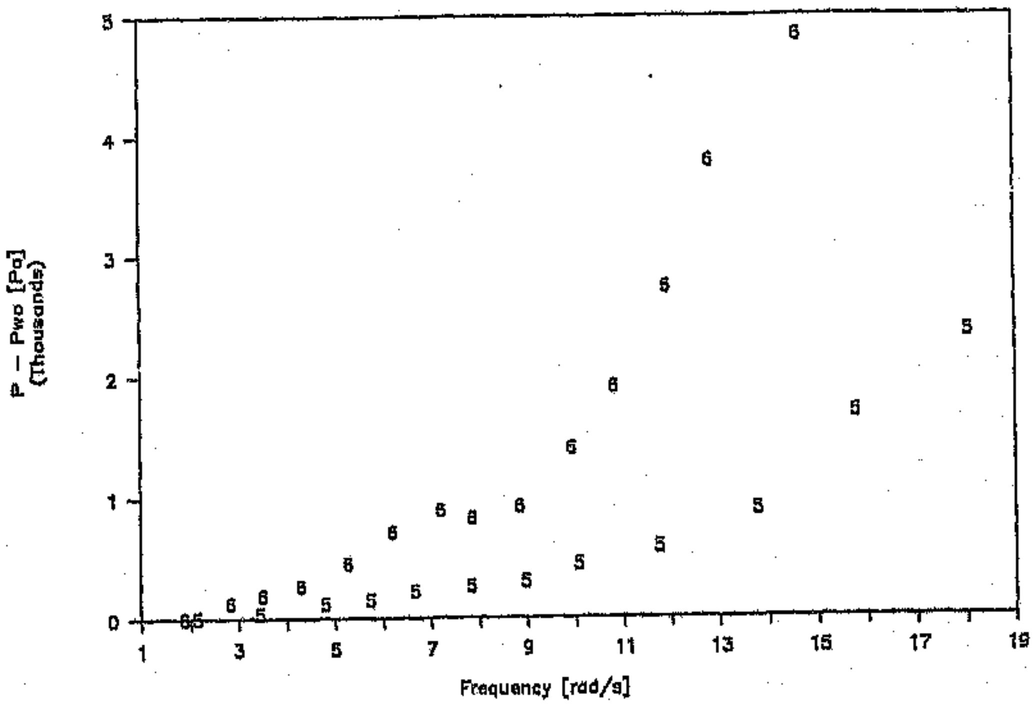

Fig. 4.12a Plot of pressure amplitude offset vs. frequency for runs 5 and 6

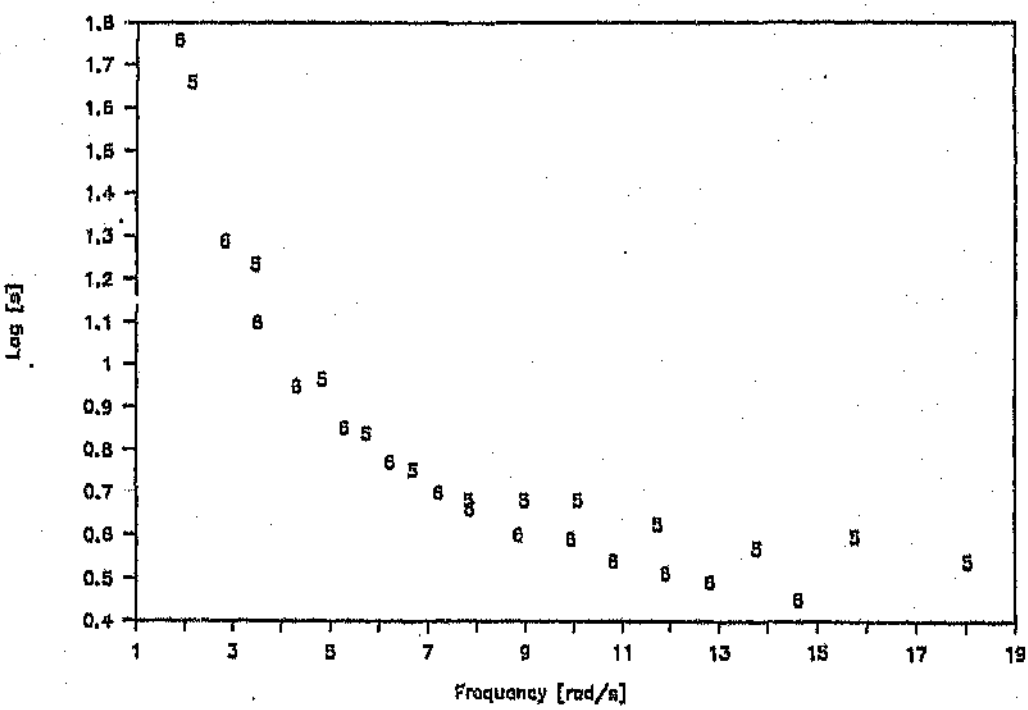

Fig. 4.12b Plot of lag vs. frequency for runs 5 and 6

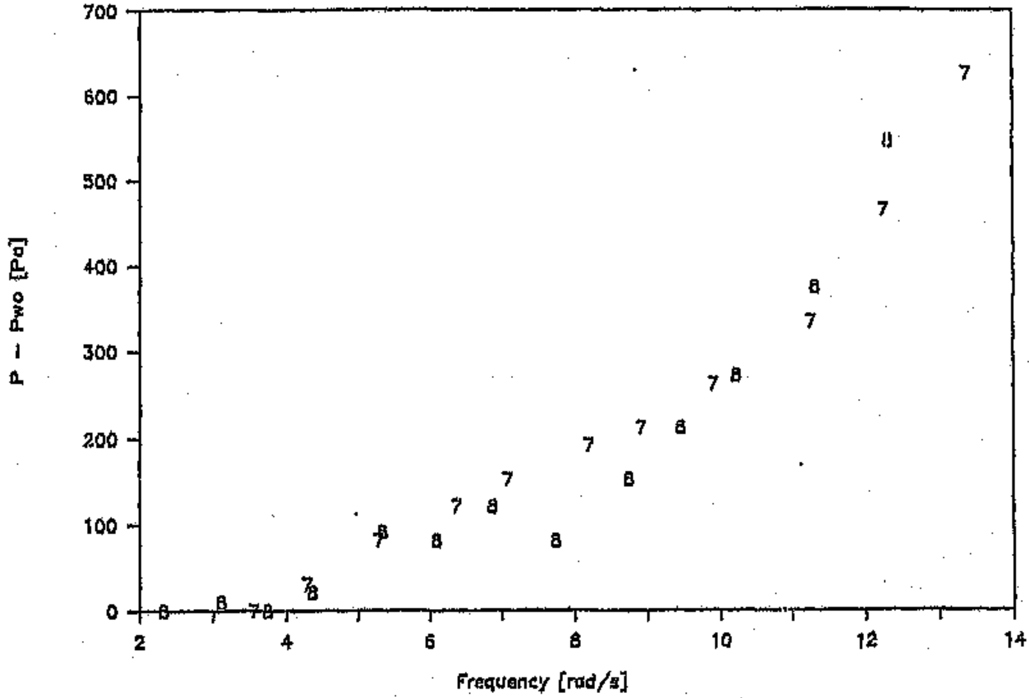

Fig. 4.13a Plot of pressure amplitude offset vs. frequency for runs 7 and 8

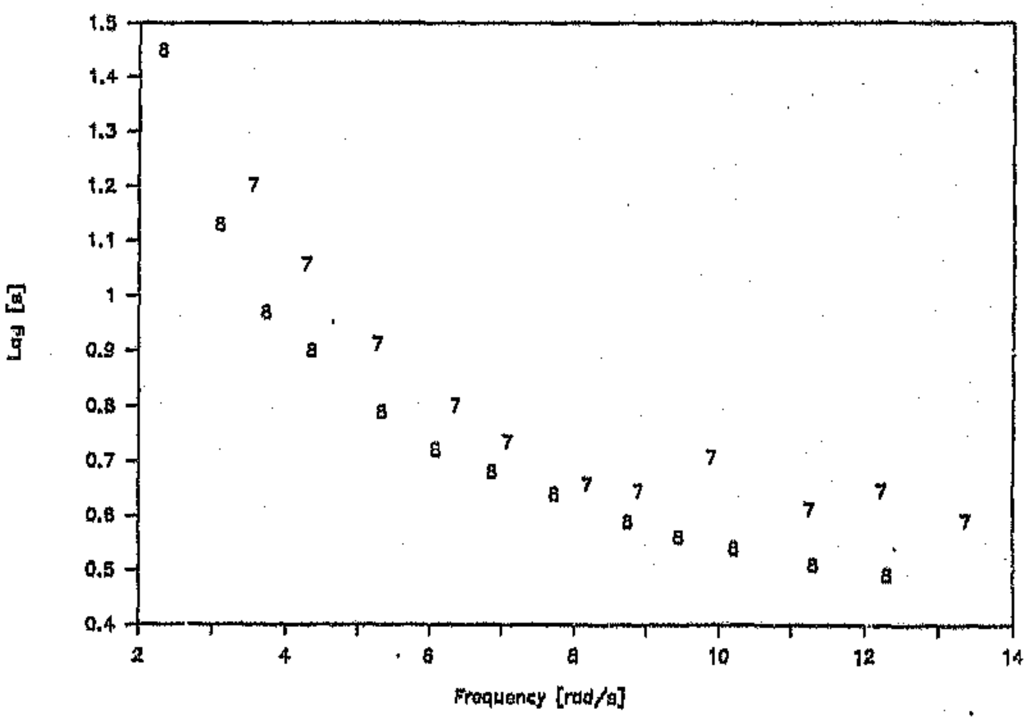

Fig. 4.13b Plot of lag vs. frequency for runs 7 and 8

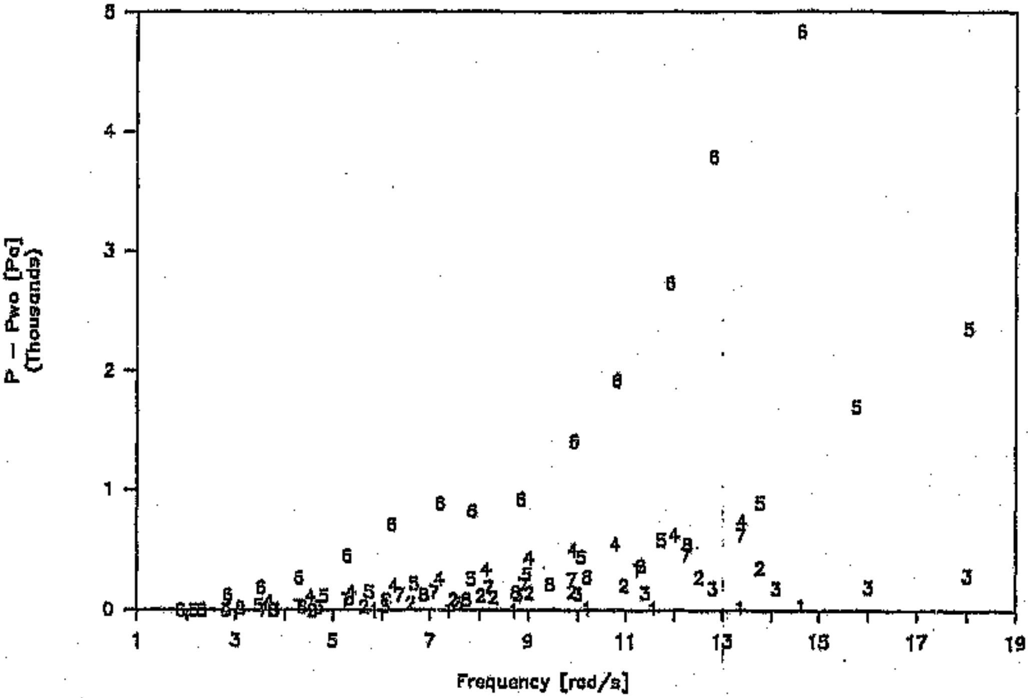

Fig. 4.14a Plot of pressure amplitude offset vs. frequency for runs 1 through 8

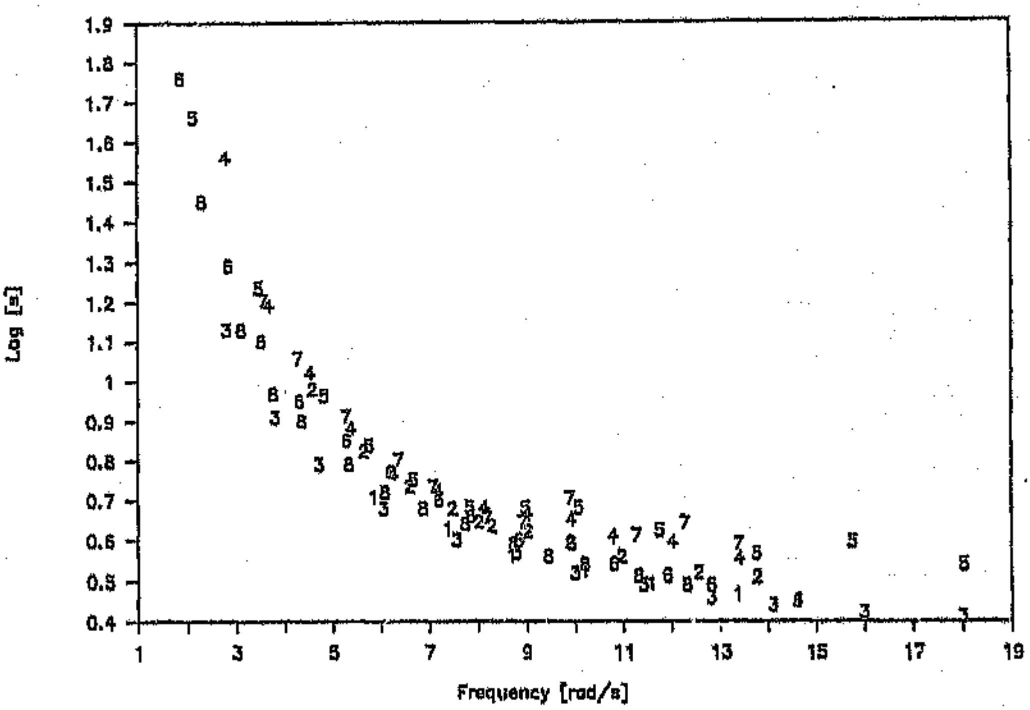

Fig. 4.14a Plot of lag vs. frequency for runs 1 through 8

As expected, the amplitude offset increases with frequency, and with increased resistance, as can be seen in Fig. 4.15a, which shows overlays of the pressure amplitude offset for the three orifice sizes. The main motivation for doing the measurements on the orifice plates, however, was to verify the intuitive conclusion that lag decreases with increasing frequency and increases with increasing resistance. This is indeed the case, as is clearly shown in Fig. 4.15b. One could use this information to assist in the interpretation of measurements on packed beds, by assigning lumped resistances to various section of the bed. This is further investigated in Chapter 5.

4.2 Discussion.

A marked feature of Fig.'s 4.1a through 4.8a is that the composite (layered) beds (no.'s 5 to 8) display sharp changes in slope (see Fig.'s 4.5a to 4.8a). The results for beds 5 and 6 are overlaid in Fig. 4.12a to emphasise the behaviour. This feature could be an indication of inhomogeneity within beds, and possibly the difference in slope between the low and high frequency sections could be correlated with permeability ratio. It may also for instance be found that the location of the sudden increase in slope gives an indication of the depth at which the permeability changes.

One would also expect (as shown in Chapter 5) that time lag behaviour could assist in deduction of the internal structure of the bed. Fig. 4.12b shows an overlay of the lag plots for beds 5 and 6, and there appears to be a digression above a frequency of 9 rad/s. However, examination of Fig. 4.14b reveals that there is little real variation in the time lag plots for the different beds if one takes measurement uncertainty into account, certainly too little to make generalised conclusions.

Fig. 4.13a shows the pressure amplitude offset for runs 7 and 8

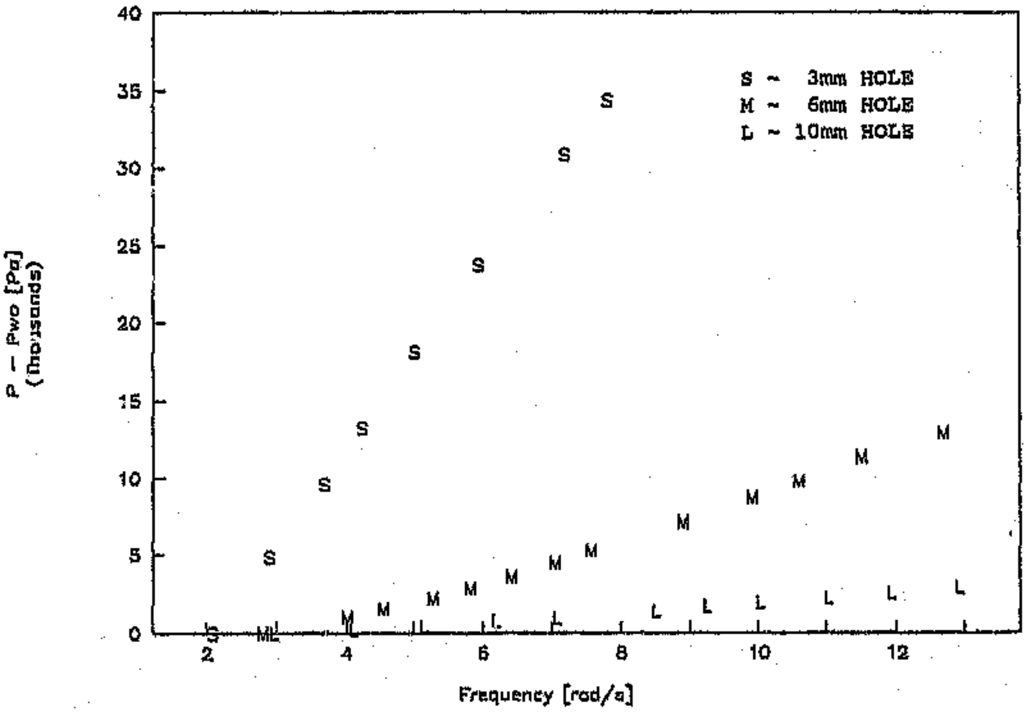

Fig. 4.15a Plot of pressure amplitude offset vs. frequency for 3mm, 6mm & 10mm hole

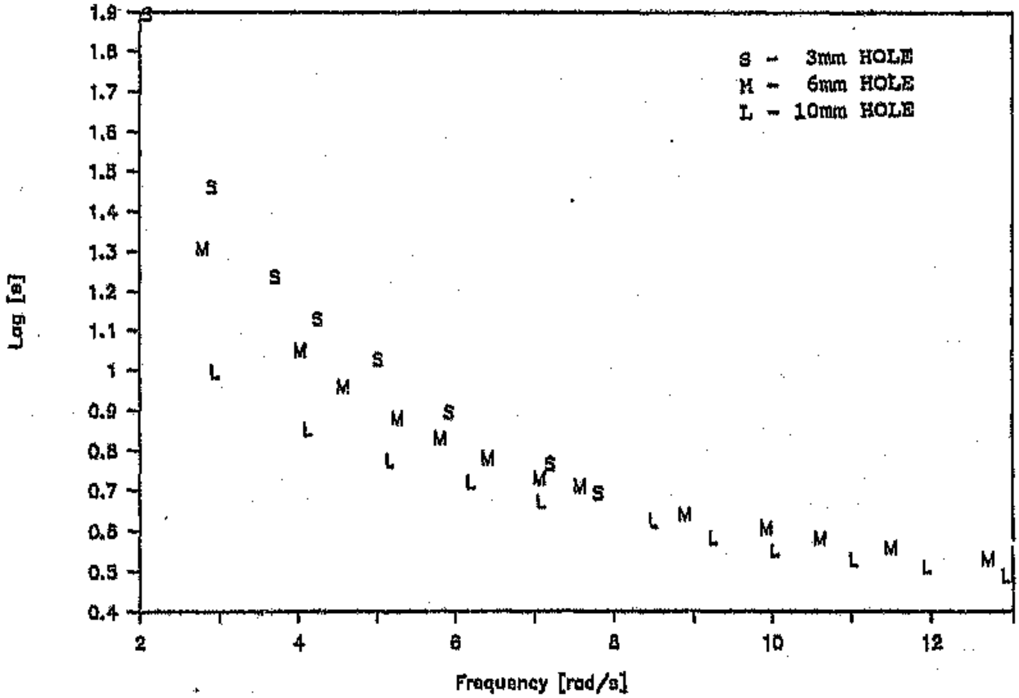

Fig. 4.15b Plot of lag vs. frequency for 3mm,6mm & 10mm hole

(the same bed, left undisturbed for two weeks). Apart from an inexplicable deviation between 7 and 9 rad/s, the correspondence between these two runs is good, thus confirming that these measurements are reproducible. Note, however, that the lag plot for these same two runs in Fig. 4.13b shows that the later run (run 8) has a consistently lower lag at any given frequency. No reasonable explanation for this could be found, though future studies should address this issue.

4.3 Summary

Due to shortcomings in the design of the apparatus, it was difficult to locate the compressor on the surface of the bed without disturbing the bed at all. As a result of the disturbance, which generally took the form of compression of the bed, it is not possible to compare measurements on an absolute basis. This, however, is not a serious problem when considering application in the field, since the methods of stacking the piles are not well controlled, and even apparently identical piles will have different internal structures.

In any case, the major application envisaged for this technique is the identification of gross differences in behaviour, which would indicate whether one bed (or a region of a bed) was substantially more permeable than another. The presence of a large region of high permeability might for instance make a bed more susceptible to combustion, so identification of gross differences in permeability is considered a worthwhile pursuit.

Little of value could be deduced from measured lag curves due to lack of resolution in the results. This is possibly due to disturbance of the different beds during location of the reciprocating device on the surface, which generally took the form of compression. The results have, however, been reported here in case any future analysis is to be attempted.

It is believed that some information of value can be deduced from the pressure amplitude results reported here. In any case, before the method can be applied to the analysis of large scale beds, it is necessary to address four main issues:

1 the apparatus must necessarily make contact with the bed in question. It is essential that disturbance in the region of contact be kept to a minimum.

2 some means must be found to prevent the majority of air escaping from the bed surface immediately adjacent to the compressor, or a means to account for these losses.

These first two issues are not of crucial importance, since it is envisaged that the method will be used for comparative analysis of beds, just as the surface temperature method for estimating total energy release within a bed does not require exact heat transfer coefficients if comparison is required.

3 in the case of a mega-ton stockpile, it is clear that a substantial pneumatic pulse would be required to probe the bed to any significant depth; furthermore, the average coal particle in such a pile has a diameter fo the order of 10-30mm. The permeability of such a bed, even with a sizable portion of fines, is two orders of magnitude greater than that used in the numerical experiments discussed above and the measurements described in Chapter 4. A large bed composed of 10-30mm particles would therefore require either very rapid pulses of air, or impossibly large pulses in order to register any increase in pressure. In such a case, alternative pulse methods would have to be investigated.

4 The analysis of the amplitude-frequency curve to produce quantitative information about the bed is clearly a difficult task, and a large amount of work is required in order to develop such an analysis.

It is believed that the technique could be developed into one which can be used to make meaningful and effective deductions regarding the interior of a bed.

5 Development of Some Surface-based Measurement Techniques

As discussed in 1.1 and 1.3, modelling transfer processes in porous media is exceedingly important to developing the state of understanding, and improvement of systems in a wide range of fields. In this chapter models are applied to different artificial systems to estimate parameters and attempt to understand the phenomena involved. Published attempts to model transport in porous bodies in both natural and artificial surroundings have shown that:

- little is known about relevant boundary conditions at exposed surfaces. The earliest warning of combustion deep within a coal stockpile is the appearance of 'hot spots' on the surface of the pile. Knowledge of the relationship between the surface temperatures and the state of the interior of the stockpile is vital to the early diagnosis of combustion dangers.

- multidimensional convective-conductive modelling is computationally very expensive, and often of limited use in practical applications due to lack of knowledge regarding internal structure. Alternative approaches to these extremely expensive and complex calculations are required, for reasons of economy of both time and effort.

This chapter attempts to specifically address the above two issues, with a view to developing a system for the practical monitoring and management of coal stockpiles, using only realistically attainable measurements and parameters.

5.1 Modelling Natural Thermal Convection in Porous Media

Although the applicability of conductive-convective equations has become accepted, a number of questions remain unanswered, one of which is the treatment of boundary conditions. Boundary conditions are taken for granted, but no evidence of research into validity and efficacy of the boundary conditions was found. One of the aims of this section was therefore to test the application of surface heat transfer coefficients to convective heat transfer modelling in porous media.

In particular, the surface heat transfer coefficient of an experimental coal bed was estimated by fitting model predictions to measured temperatures. An attempt was made to determine the dependence of effective permeability and surface heat-transfer coefficient on particle size, by fitting calculated internal temperatures in a packed bed to experimentally measured temperatures. No general conclusions could be reached regarding dependence of surface heat transfer coefficient on particle size, due to inadequacies in experimental design, but values commensurate with free convection from solid bodies were obtained, and may be used as a guideline for future studies. Since no evidence of any studies regarding heat transfer coefficient at the exposed surface of porous media are evident, this aspect is considered worthy of study.

Due to the complexity of two-dimensional conductive-convective simulations, several workers (Brooks & Glasser 1986, Hughes, Klein & Close 1976, Audibert & Gaudet 1987, to name only a few) have developed simplified models. These models are useful for general applications such as the general monitoring of stockpiles of coal or other fuels, or thermal storage beds. In particular, models dealing with the grading of coal-stockpile combustion hazards, and the approximate analysis of thermal storage beds have been published (Brooks & Glasser 1986). The studies mentioned do not directly address the issue of monitoring internal processes using only measurements accessible at the surface of the beds, and since indications from the field are that such methods would be welcome, a simple, fundamentally sound model was developed and tested. The technique was found to produce consistent estimates of energy release in coal beds using only surface temperatures and the heat transfer coefficients discussed above.

The major application envisaged for this model is in the management of solid-fuel stockpiles, which often represent large investments, and considerable environment hazards in the case of combustion. The strength of the model is that it is inherently fundamental in nature, is very simple to apply, and effectively has only one parameter, namely the heat-transfer coefficient at the exposed surface of the body. Since this parameter can reasonably take on only a limited range of values, it is possible to use the model to consistently grade and compare hazards over a period of time, or between various stockpiles.

5.1.1 Two-dimensional conductive-convective modelling

The work and results discussed below culminated in a publication by Anderson & Glasser (1990), the content of which has been extracted from this thesis.

Conductive-convective models are discussed and justified in 2.3, and at great length in the literature. The motivation for undertaking further work in this much-studied field is to develop an understanding of the model parameters permeability and surface heat-transfer coefficient. Young *et al* (1986) estimated permeability and effective thermal conductivity of one bed-type by minimising the sum-of-squared errors in model temperature predictions, but subsequent investigations (see below) have shown that the surface heat-transfer coefficient is an extremely important parameter if the results of such modelling are to be of real use.

A large volume of work on thermally driven convection in porous media has been published, much of which is discussed in a review article by Cheng (1986) . The early work was by Lapwood (1948), who analysed the stability of free convection of fluids in horizontal porous layers heated from below. Lapwood made use of the Darcy-law and the Boussinesq approximation and assumed the temperatures of both the upper and lower surfaces to be known. An approximate analysis was applied to the simplified equations to show that there existed a critical value of the Rayleigh number, below which no convection occured.

More recent work by Bejan (1978) dealt with flow and temperature distributions about a concentrated energy source in an infinite porous medium. An approximate analysis of the model equations made comparisons between coupled convection/conduction and pure conduction temperature profiles. This clearly demonstrated the effect of convection, which is to distort temperature profiles from those of pure conduction, shifting them locally in the direction of the convective flow.

Bejan (1981) also investigated the phenomenon of lateral penetration of convection into the vertical sides of heated porous media. The two dimensional model was shown to be essentially one-dimensional due to the large difference in the natural horizontal and vertical scales. Approximate analysis of the one-dimensional model gave information on the amounts of penetration to be expected under various circumstances; this was illustrated by application of the results to a helium-cooled winding.

Further work by Bejan (1984) on vertical penetration into the base of porous structures caused by local surface-temperature variations (hot- or cold-spots) examined the degree of penetration of flow- and temperature disturbances.

In all of the work mentioned above, the porous bodies have been infinite (no surfaces), or the surface temperatures have been assumed to be known, or of known spatial variation, and in every case the physical geometry was well defined. However, in practice, surface temperatures are seldom explicitly known, but rather take on values dependent on internal temperatures and power dissipation. Young et al (1986) assumed that the temperature of the top surface of the coal bed was approximately ambient, which for a line heater gave acceptable results. However, the assumption of ambient surface temperature is, by definition, of no direct use in the study of boundary conditions and surface hot spots. This necessitates the use of boundary conditions dependent on the local surface temperature and temperature gradients, (Cauchy boundary conditions). The use of a Cauchy boundary condition for temperature at exposed surfaces of the bed is examined in this work.

Various reliable and corroborating estimates (including Young *et al's*) for effective coal-bed thermal conductivity are available (see Brooks 1986). Young *et al's* temperature data were used, but this time permeability and surface heat-transfer coefficient were estimated.

The two-dimensional conductive-convective model equations (see 2.3) were solved using a Galerkin finite element method with a graded mesh, (see Gresho & Lee 1981), using 4-noded bilinear elements, as well as 8-noded quadrilateral elements. Using the guideleines presented by Gresho and Lee, it was found that a 15x15 bilinear mesh, graded finer in the vicinity of the surface and the heater, adequately represented the solution (see Appendix C for a representation of the mesh). The parameters were estimated by minimising the sum-of-squared errors in predicted temperature at the thermistor positions. APPENDIX C contains a detailed description of the procedure used to solve the equations for a given set of parameters, as well as a representation of the finite element mesh used. Michelsen (1979) describes in detail the procedure used to find the best-fit set of parameters.

The resultant parameter estimates are listed in Table 5.1, along with their 90% confidence intervals (see Michelsen 1979).

Table 5.1 - Fitted Parameters - Rod Heater

Q'	h	h_{min}	h_{max}	K	K_{min}	K_{max}
$[W.m^{-1}]$	$[W.m^{-2}.K^{-1}]$			$[m^2 x\ 10^7]$		
15	6.8	2.9	11.5	1.5	1.3	1.8
20	6.9	2.7	15.7	1.4	1.2	1.6
30	8.9	2.9	15.8	1.9	1.8	2.2

It is clear from Table 5.1 that little confidence can be placed in the surface heat-transfer coefficients. Part of the reason for this is that surface temperatures were small, and heat-transfer at the surface was very much convection dominated.

The measurements of Benson-Armer & Leibowitz (unpublished) have been analysed as described above. The results are summarised below.

In analysing their results, a 15x15 mesh, similarly graded to that mentioned above, was used to solve the equations, this time using the cylindrical equations (see 2.3). Fig. 5.1.1 shows an idealised sketch of the arrangement of Benson-Armer and Leibowitz's experimental apparatus. The fitted parameters are summarised in Table 5.2.

Table 5.2 - Fitted Parameters - Cylindrical Heater

Q" [W]	h	h_{min} [$W.m^{-2}.K^{-1}$]	h_{max}	K	K_{min} [m^2x 10^7]	K_{max}	d_p [mm]
5	1.7	1.0	2.9	0	0	0	
7.5	0.8	0.5	1.4	0	0	0	< 5
10	1.6	1.0	2.6	0	0	0	
5	10.8	5.3	15.7	1.67	1.4	1.9	
10	9.6	5.0	15.4	1.43	1.1	1.5	10
18	8.3	4.8	15.1	1.31	1.1	1.4	
5	3.5	2.3	5.2	2.9	2.7	3.6	
7.5	4.0	1.9	7.1	2.7	2.6	3.1	20
10	3.1	1.3	5.5	2.3	2.2	2.7	

Fig. 5.1.2 shows contours of measured and best-fit temperature profiles in the bed, in the r-z plane, for a 10W source in a bed composed of particles nominally 20mm in diameter. Agreement between measured and calculated temperatures is acceptable, thus demonstrating that suitability of this type of model to the situation. Fig. 5.1.3 shows the streamlines of the velocity field corresponding to the temperature profile in Fig. 5.1.2. Fig. 5.1.4 shows an alternative comparison between experimental and calculated temperatures; experimental temperatures are plotted against calculated temperatures for each thermistor position. If temperatures were fitted exactly, all the points would lie on the 45 degree line (Texp=Tmod). The figure shows a distribution of points around the line, as expected.

Plots similar to Fig.'s 5.1.2 through 5.1.4 were viewed for each of the remaining estimation runs. There was little to distinguish them from those already plotted, aside from changes in scale, so they have not been included here.

Fig. 5.1.5 shows a plot of the sum of squared errors contours vs. Ra and Bi (equivalently K and h), for the cylindrical heater

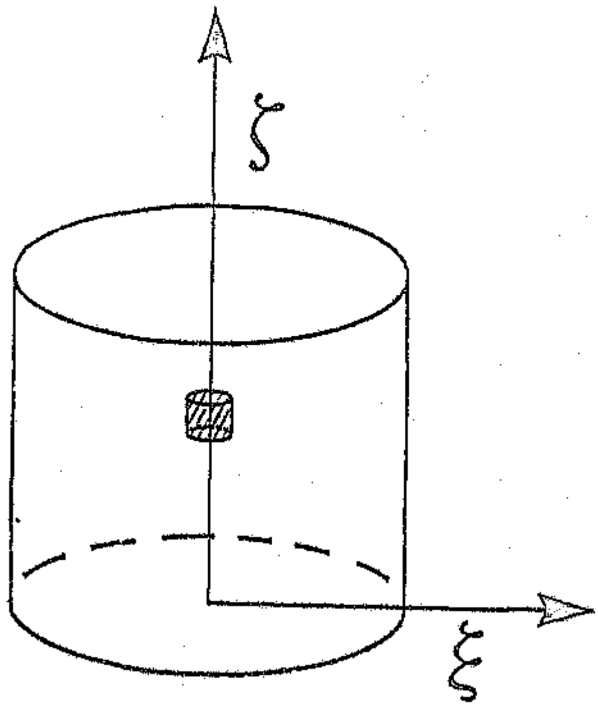

5.1.1 Sketch of idealised bed with cylindrical heater

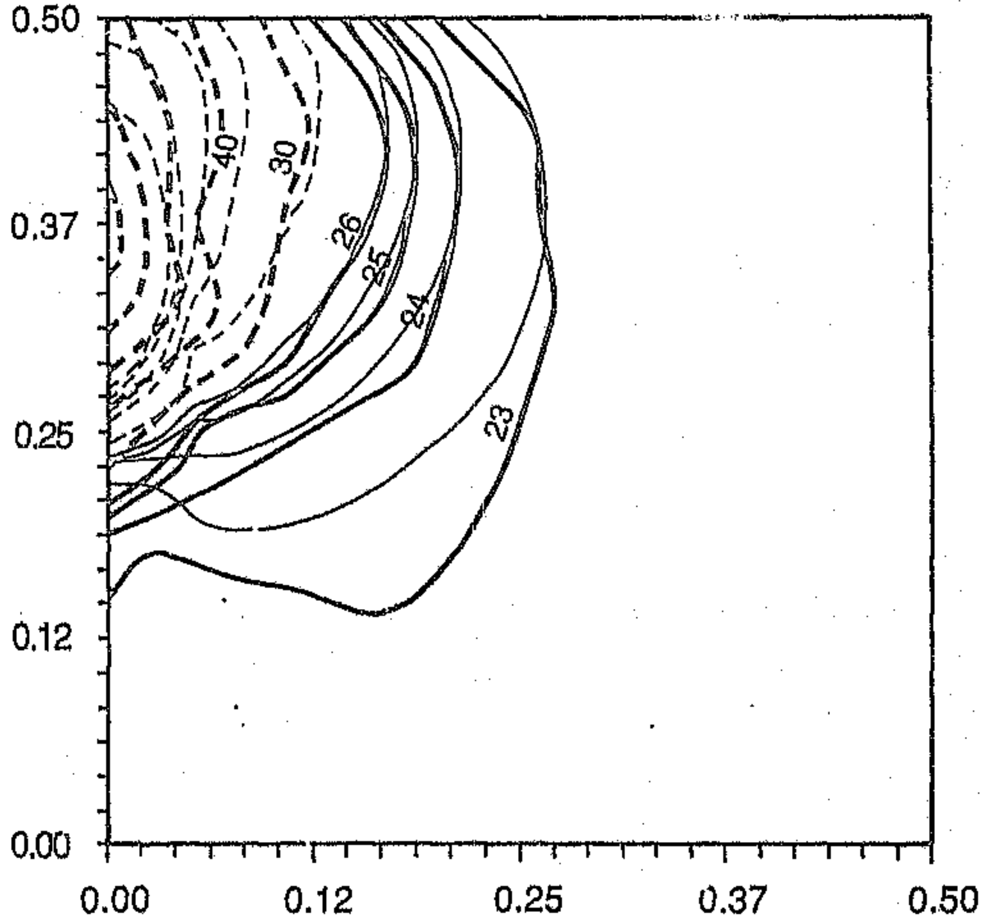

5.1.2 Plot of experimental and best-fit temperature contours (Q=10W, d_p=20mm). Contour intervals are 1°C for solid lines, and 10°C for broken lines. Bold=experimental, Faint=calculated

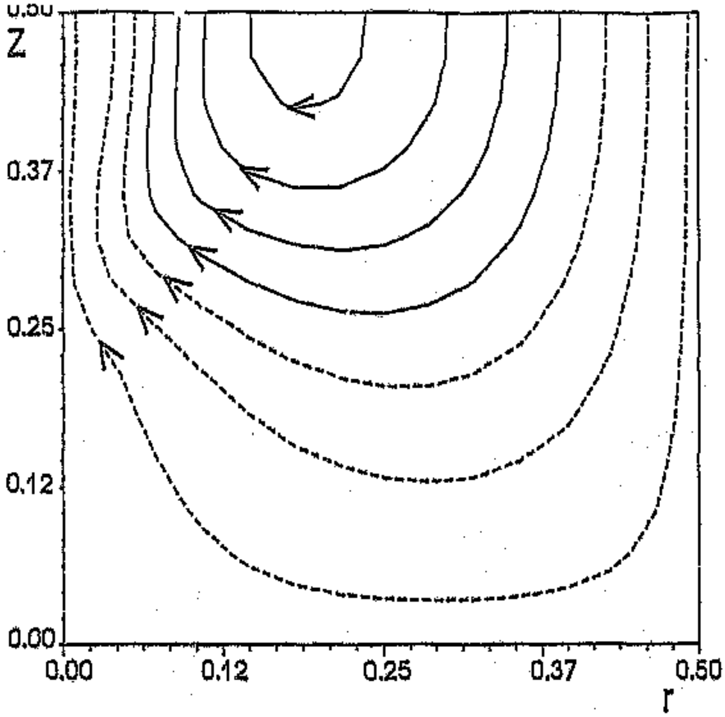

5.1.3 Plot of calculated streamlines (Q=10W, d_p=20mm)

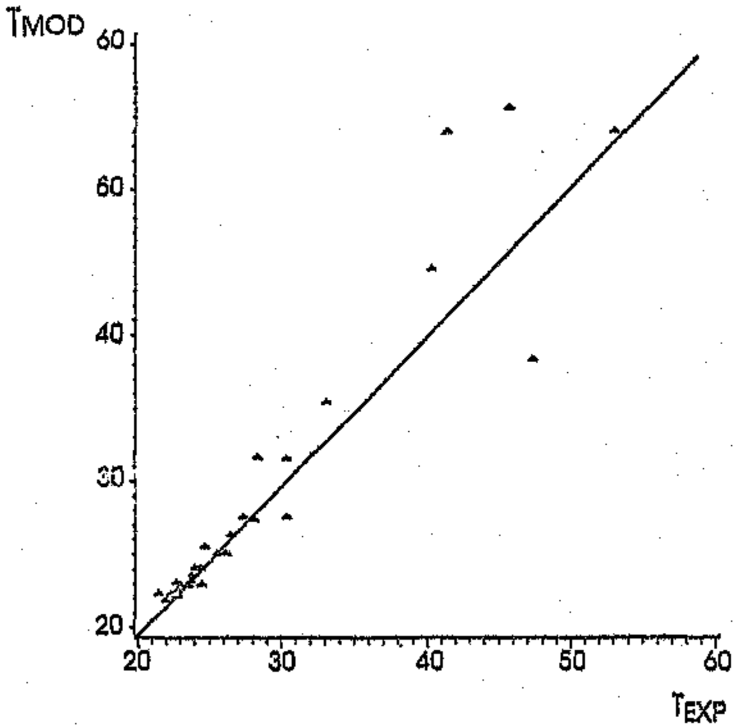

5.1.4 Alternative comparison of measured and calculated temperatures (Q=10W, d_p=10mm)

90% confidence interval is shaded

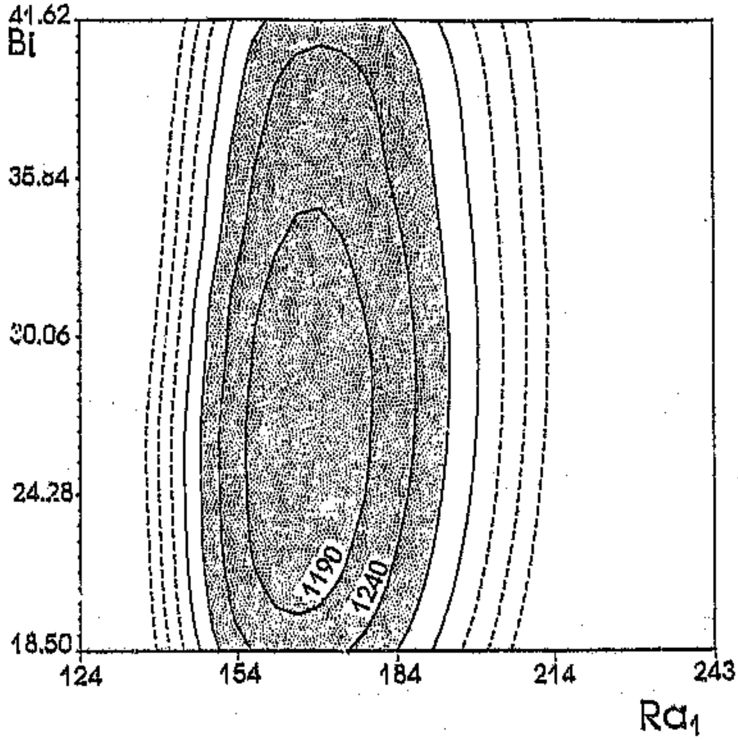

5.1.5 Plot of sum-of-squared errors contours ($Q=18W$, $d_p=10mm$)

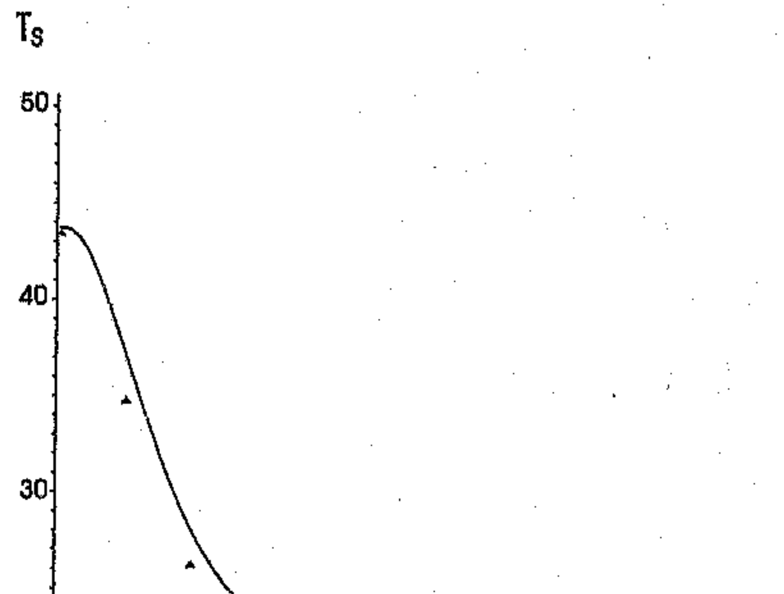

5.1.6 Plot of surface temperature ($Q=7.5W$, $d_p=20mm$)

(power ~ 18W, nominal particle diameter ~ 10mm). The contour shape for all of the remaining cases was the same, however, with variations in scale only, so no further contour plots have been included here.

Since the sum-of-squared errors contours are approximately ellipses with their major and minor axes aligned with the Rayleigh and Biot number axes, it may be concluded that there is little covariance between these parameters.

It can be seen by comparing Tables 5.1 and 5.2 that there is reasonable agreement between permeability estimated for beds of 10mm particles for the different heater types. Furthermore, the confidence intervals for heat transfer coefficients in Table 5.2 are a little better than those in Table 5.1. The variations are still too large, however. The reason for this is that the permeability variable is very influential in comparison to heat-transfer coefficient, that is, a small variation in permeability affects the prediction considerably more than an equivalent change in the heat-transfer coefficient.

Since the beds (listed in Table 5.2) were not disturbed between runs using different powers, the permeabilities should be identical; ideally one permeability only should be fitted for each bed type, allowing only Biot number to vary for the different power inputs. Such an approach was found to be highly inconvenient, so individual permeabilities were fitted for each run; the variation in permeability obtained for a single bed ($1.3 - 1.7\times10^{-7}$ m^2 for 10mm particles and $2.3 - 2.9\times10^{-7}$ m^2 was for 20mm particles) deemed acceptable. Note that since the particle sizes quoted are nominal, it is quite acceptable that permeability of the bed comprised of 20mm particles is not four times larger than that of the bed comprised of 10mm particles, as would be predicted by the Ergun-derived relation in 2.1.

An attempt was made to solve the problem of obtaining reliable estimates for heat-transfer coefficient by assigning a single, (constant) average permeability to each bed-type and re-estimating the heat-transfer coefficient only, using the methods described above. These results are summarised in Tables 5.3 and 5.4.

Table 5.3 - Fitted Heat Transfer Coefficients - Rod Heater

Q'	h	h_{min}	h_{max}	K	d_p
$[W.m^{-1}]$	$[W.m^{-2}.K^{-1}]$			$[m^2 x\ 10^7]$	[mm]
15	6.8	2.9	11.5		
20	6.9	2.7	15.7	1.6	10
30	8.9	2.9	15.8		

Table 5.4 - Fitted Heat Transfer Coefficients - Cylindrical Heater

Q	h	h_{min}	h_{max}	K	d_p
[W]	$[W.m^{-2}.K^{-1}]$			$[m^2 x\ 10^7]$	[mm]
5	1.48	0.99	1.97		
7.5	0.74	0.49	1.15	0	< 5
10	0.33	0.13	0.66		
5	10.78	6.74	16.17		
10	11.04	6.36	15.72	1.468	10
18	10.89	6.85	14.94		
5	4.02	2.31	5.53		
7.5	5.25	3.35	6.82	2.63	20
10	4.57	3.31	6.32		

Two further attempts were made to improve confidence in estimated parameters: firstly, variation of surface heat transfer coefficient with surface temperature was allowed, in two forms. The first form followed the well known result for convection from flat horizontal plates, where film coefficient varies according to the one-fourth power of the temperature difference between surface and ambient temperatures. The second form allowed for a different contribution depending on whether air was entering or leaving the bed. Neither of these models showed any discernable difference in the calculated results, fitted Rayleigh number or surface heat transfer coefficient. Further, following the methods used by Horne & O'Sullivan (1978), temperature dependence on viscosity and density of the air (i.e. not making use of Boussinesq's assumption) were allowed for. This measure did not result in better confidence levels in estimated parameters, possibly due to experimental design or measurement inaccuracy; these results are therefore not included here.

Secondly, all of the parameters were re-estimated to determine what effect (if any) would result from allowing the heater to be solid (note that the parameters reported above were estimated using a model that assumed the heater to be porous. Fig. 5.1.7 shows the streamlines calculated assuming a solid heater. A porous heater would most accurately represent the case of a combusting stockpile, but no noticeable difference in the calculated results or parameters could be detected. This is shown clearly in Fig. 5.1.8, which compares calculated surface temperatures for a porous heater and a solid heater. There is clearly little to be gained by rigorously representing the heater as solid.

It may be concluded that heat transfer in porous media may be adequately modelled using conductive-convective equations, with permeability and surface heat-transfer coefficients as parameters. Furthermore, the parameters estimated above may be used with fair confidence in situations not far removed from the laboratory conditions, particularly since it was shown that the presence of the solid heater makes no noticable difference to the model results.

5.1.2 Development of a simplified one-dimensional model

When attempting predictive modelling of coal stockpiles the rate of combustion (if any) is not known, and a simple model such as that applied above, is of little use, and is furthermore exceptionally expensive to solve for beds of any appreciable size. Also, the actual temperature and flow profile in the bed are of little direct use in assessing combustion hazards. Ideally, one would like a model which allows reasonable prediction of energy dissipation from simple and accessible (therefore restricted to the surface) measurements. This was the motivating factor in the development of a simplified model for estimation of energy dissipation from readily accessible measurements.

Examination of the contours in the region z=1 in Fig. 5.1.2 shows that surface temperatures are adequately represented by the conductive-convective model. Fig. 5.1.6 shows this more clearly on a T-r plot at the surface. Prompted by the above observation, an attempt was made to estimate power input from measured surface temperatures alone. After fixing surface heat-transfer coefficients and permeability as originally estimated (see Tables 5.1 and 5.2), the source power which minimised the sum-of-squared temperature prediction errors *on the surface only* (internal temperatures were not fitted) was calculated.

Note that in these calculations the position of the source was not varied, and was assumed to be the same as in the experiments. The results of these early attempts are not reported here since they are of no constructive use. In all cases, however, a close fit to the surface temperature was obtained, and the predicted power input in every case was within 10% of what was actually used in the experiments, demonstrating that surface temperature may be used as an indicator of the energy input to the bed. This concept is clearly applicable to solid bodies, and is easy to justify in the absence of convection currents through the body itself.

Encouraged by these numerical experiments, development of a simplified one-dimensional model was undertaken. The model was developed to investigate the variation of surface temperature with surface heat-transfer coefficient and energy input.

The system modelled consists of a horizontal porous layer, heated along the bottom surface by a porous heater (see Fig. 5.1.9 for a schematic sketch of the system). Note that the layer does *not* rest on an impermeable support, as in Lapwood (1948) or various other similar studies. Using the Boussinesq

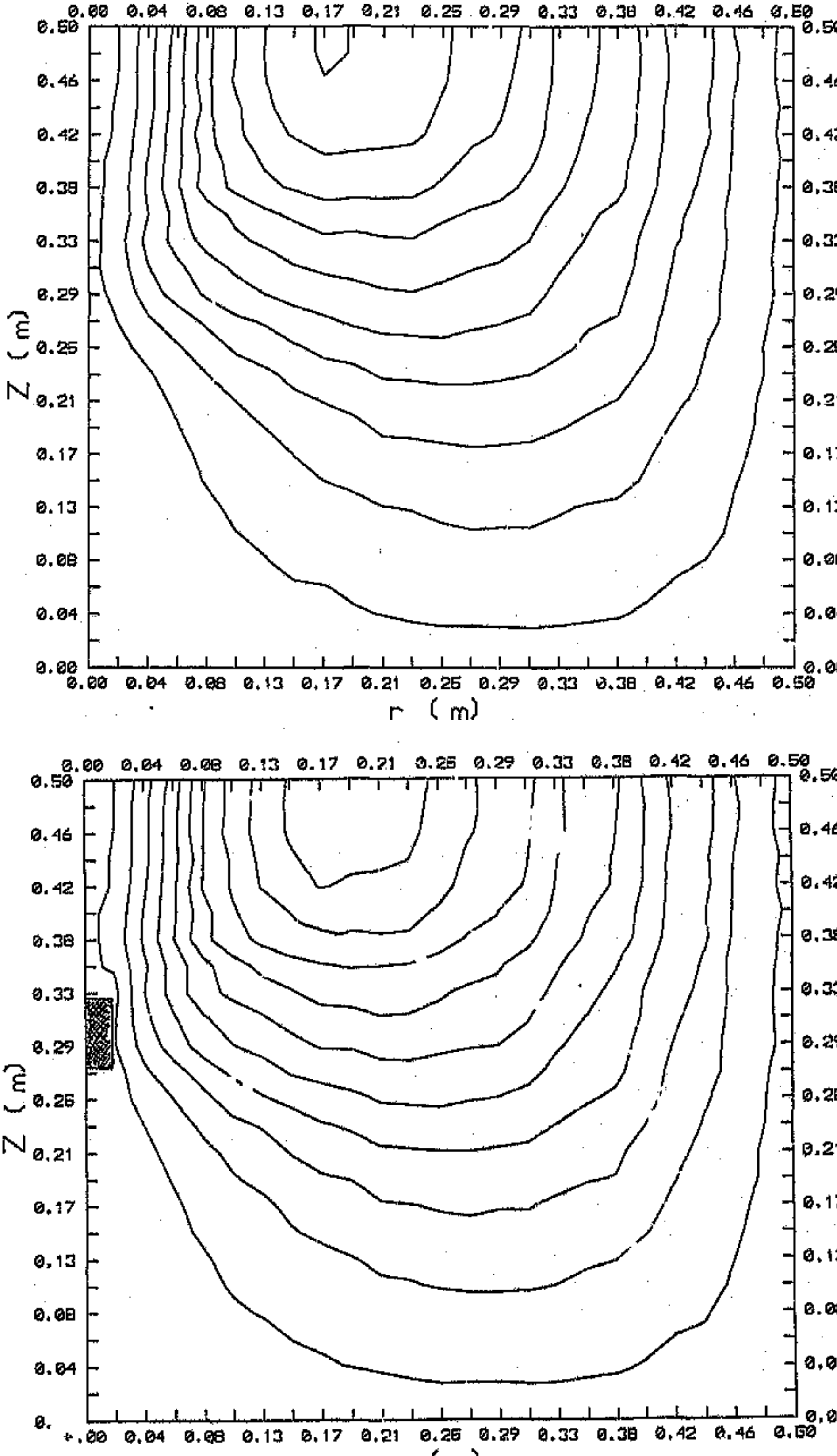

5.1.7 Plot of streamlines showing effect of solid heater (Q=10W, d_p=20mm)

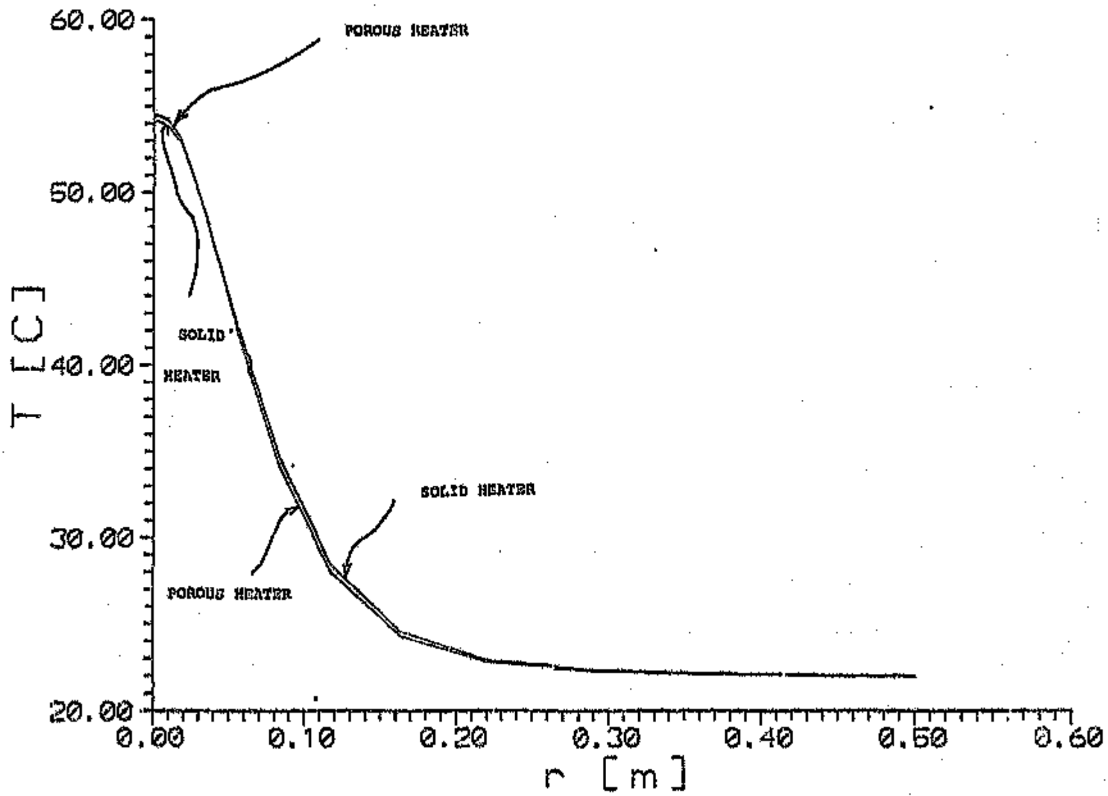

5.1.8 Comparison of calculated surface temperature profiles for porous and solid heater

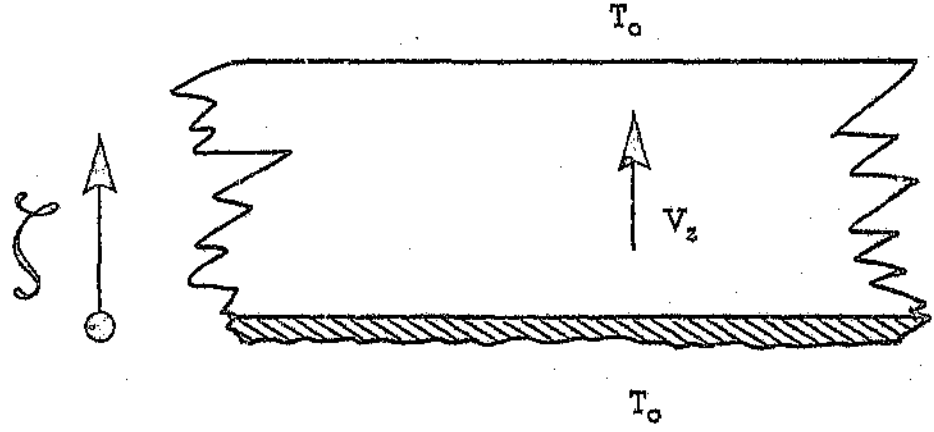

5.1.7 Sketch of theoretical one-dimensional layer

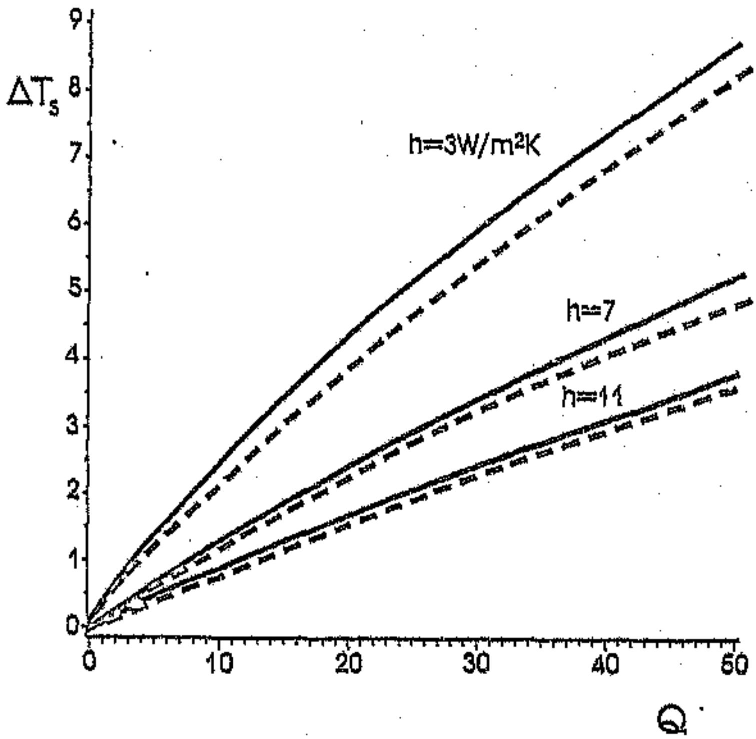

5.1.8 Variation of energy dissipation with surface temperature difference and heat transfer coeffcient assumption, the Darcy law, and the equation of continuity, the following expressions are obtained for temperature and velocity of convection in the layer (see Appendix C for derivation):

$$v_z^* = \frac{KgL\rho_o}{\mu\alpha}\left[1 - \int_0^1 \frac{d\zeta}{1 + \theta(\zeta, v_z^*, q, Bi)}\right] \tag{5.1}$$

where

$$\theta(\zeta, v_z^*, q, Bi) = \frac{q}{v_z^*}\left[1 - \frac{Bi}{v_z^* + Bi}\exp\left(v_z^*(\zeta - 1)\right)\right] \tag{5.2}$$

The temperature and velocity in the layer, as expected, are interdependent on each other. For given physical properties and energy input per unit area, q, v_z^* must be calculated by solving equation 5.1, which is clearly transcendental in v_z^*. Solution is only possible if done numerically, and a FORTRAN 77 program called 'LAYER' (see Appendix C) was written to achieve this. Fig. 5.1.10 shows the variation of the surface temperature (ζ=1) with q and Ra_l ($KgL\rho_o/(\mu\alpha)$).

A most interesting feature of Fig. 5.1.10 is that despite the variation of Ra_l over two decades (40 to 4000), very little variation in the surface temperature difference appears (for a given heat-transfer coefficient). The surface temperature difference may therefore be taken to depend only on energy input per unit area, q, and surface heat-transfer coefficient h. Since Ra_l between 40 and 4000 covers most situations of practical interest, and since that parameter includes both the vertical length scale and the permeability, it is possible to calculate the energy input to the layer knowing only the surface temperature and surface heat-transfer coefficient. Surface temperature of a coal stockpile is relatively easy to measure, thus leaving only the surface heat-transfer coefficient to be determined. This need for a reliable surface heat-transfer coefficient was a major factor motivating the research on that parameter, discussed above.

This result is applied to practical situations as follows:

The temperature is measured at an adequate number of points on the surface of the medium. In the case of coal stockpiles, this may be done by aerial thermography. The energy input per unit area is calculated using the above method and the measured surface temperatures, and these contributions are summed or integrated over the surface of the medium.

$$\int_S q\left[\Delta T_s(\underline{x})\right] dS \qquad (5.3)$$

Where S is the exposed surface, and vector x is position on S. Q then is the total energy being dissipated in the bed. The applicability of the model has been tested, as discussed below, and found to be adequate for the intended purpose.

Test of the one-dimensional model

For each set of measured experimental results the power dissipation was estimated as shown above. For the cylindrical heater eqn.(5.3) takes the following form:

$$Q = 2\pi\int_0^{0.5} rq\left[\Delta T_s(r)\right]dr \qquad (5.4)$$

In doing these calculations three separate values of h(3.0, 7.0 and 11.0 $W.m^{-2}.\ K^{-1}$ were used. The results are presented in Table 5.5 below.

Table 5.5ℓ- Energy Estimated from Measured Surface Temperatures

Q input	Q [W] estimated	h $[W.m^{-2}.K^{-1}]$	d_p [m]	H_q [m]
	5.5	3.0		
5.0	11.0	7.0	0.005	0.3
	16.5	11.0		
	11.2	3.0		
7.5	21.6	7.0	0.005	0.3
	31.6	11.0		
	9.9	3.0		
10.0	18.9	7.0	0.005	0.3
	27.5	11.0		
	2.8	3.0		
5.0	5.6	7.0	0.01	0.3
	8.6	11.0		
	5.9	3.0		
10.0	11.0	7.0	0.01	0.3
	15.6	11.0		
	13.3	3.0		
18.0	23.8	7.0	0.01	0.3
	32.4	11.0		
	3.2	3.0		
5.0	6.2	7.0	0.02	0.3
	9.5	11.0		
	4.4	3.0		
7.5	8.4	7.0	0.02	0.3
	12.4	11.0		
	4.7	3.0		
10.0	8.7	7.0	0.02	0.3
	12.2	11.0		

Clearly, if a reliable heat-transfer coefficient is used when applying the simplified model, the accuracy of the estimated power input is quite acceptable, and the model is suitable for application as suggested.

Since independent data on power input and surface temperatures of porous media are extremely scarce, it was necessary to simulate additional results with which the model could be further tested. Surface temperatures on a large, cylindrically symmetrical bed were therefore simulated using the conductive-convective model discussed above. This is justified since it has been clearly demonstrated in this chapter and other publications that temperatures in porous media are adequately modelled by such an approach.

The bed simulated had a radius of 10m and a height of 10m, and was composed of 10mm particles. The power source had both radius and height equal to 1.1m, and was located in various positions. The power input was also varied; a surface heat-transfer coefficient of 11 $W.m^{-2}.K^{-1}$ was used for all of the simulations. The purpose of these simulations was to obtain surface temperatures for large beds, with sources of varying size, so that the effects of these changes (if any) on the estimates could be examined. The power input to the simulated bed was estimated using equation (5.4); the results of this are shown in Table 5.6.

Table 5.6 - Energy Estimated from Simulated Temperatures

	Q [W]	h [$W.m^{-2}.K^{-1}$]	d_p [m]	H_q [m]
5.0	6.3	11.0		
50.0	53.5	11.0	0.01	6.1
500.0	507.6	11.0		
5.0	6.9	11.0	0.01	8.3
500.0	534.5	11.0		
5.0	4.8	11.0	0.01	2.8
50.0	50.4	11.0		

From the results in Table 5.6 it can be seen that the position and size of the source are also not important in estimating the power input from the surface temperatures and so we may conclude that this simplified model over the range of parameter values used, which is reasonable for coal stockpiles, is a useful one for monitoring spontaneous combustion.

The only major discrepancy could be caused by having an incorrect value of the surface heat transfer coefficient. Since in most cases measured surface temperatures are compared to those taken at an earlier time, the actual value of h is not too critical. Furthermore, values of h for different coal stockpiles are not likely to vary significantly, so that comparison between different piles should also be valid. Finally, once a body of measurements has been built up, including occasions where burning has actually occurred, one should be able to more readily interpret such results.

Discussion

Real coal stockpiles and waste dumps tend to be very large and inhomogeneous and the task of modelling the dumps is well nigh impossible. If one could have a simple overall estimate of energy dissipation this could be very valua le for two reasons.

One would like to have such a measure of energy dissipation for burning dumps in order to try to estimate the amount of pollution such as sulphur dioxide being discharged into the atmosphere. If one knew the energy dissipation rate one could reasonably estimate the burning rate using a known heat of reaction and hence through the known concentration of the material in the coal, the pollutant discharge rate.

Furthermore one would also like to be able to use the result to decide when spontaneous combustion in a dump or stockpile is becoming a problem so that the necessary preventitive action, such as "digging the hot spot out", could be taken. It is expensive and difficult to do this "digging out", and one would like to be sure there was a real problem before taking such action; on the other hand if one waits too long and the material is too hot, exposing it to the atmosphere is dangerous and the ensuing fire difficult to extinguish.

For monitoring of large dumps the only really feasible approach is to use infra-red thermography preferably done from a helicopter. Only in this way is it really possible to identify "temperature anomalies" in the surface temperatures at some points relative to the rest of the surface.

Experience has shown that it is essential to do such surveys under some sort of "standard conditions" in order to interpret the results. It is most convenient to do these surveys on a cloudless still night just before dawn. This is often done at full moon in order to ease the navigation problems involved.

In order to turn these surface temperature measurements into some sort of quantitative measure of the energy dissipation rate, it is clear one needs an estimate of the surface heat transfer coefficient. It is also clear from the analysis in the previous section that the result is fairly sensitive to the value of this parameter. Thus to effectively use this simple model it is necessary to obtain some value for this quantity and preferably know how or if the value changes with the weather conditions.

The value of the heat transfer coefficient used by Brooks and Glasser (1986) in their calculations was one estimated by assuming the main mechanism for heat loss from the surface (other than that removed by the flowing gas) was radiation. In this case assuming black body radiation to ambient temperature the value of the heat transfer coefficient one can calculate is about 6 $W.m.^{-2}k^{-1}$ which is entirely consistent with the estimated values in Table 5.5, but does not show the variations for the different particle sizes.

Brooks [18] in some experiments on an insulated coal bed open at both ends, found that his temperature-time results on both cooling and reaction runs could be fitted using heat transfer coefficients at the bottom and top of the bed with values of 3.7 $W.m^{-2}. K^{-1}$ and 9.3 $W.m^{-2}. K^{-1}$ respectively.

As seen from the values in Tables 5.3 and 5.4 there is not a consistent variation of heat transfer coefficients with particle size, though the values for each particle size do not appear to vary with power input. Of course different coals have very different surfaces ranging from bright shiny to dull matte and it could be expected, certainly, if radiation is important, that this alone would give rise to a range of values.

The problem is made worse by diurnal temperature variations being superimposed on the surface of the dump. However as it is the difference between the "anomaly" and the rest of the surface that is being measured this effect is not as large as one might at first think. Obviously rain can also have a major effect on surface temperatures and wind has the dual effect of changing the surface heat transfer coefficient as well as forcing air through the dump, and so possibly changing the oxidation rate.

All one can say is that the larger the energy dissipation rate, the smaller the problems caused by these other effects, thus in these surveys one is looking for consistent patterns. It has often been observed when one is doing the measurement just before dawn that at such an "anomaly" one first sees a "surface cold spot" which is later followed at the same or a neighbouring place by the "surface hot spot". It would appear that this is caused by the cool air moving into the dump having a larger effect on surface temperatures in the early stages of self-heating, than the hot air leaving it. This situation then rapidly changes over to a hot-spot which then exhibits ever increasing surface temperatures.

In practice dumps of different particle sizes show very different types of "surface" anomalies. One can use this model to combine all the information into a single useful criterion by which one can decide when further confirmatory action is needed. This action usually takes the form of sending a person to the suspect area and knocking a temperature and oxygen probe a metre or two into the material, to confirm if there is a real problem.

In the case of burning dumps again the manner of burning is very differant for material of different particle sizes. For larger particles burning tends to take place much deeper in the dump and to be spread over a larger area than for smaller particles, where burning is often in the toe of the dump. Again the criterion can be used in combining all the results into a single measure of the burning or energy dissipation rate.

From this discussion it is clear that a theory describing variation of surface heat-transfer coefficient with convection rate, surface characteristics, energy dissipation etc. would be most useful in developing and maintaining a database of surface heat transfer coefficients which may be expected in such situations. Such a theory has been developed by Glasser, Williams, Brooks, Burch and Humphries (1990) The predictive surface-temperature model, together with the heat-transfer coefficient theory, provides a simple and reliable method for monitoring and grading combustion hazards in the field.

Because of the insensitivity to other parameters (depth, permeability, etc.) the surface temperature theory discussed above provides a basis for comparison between a wide variety of situations with differing surface temperature patterns, even in the absence of a heat-transfer coefficient model. As a result of this it should prove possible in the future for the whole process of monitoring and protecting dumps and stockpiles to be done on a much more scientific basis.

In reality of course the heat source is not a heater but a section of the coal oxidizing (undergoing a chemical reaction). This fact should in no way significantly alter the conclusion as the flow and heat transfer mechanisms will be relatively unaffected by the chemical reaction. Furthermore if all the oxygen is adsorbed the molar flow rate of the air will only be reduced by 20%. Conversely if all the oxygen is turned into carbon monoxide the molar flow-rate will be increased by 20% while if it is all turned to carbon dioxide the flow rate will remain unchanged with only a change in the mean molecular weight of the gas. All of these effects are essentially negligible relative to the purposes to which the model is intended to be used. Thus one can see that the model is directly applicable to self-heating situations in real stockpiles of coal.

5.2 Modelling Transient Momentum Transfer in Porous Media

Steady-state momentum transfer experiments may be used to determine the *effective* permeability of a bed by using equation (1.1), in much the same way as effective thermal conductivity of a solid body is determined by measuring energy flux and temperature gradient (Flumerfelt & Slattery 1969).

Such effective values are of little use under conditions different to those of the experiment, particularly if unsteady behaviour is being investigated, where certain inhomogeneities may play no role at all (such as a layer of material located at depths to which cyclic surface-disturbances do not reach) Furthermore, in the case where the porous body is not contained by well-defined, impermeable walls, steady flow methods are difficult if not impossible to apply, for the simple reason that there is either no defined end-point at which to measure any variable, or any such 'endpoint' is totally inaccessible.

Furthermore, if estimates of conductivity or permeability of materials are required under circumstances which would not allow extraction of a sample, or where such extraction/sampling were either impossible or self-defeating, the steady-state measurement technique would be completely unsuitable. For example, it is impossible to sample a nonhomogeneous body of loose particles in its natural form, and therefore the steady-flow method of permeability or thermal conductivity measurement is extremely difficult to apply.

Such circumstances call for a method which does not rely on the dimensions of the 'container', such as seismology ultra-sound imaging. All such techniques rely on the analysis of reflections of disturbances imposed on the 'system'. A common feature of the abovementioned examples is that the disturbance (seismic explosion or ultrasonic vibration) must be reflected to a degree by the entities which are to be probed. Hence, the signal energies and frequencies used for ultrasonic imaging depend on whether one is testing for defects in materials, or whether one is scanning a human to monitor the progress of an unborn infant. The energy used to scan a metal component for defects would pass straight through a human body, or cause considerable damage and pain at any rate.

In summary then, a measurement technique applicable to uncontained porous bodies of arbitrary geometry must possess the following characteristics:

- the points of disturbance and measurement must be readily accessible, preferably at the same point

- the disturbance signal must be adequately 'reflected'

- the technique must not require the porous body to be contained within walls of any sort.

Since permeability and voidage are properties of porous media which primarily affect flowrate/pressure distributions, it would make most sense if flow and pressure were used to probe porous media, using principles which parallel seismology and ultrasound techniques.

The development of a measurement technique which avoids the problems associated with steady-state methods and does not require the porous body to be contained, is discussed and applied below.

5.2.1 Development of a surface-based method for characterising porous media

A method of permeability measurement has been devised which has similarities to seismic probing of the earth's crust, and to general frequency testing methods used in engineering, particularly in the fields of process control theory (Luyben,1982) and reactor analysis (Levenspiel, 1972). The method proposed is summarised below:

If one were to force a cyclic flow of fluid into a porous body from a free surface (for example by mounting a reciprocating compressor on the bed), it would be expected that the pressure variation within the bed would depend on the internal structure of the bed, at least to the extent that the flow penetrated. By increasin the frequency of the flowrate cycle, one would expect that varying portions of the bed would exert influence on the flow, by means of resistance to flow (permeability) and capacitance for retaining the fluid in interstitial spaces (voidage). By analysing the differences between the pressure history measured at various frequencies, one could in principle deduce the internal structure of the bed.

Although the basic principle of this frequency-response method is very common, as referenced above, the author could find no evidence of this particular type of application in the literature. One study that bears some small resemblance is that of Nemeth and Virag (1989), who modelled the equalisation of gas pressures in packed beds. The major difference between that study and this is that Nemeth and Virag assumed the pressure at the surface of the bed to be an 'a priori' known function, and that they used step changes in this surface pressure; furthermore, the study did not address the effects of inhomogeneity on the pressure history.

It is thus believed that this method of probing porous media by imposing only surface disturbances is novel and well worth investigating.

Although the idea is applicable (in theory at any rate) to a general inhomogeneity, it is conceptually and mathematically simpler to allow inhomogeneity only in the direction normal to flow, i.e. in the case of infinitely large surface for flow, inhomogeneity is allowed only in planar layers, normal to the direction of flow, and for a point- or sphere-shaped surface, only spherically- (or hemispherically-) symmetrical layers of inhomogeneity are allowed. The assumption of planar flow clearly does not apply to the situation where a compressor is mounted on the surface of a bed, since the flow pattern would tend to be largely spherical; furthermore, the majority of the flow would tend to reverse, and leave the bed in an annular region close to the circumference of the compressor 'mouth'.

Although it greatly simplifies modelling of the situation, restricting flow and inhomogeneity to a planar configuration prevents direct application to practical situations. Such simplifications do however allow for primary verification and demonstration of the method.

The modelling of such a system is conceptually simple (within the limits of available phenomenological laws describing flow in porous media), and the derivations of models which use Darcy's law to relate pressure gradient and flow are detailed in Appendix D. The most rigorous model allows for spherical geometry and compressibility of the fluid, and spherical inhomogeneity; the simplest model allows for planar, incompressible flow in homogeneous bodies only.

The equations describing the pressure within a porous body, for planar, compressible flow, are reproduced here for convenience.

$$\frac{\partial}{\partial x}\left(KP\,\frac{\partial P}{\partial x}\right) = \epsilon\mu\,\frac{\partial P}{\partial t} \qquad (5.5)$$

$$P(x,0) = P_{amb} \quad (5.6) \qquad\qquad \left.\frac{\partial P}{\partial x}\right|_{x=L} = 0 \quad (5.7)$$

$$P_c(t) = \frac{P_c(0)V_c(0) - \int_0^L \epsilon A\left[P(x,t) - P(x,0)\right]dx}{V_c(t)} \qquad (5.8)$$

where P_c is the pressure inside the reciprocating device which is used to impose the pressure fluctuation. By definition, this is also $P(x=0,t)$ [Pa]

V_c is the (sinusoidally) varying volume of the reciprocating device [m^3]

L is the depth of the porous body [m]

x is distance, measured in the direction of flow [m]

ϵ is voidage [-]

P_{amb} is the ambient pressure [Pa]

A is the area of the one-dimensional bed measured normal to the flow [m^2]

Some important features of the above equations are:

- K appears inside the brackets on the left hand side of equation (5.5), (see Appendix D for derivation), resulting in a nonlinear equation for cases where K is not constant. It is primarily this term which influences the pressure gradient in nonhomogeneous bodies, as will presently be seen.

- Note that although void fraction of the medium (ϵ) directly affects the permeability K, the term ϵ appears in the coefficient of the time derivative as well as the boundary condition (5.8), in its own right. This means that porous media with equal permeabilities but different voidage characteristics will have different amplitude-frequency characteristics, as demonstrated below.

- The boundary condition (5.8) contains the volume integral of the pressure within the body; as a result, the solution of this set of equations is not a simple task. Nemeth and Virag (1989) use a Newton method to solve their somewhat simpler equations, but the author is not aware of a simple technique for the solution of the equations listed above, especially in the case of varying K (and more particularly discontinuous K, as in the case of layered beds, or strata).

A numerical method of solution has been used, for the reasons discussed above. A FORTRAN 77 program using Nag routine D03PGF (1982) as the core PDE solver was written. The complex boundary condition (5.8) and supporting code was developed by the author, and a printout of the program is presented in Appendix D.

5.2.2 Application of the model

5.2.2.1 Trends in pressure 'measured' at x=0

The scenario discussed in 5.2.1 above was modelled using the method described in Appendix D, for a range of pulsation frequencies. Table 5.7 summarises the model parameters used. Note that a permeability ratio of 9 is caused by a particle diameter ratio of only 3 (all else being equal); such a ratio in particle diameters is not difficult to imagine or encounter. The location of the interface between the more permeable material (upper region) and the less permeable material (lower region) was varied from 0.2L to L in steps of 0.2L. See Fig. 5.2.1 for a schematic representation of the composite bed. The maximum pressure at the surface was determined for each frequency, and these figures plotted against each other. The procedure was repeated for each of the interface positions.

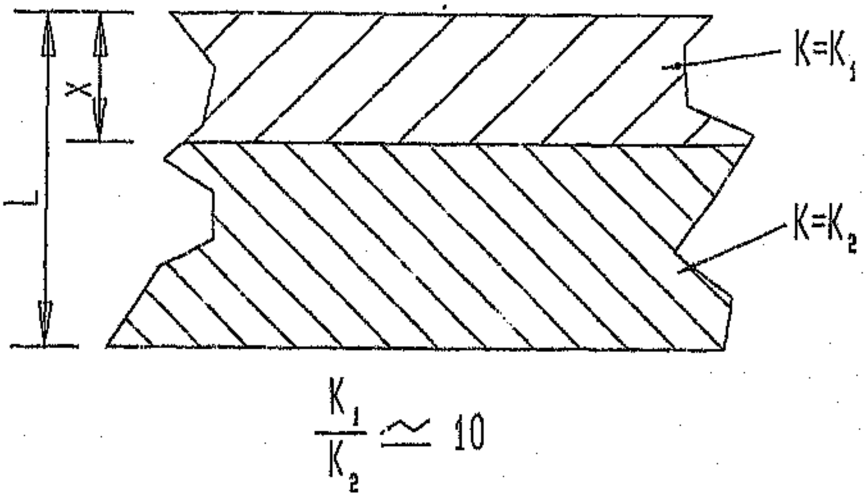

5.2.1 Schematic sketch of layered bed

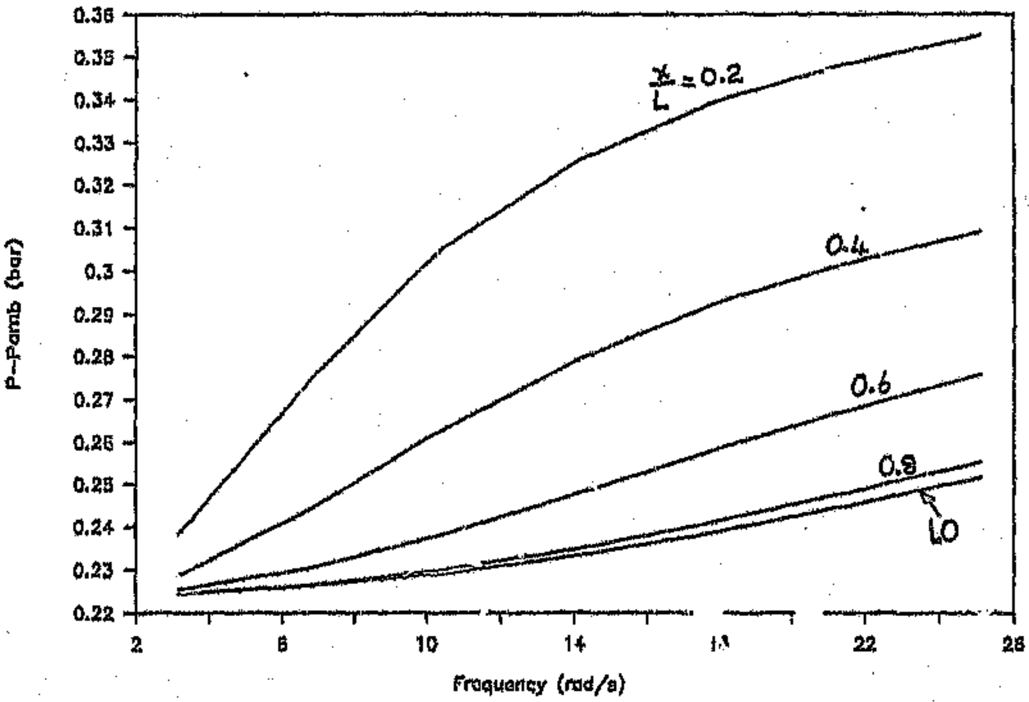

5.2.2 Plot of pressure amplitude offset vs. frequency

Table 5.7 - Base Case Parameters for Pneumatic Test Simulations

ϵ	(-)	0.42
d_p	(mm)	0.4/0.12
φ_s	(-)	0.6
V_o	(m^3)	5.0
ΔV	(m^3)	0.002
L	(m)	0.45
A	(m^2)	0.031

$\Rightarrow K = 4 \times 10^{-11}\ m^2$ or $4 \times 10^{-12}\ m^2$

c.f. measured permeabilities, see section 4.1.1

Fig. 5.2.2 shows the plots of amplitude vs. frequency for the five different bed compositions, superimposed on one graph. As expected, in the limit of low frequency, where neither section of the bed presents any appreciable resistance to flow, the pressure measured at the surface does not depend on bed composition.

Note: Numerical modelling of such a system at very low frequency is difficult and prone to numerical instability due to very small pressure gradients, as well as computationally expensive. Model results therefore begin at a frequency of approximately 2 radians per second.

A further measure which may be informative here is the relation between the maximum pressure measured at the surface of the bed and the position in which the piston is at that time. For a totally impermeable bed, the maximum pressure will coincide with bottom- dead-centre of the piston, and likewise for an infinitely permeable bed. However, for a finite permeability, the retarding effect of the bed on the flows would alter this, and therefore investigation of the 'lag' is considered worthwile. For instance, experiments conducted using orifice plates as (lumped) resistance to flow (see Chapter 4) show that time lag increases as resistance to flow increases, and that this effect diminishes as frequency increases.

Definition: 'Lag' here is defined as the (angular or time) difference between the occurrence of maximum pressure and bottom- dead centre of the piston.

Fig. 5.2.3 shows variation in time lag with frequency, for the parameters listed in Table 5.7. The character of these results is in general agreement with measured lags (see Chapter 4), but no quantitative conclusions can be made without further work, both experimental and theoretical. In any case, the behaviour of lag with frequency is as expected: a more permeable, homogeneous bed (curve a) experiences a smaller lag than a bed whose bottom 80% (curve e) is one tenth as permeable as the former bed. Further work on this aspect is required if quantitative results are to be obtained.

5.2.2.2 Trends in pressure profile within the bed

It can be seen in Fig. 5.2.2 that the amplitude measured at $x=0$ increases faster for beds in which the less permeable layer occurs nearer to the surface. The reason for this is that as frequency increases, larger velocities (and therefore larger pressure gradients) are caused in the bed. Flows in the lower, less permeable layer of the bed are retarded, to the extent where increasing portions of the lower, less permeable region experience smaller and smaller deviations from ambient pressure. As smaller regions of the bed become 'available' to accomodate compression taking place in the piston, pressure must increase accordingly. The presence of larger and larger portions of less permeable material in the bed amplifies this effect, hence the behaviour of the curves in Fig. 5.2.2.

When varying the bed composition, one would expect to see evidence of the 'availability' (discussed above) in the pressure profiles. This is indeed the case, as shown in Fig. 5.2.4, which compares the pressure profiles for the various layered beds, for the same parameters as Table 5.7, except that $\Delta V=0.0045m^3$ (demonstrating that small pressure variations, and hence gradients, still show adequate resolution). The point in time

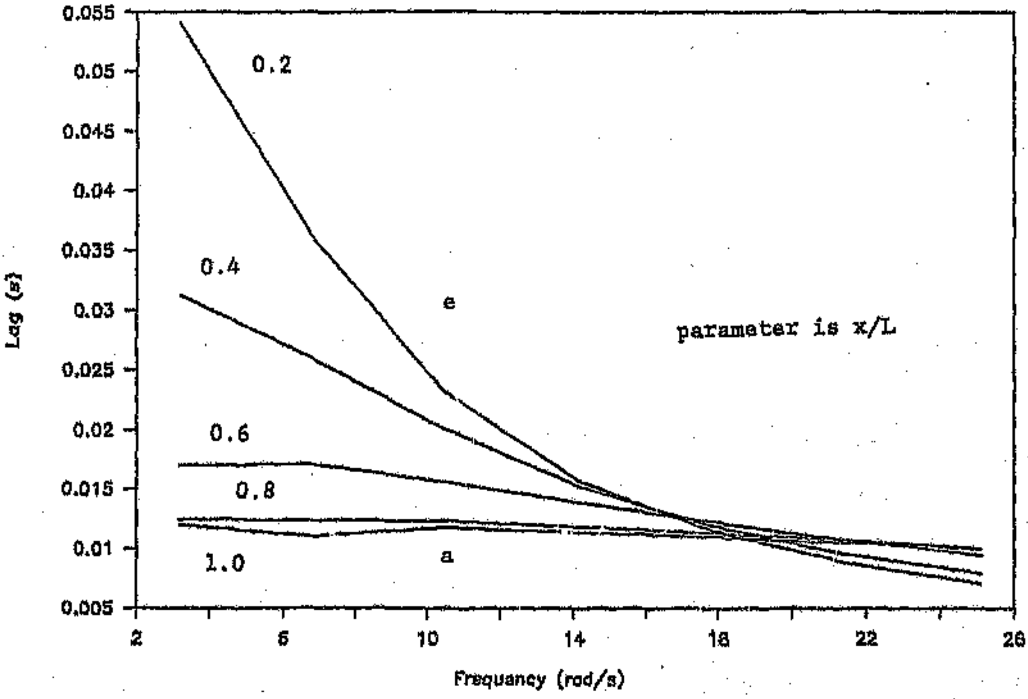

5.2.3 Plot of lag vs. frequency - effect of bed composition

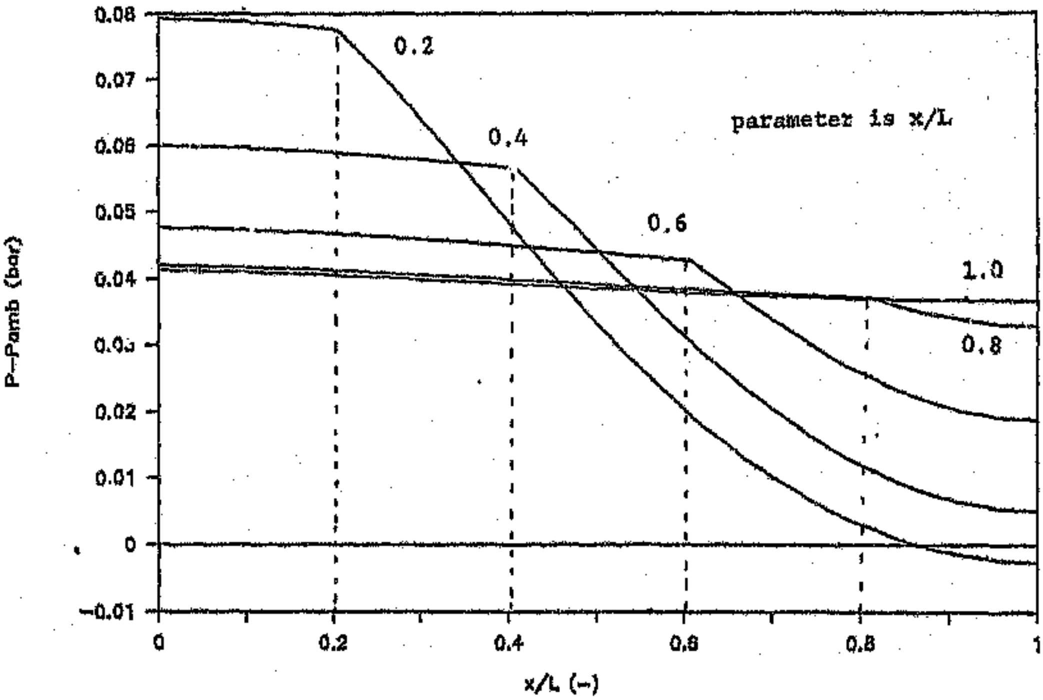

5.2.4 Plot of pressure profile - effect of bed composition selected for 'freezing' the pressure gradients is when the reciprocating device is at bottom-dead-centre (for maximum clarity and contrast in the profiles); in this case, pulsation frequency is constant at 4 revolutions per second.

It is very clear from this graph that, as expected, there is little or no gradient in the upper (higher permeability) section of the bed, and comparatively large gradients in the upper regions of the less permeable sections. As the volume of the less permeable section becomes a smaller and smaller fraction of the total volume, the effect becomes less marked, as expected, to the point where no pressure gradient is evident (see curve e). Note also the slightly less-than-ambient pressure of curve a, above approximately $x/L=0.9$.

In the limit as frequency becomes large, the layered bed will begin to behave as a shallow bed with depth equal to the depth of the upper, more porous layer. This behaviour is a clearly evident in Fig. 5.2.5, calculated using the base case parameters in Table 5.7. Fig. 5.2.5 compares the pressure profile at various frequencies, for a bed with a less permeable layer located at 40% of total depth (once again, the profile was 'frozen' with the reciprocator at bottom dead centre). It is clear from the graph that that the gradients in the two regions of the bed differ more and more as frequency increases. The higher the frequency, the less gas is contained in the lower region of the bed, due to its higher resistance to gas flow (see curve e)

It has therefore been demonstrated that by varying the frequency of the disturbance at the surface, the bed is 'probed' to varying depths (small frequencies probe deeper than high frequencies). Bed structure can thus be deduced by comparing the amplitude-frequency characteristic to that of a simple, known bed.

One might also be interested in the void fraction variation of a bed, (bearing in mind that for beds of particulates,

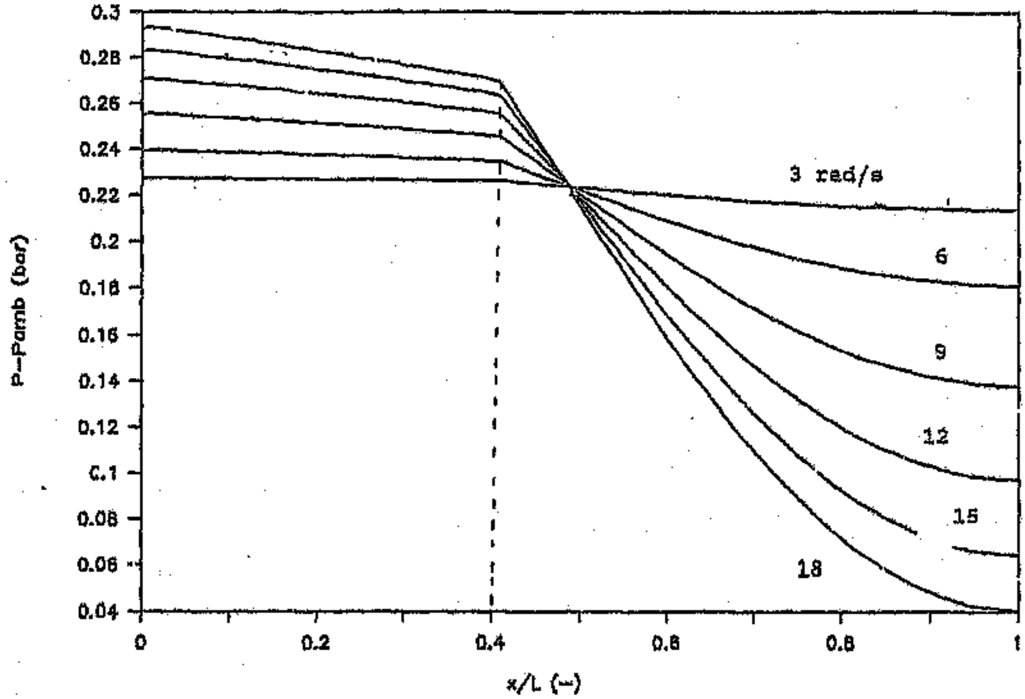

5.2.5 Plot of pressure profile - effect of frequency

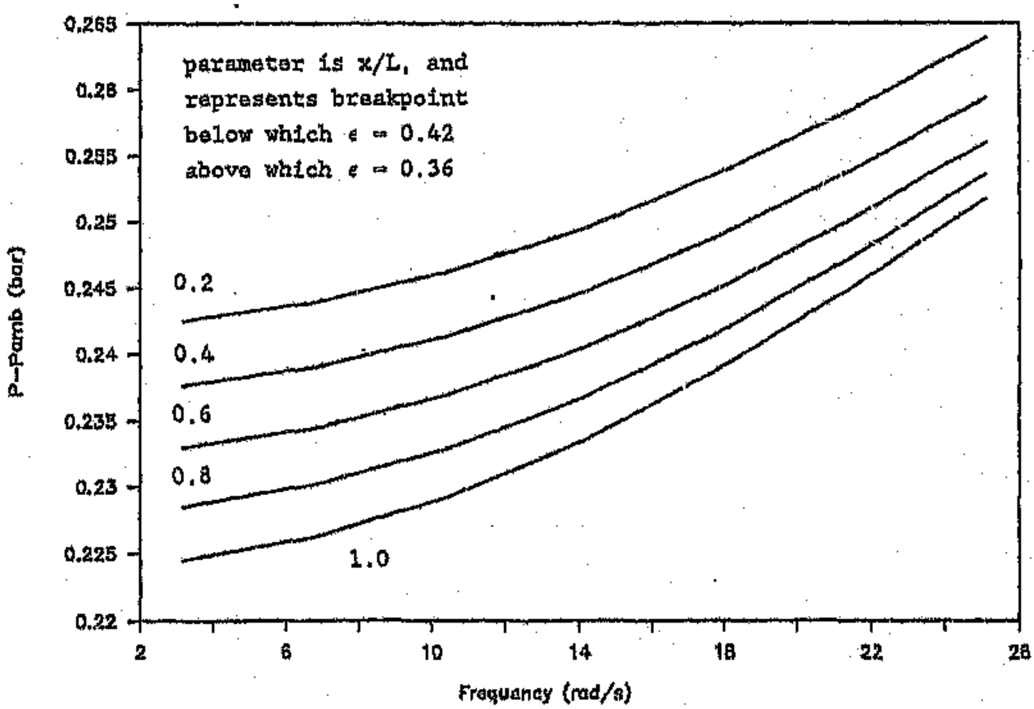

5.2.6 Plot of pressure amplitude offset vs. frequency
effect of layer of different voidage

permeability is strongly dependent on void fraction). It is possible, though, for layers of similar permeability to have different void fractions if the shape of the particles in the layers is different (consider sand shape particles vs. shale-type particles of the same characteristic diameter).

The effect of a layer of different void fraction (parameters as in Table 5.7) is shown in Fig. 5.2.6; the graph shows the amplitude-frequency characteristic for a bed of fixed size, whose lower portion has a void fraction of 0.36 as opposed to 0.42 in the upper section. Note: to isolate the effects of voidage here, the permeability of the entire bed was kept uniform at $1.48 \times 10^{-11} m^2$.

The depth of the section with 0.42 void fraction varies from 20% of total bed depth to 100% of total bed depth; in all cases, permeability was kept constant. To facilitate comparison, each curve in Fig. 5.2.6 was normalised by its own low-frequency value; the resultant curves are shown in Fig. 5.2.7. It is clear that voidage has a significant effect in its own right, quite apart from its effects on permeability. Fig. 5.2.8 shows the variation of lag with frequency for the beds with different voidage layers. Thus one can in principle detect the presence of layers with varying voidage by such measurements, though the resolution between amplitudes or lags for the different beds is small, and measurements will have to be taken with great care.

5.2.3 Interpretation of model results

Ideally, one would like to be able to analyse the amplitude-frequency and lag-frequency characteristics and arrive at a quantitative description of the bed. Since increasing the frequency leads to a diminishing portion of the bed being active, in theory one could devise a 'deconvolution' which would give some quantitative measure of the permeability-depth relationship from the amplitude-frequency response curve. All disturbance- reflection measurement techniques require analysis

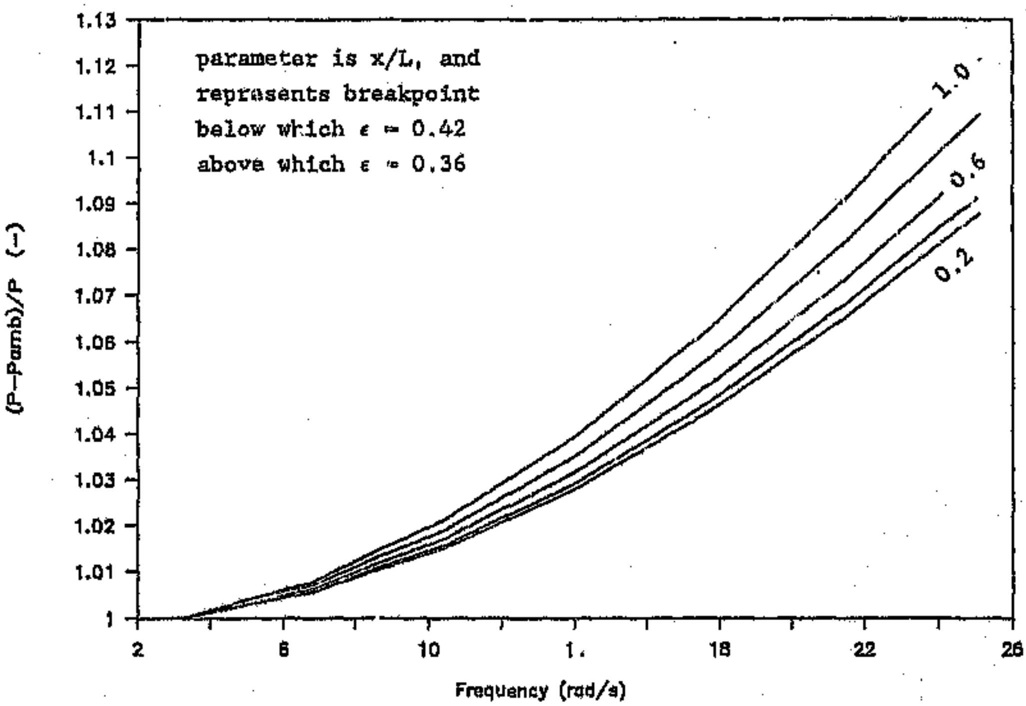

5.2.7 Plot of normalised pressure amplitude offset vs. frequency-effect of layer of different voidage

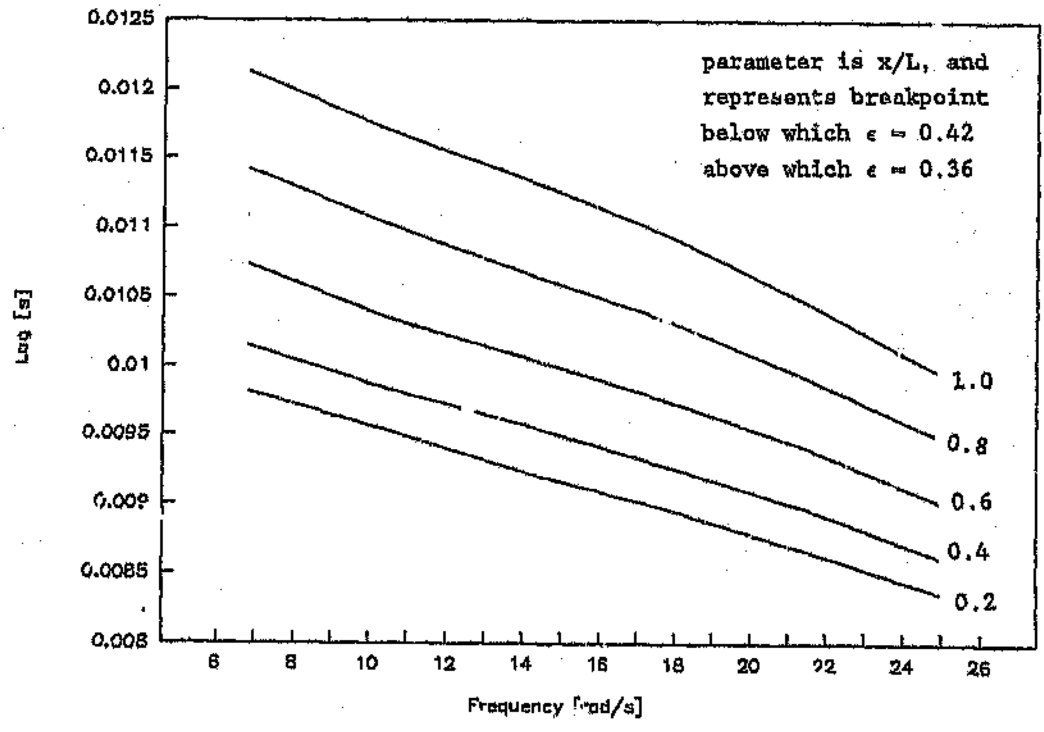

5.2.8 Plot of lag vs. frequency - effect of layer of different voidage of the results in some such way, since all results, right across the frequency range, are affected by the material nearest to the surface, and to a lesser extent (dependent on frequency in this case) by the material further away.

To actually determine a suitable deconvolution would require a substantial effort and considerable mathematical sophistication, as well as a large amount of further experimental results for verification. One might study the methods used to deconvolute sonic and ultrasonic imaging measurements, or the seismic analysis methods used by geologists and geophysicists, though such an in depth study is not within the scope of this thesis.

5.2.4 Discussion.

Although the above application is artificial in that model results are explained with prior knowledge of bed structure, and the bed is artificially contained in an impermeable container, the results do demonstrate that inhomogeneity of a porous medium may in principle be deduced from surface measurements only. Furthermore, these results were sufficiently encouraging to prompt experimental investigation of the method.

The experimental procedure is discussed an Chapter 3, and the results presented in Chapter 4. The measured frequency response behaviour displayed a particular feature which requires mention here, namely that for layered beds (such as that described in 5.2.2 above), there was a sharp transition in the amplitude-frequency behaviour. In particular, the slope of the amplitude-frequency curve increased sharply at a point. This feature is clearly not apparent in the model results presented above, and no attempt at building a model which explains this phenomenon succeeded.

The presence of an inflexion just above the low frequency region is a feature of a number of flow-resistance models including a single lumped-resistance model, and a multiple resistance model (see Appendix D, D.1.2), and would therefore not satisfactorily explain the sudden transition. Fig. 5.2.9 shows a sketch of the multi-resistance model referred to above. Fig.5.2.10 shows a plot of the frequency-amplitude behaviour for four related sets of resistances, and Fig. 5.2.11 a plot of time lag vs. frequency. The model parameters used are summarised in Table 5.8 below (see Appendix D for model derivation)

Table 5.8 - Parameters for Lumped Resistance Model

	Case A	Case B	Case C	Case D
κ_1	5	5	5	5
κ_2	5	5	5	0.5
κ_3	5	5	0.5	0.5
κ_4	5	0.5	0.5	0.5
V_1	0.2	for all cases		
V_2	1			
V_3	1			
V_4	1			

κ_n (in arbitrary units) is effective permeability of hole n

V_n in arbitrary units is volume of chamber n

Case A corresponds to a completely homogeneous bed, and cases B through D correspond to beds with a less permeable layer at the bottom, in various positions. The inflexion at low frequency is obvious, even in Case A. The presence of the inflexion at low frequency, also apparent in the single lumped resistance case, is therefore not indicative of inhomogeneity.

It would appear however, that the upward inflexion in the measured amplitude (see Fig.'s 4.1a through 4.8a) for layered beds is not evident in these model results. The cause of the inflexion in the measured results is not clear yet, though a number of possible causes exist:

1) A transition from laminar to turbulent flow above a certain frequency, in such a manner that it manifests itself particularly in the lower, less permeable layer. This could result in a sharp increase in frictional losses (analagous to the peak in friction factor evident in single-phase flow in pipes and channels), in turn giving a transition in the amplitude-frequency behaviour.

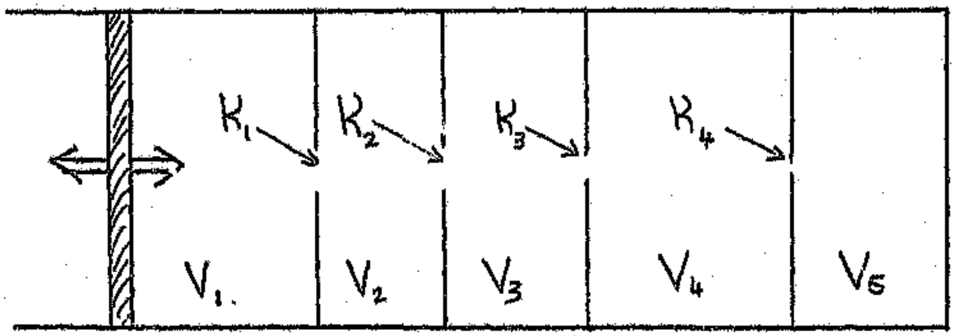

5.2.9 Sketch of multi-chamber model

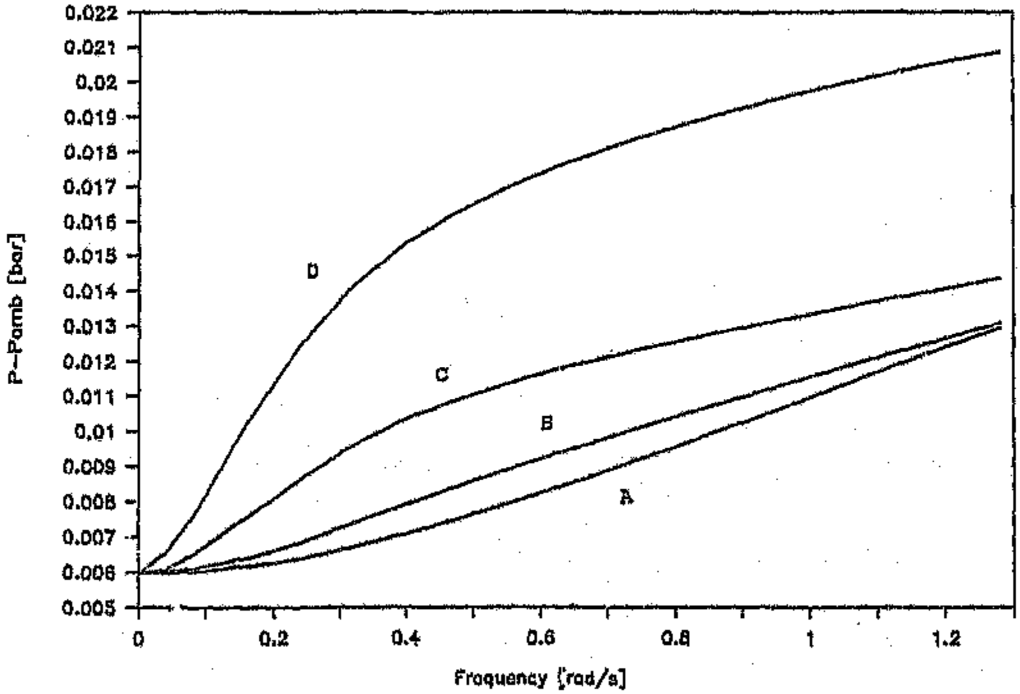

5.2.10 Plot of pressure amplitude offset vs. frequency for multi chamber model - effect of permeability 'profile'. See Table 5.8

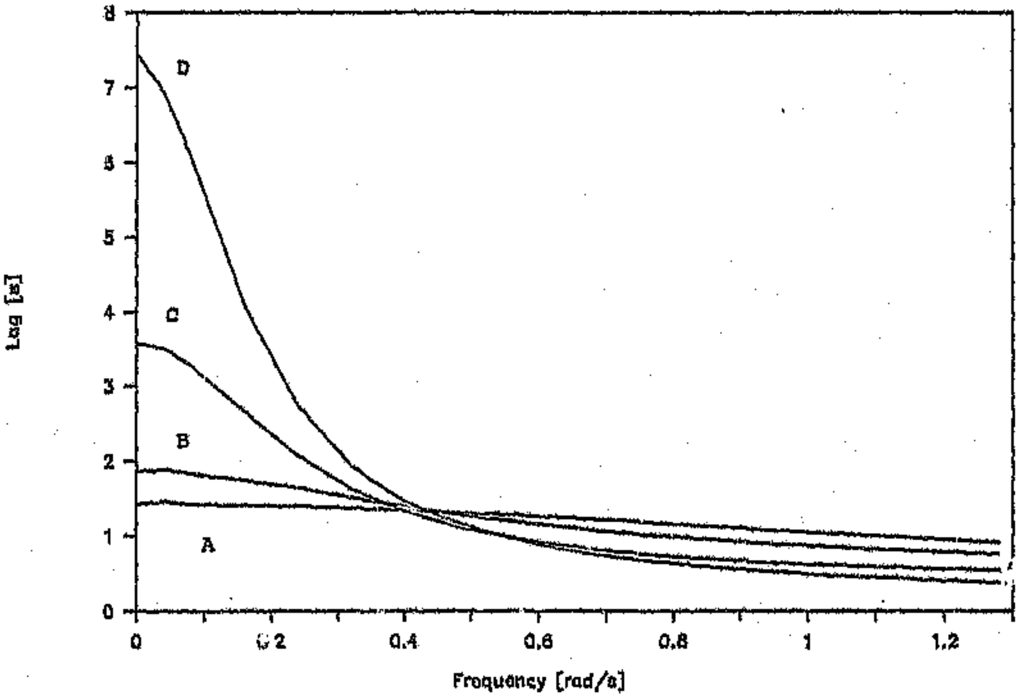

5.2.11 Plot of lag vs. frequency for multi chamber model
See Table 5.8.

2) Inadequacy of the Darcy Law in describing the flows present. Indeed, the major restriction of Darcy's law is that it is valid only for laminar flow in homogeneous media only. The modelling work described above has planar flow at all times, whereas the experimental apparatus employed (see Chapter 3) made use of what approximated spherically symmetric flow patterns. The result of this is that the area for flow would have been small near to the source, resulting in higher velocities, and therefore higher pressure gradients. It is believed that the magnitude of pressure gradients present in the bed render the Darcy law inadequate.

It is tempting to draw the general conclusion that a sudden transition in the amplitude-frequency curve is an indicator of large-scale inhomogeneity. There is, however, not sufficient information at this stage to support such a conclusion, and further work is required, both on the model and the experimental equipment and techniques.

Note, however, that there is reasonable agreement (in character) between the time lag results of the rigorous numerical model and the lumped-parameter multi-chamber model; while such qualitative results are encouraging, they are not useful in their present form, and more modelling work is required to develop the technique adequately

It remains to perform an in-depth modelling and experimental study of the phenomena discussed in this section, particularly with a view to understanding and improving on the phenomenological laws which describe the unsteady, compressible flow which occurs in the experimental beds.

5.3 Conclusions

The above discussions and applications have demonstrated that management of coal stockpiles based on surface measurements is a viable proposition. In particular, the energy release within stockpiles may now be estimated using a scientifically based theory, which appears to give consistent estimates based on comparison with laboratory results. The major uncertainty of the estimates arises from the value of surface heat transfer coefficient assumed. In the event that only comparative estimates for stockpiles under certain similar conditions are required, this is not a major shortcoming, since the heat transfer coefficients on the different piles may, to a first approximation, be assumed equal.

The most likely positive development regarding the energy estimation technique would be a reliable theory for heat transfer coefficients on exposed surfaces of porous media.

Further work on the aspects of modelling unsteady momentum transfer (as discussed in 5.2 above) is required to develop the method to a level where the time and effort are justified by the quality of the results obtained. Reliable and efficient modelling provides the key to improving and adapting measurement and monitoring techniques; further work on the models is required, both to define the limits of validity and to make such calculations more effective and accessible to practitioners in related fields.

6 A Systematic Approach to Coal Stockpile Management

Preceding chapters have developed and verified some concepts which are applicable to coal stockpile monitoring and management, namely:

- the efficacy of classical heat transfer coefficients in modelling surface temperature of coal stockpiles

- the predictable relationship between surface temperature of a stockpile and the energy dissipation within

- the relationship between the measured response of a bed to a periodic pressure disturbance and the internal structure of that bed

The intention of this chapter is to describe a systematic approach to monitoring coal stockpiles, one which combines previously published findings and the ideas mentioned above. The basic system which is discussed in the remainder of this chapter is intended to specifically address the following questions:

- whether a stockpile (or section thereof), previously known to be stable or non-combusting, is steadily developing into a combustion hazard

- in the event of an existing or developing combustion hazard being identified, some scientifically informed measures of controlling and possibly eliminating the combustion are required. This would include the type of measures to be taken as well as the location at which action would best be taken.

- In the c a where a new stockpile is to be built, preventative measures should be taken; effective and practical measures must be devised, and this is best done using a scientific approach.

The discussion below proposes an approach that is systematic and makes use of the techniques which have been developed in this thesis. As these methods are further developed, improvements to the system can be made, particularly with regard to the quantitative nature of the permeability probing technique. The most obvious route for improvement of any of the techniques is the adjustment of parameters, so that model results more accurately correspond to observed behaviour. All observations, measurements, and subsequent calculations should be recorded, and a systematic database maintained, so that model parameters can be regularly assessed and updated.

Existing data on behaviour of the interior of coal stockpiles is very very scarce, so the accuracy of any of the techniques developed here can not be assessed a priori; it is for precisely this reason that simulated temperatures were used for preliminary verification of the energy release estimation technique (see 5.1.2). It is only by combining field observations with theories that the suitability of the results to practical applications will be improved, thus bridging the gap between laboratory and stockpile.

Due to the sheer size of most stockpiles, and the methods used to lay them, it is necessary to have some form of map of the surface, such as a cartesian or polar coordinate system, with reference point/s which are visible from a height suitable for helicopter based infra-red thermography measurements. For the remainder of the discussion it will be assumed that the stockpiles(s) has been surveyed, and that a suitable map has been drawn up.

It is suggested that preliminary infra-red thermographs be recorded and studied to decide on the initial resolution required for temperature measurements.

6.1 Identification of Developing Combustion Hazards

Having decided on a grid, infra-red thermographs (IRT) must be measured regularly, at two or three day intervals, until other indications of the required frequency become available. In the case of a recently laid stockpile, it may be necessary to wait for weeks or months before any significant surface temperature variations become apparent. In this case, initally, weekly IRT's should be adequate. Every attempt must be made to measure the IRT's under standard conditions, such as discussed in Chapter 5 (just before dawn, and at full moon in the case of navigational problems, etc.), and considerable care is recommended in the selection of temperature intervals. Fig. 5.1.8 shows that a temperature difference of only 3°C can indicate an energy flux as high as 40 $W.m^{-2}$. It is recommended that the IRT range be set from ambient temperature to ambient plus 5°C; it will soon become apparent whether a smaller or larger range is required.

As soon as measureable differences between surface and ambient temperatures start to occur, it will be noticed that higher temperatures occur in 'islands' surrounded by regions of lower temperature. This is characteristic of convection in large beds, see Bradshaw (1990). At this stage, the energy associated with some of the more extreme hot 'islands' (hot spots) should be calculated using the methods described earlier. The map discussed above is necessary to reference the hot spots (which may mov or change size with time, thereby becoming unrecogn.. ble) and so that the scale of the IRT is known. Without the scale, the IRT cannot be used to estimate total energy associated with a hot spot. In the absence of any data to the contrary, it is recommended that a heat transfer coefficient of 7 $W.m^{-1}K^{-1}$ be used.

The hot spots on the surface mark regions in which hot air and volatile combustion products leave the stockpile, so the oxygen and carbon monoxide/dioxide content of the gas should be measured; this data is complementary to estimates of energy release associated with each hos spot. Due to the low gas velocities expected within the stockpile gas samples must be drawn from at least half a metre below the surface, to prevent contamination by surface air. For this reason, gas is usually sampled using a probe sheathed in a narrow pipe which is knocked approximately one metre into the stockpile.

Thus one would record the total energy release and thermographic data associated with each hot spot. as well as the composition of gas samples drawn from within the hot spots. Using the database of information so collected, together with visual observations and the input of experienced personnel, one could begin to derive criteria for combustion after a sufficient number of hot spots have been monitored. For example, one might examine the trend of energy release, area of spread of the hot spot, as well as oxygen content of the extant gas. Even in the absence of exact heat transfer coefficients, a general upward trend will indicate the development of a problem associated with particular hot spots. Once combustion is known to be occurring beneath particular spots, one might identify early trends which predict combustion. Of course, in cases where there is considerable existing experience with combustion in stockpiles, one may know sooner if a hot spot represents a combustion site, resulting in a quicker return on the investment of time and effort in measurement and analysis.

Alternatively, one could set up a number of different experimental piles, some of which will definitely combust, and obtain some initial data with which to decide on combustion criteria. This could be more economical than awaiting combustion in several different sites on a large stockpile of high value coal, though care would have to be taken in the construction of the pile to ensure that representative behaviour is obtained.

Once the database is established and is being maintained, problem hot spots can be identified with more confidence, to the point where there is enough confidence in the diagnosis to take corrective action.

6.2 Corrective Action

When potential or existing hazards can be identified from the trend of energy release with time etc., one would like to be able to take preventative or corrective action. This requires some knowledge of the location and magnitude of the combustion site, though these are difficult to determine with any certainty from the surface only. Again, the best indications of this would be experience with similar piles, although a database approach based on actual occurrence of combustion would suffice.

For example, a hot spot deep within the bed would show a greater spread than a hot-spot of similar power located near to the surface of the bed. Thus, by plotting 'radial spread' of hot spots on a vertical axis against the energy associated with each spot on the horizontal axis, one might be able to obtain an idea of the relative depths of the hot spots Some actual depths would have to be measured at some stage if any quantitative scale is to be assigned to the depth categories; this would greatly assist practitioners in making informed decisions regarding excavation of hot spots.

Note that there is considerable danger associated with 'digging' out hot-spots, since oxygen supply to the combusting region is greatly increased as digging progresses. Furthermore, conversion of coal to soft ash results in structural weakness of the bed in that region, and there is the danger of serious injury, or loss of life. This only emphasises the need for early identification of combustion, and corrective action.

An alternative or additional corrective action is to identify the regions of the bed responsible for major ingress of air which sustains combustion, and to cover those areas with some material which retards flow of air.

The results of Bradshaw (1990), among others, show that for homogeneous beds, the ingress of air takes place in a region surrounding the hot-spot. This is true also for inhomogeneous beds, with the exception that distribution will be uneven, favoring portions with higher permeability. An obvious action would be to blanket the region with some impermeable layer thus removing a source of ready oxygen. Such methods have been discussed previously; Brooks and Glasser (1986) discuss methods such as covering the stockpile with sand, or fine coal.

The problem with such measures is that imperfections in the surface coating (such as cracks or very thinly coated areas) exacerbate the situation by causing highly localised flows of air. Spreading methods which prevent imperfect sealing could be investigated, such as the controlled spraying of an inexpensive, flexible organic foam covering from a helicopter, to cover the entire surface of the stockpile. For such a method to prove economical, the cost would have to be a suitably small fraction of the value of coal in the bed, obviously favoring stockpile geometry which minimises the exposed surface area per unit volume. Should such a technique be developed, it would be sensible to coat the entire stockpile, and use the monitoring techniques suggested in the thesis to locate breaks or imperfections in the coating. The remainder of this discussion refers to unsealed stockpiles, though application to sealed stockpiles is also possible.

If it is suspected that certain regions of the bed are causing disproportionate ingress of air, reliable methods of identifying these areas would allow action to be taken where it is most urgently required. One method which could be used to locate areas of ingress (usually surrounding the hot spots identified by previous IRT) is to see in which regions artifically introduced smoke is drawn into the stockpile. Regions of major ingress will tend to be in the 'coldest' areas on the surface, so efforts should be guided by study of the IRT. Since free-convection velocities of air into or out of stockpiles are usually of the order of a few millimetres per second, care would have to be taken to exclude the effects of very light, otherwise unnoticeable breezes. For example, one could construct a box out of clear perspex, and make provision for introducing a small amount of smoke near the surface of the stockpile. It would then be evident after a minute or so whether air is being sucked into the stockpile, or being expelled; diagnosis can be confirmed by analysing samples of gas drawn from those regions of the stockpile.

The pulsed-air technique described in 5.2.1 could be used to supplement the above techniques once suitably developed, though in any case one would at this stage have a fair idea of the general regions responsible for ingress of the air which is sustaining combustion. Although it will not be possible to totally prevent air ingress from sustaining a particular hot spot (short of covering the entire stockpile as discussed above), it will allways be beneficial to seal off as much of the high permeability region as possible.

6.3 Construction of new stockpiles

The old adage 'prevention is better than cure' is as true as ever in this case. The cost and difficulty of cure, evident in the above discussion, can be avoided by preventing the formation of areas of high permeability, at least at the surface of the stockpiles. Brooks (1985), Brooks and Glasser (1986), and Bradshaw (1990) discuss the effects of particle size on tendency to combustion, and it is to be expected that stockpiles of very large particles or of very small particles do not easily combust. The reason is insufficient surface area for reaction in the former case, and difficulty of convection due to low permeability in the latter. It therefore stands to reason that for a particular coal type, there is a particle size for which combustion is most likely; efforts to identify the criterion for this diameter are ongoing, and are complicated by numerical difficulties, among other issues. See Brooks and Glasser (1986), and Bradshaw (1990) for discussions of the techniques used.

The effects of voidage, very influential in permeability of the stockpile, have also been studied by the above researchers, though it is not yet completely clear when compacting of stockpiles (to reduce permeability) is economically advantageous, though the grade (and hence value) of the coal being stockpiled clearly has a drastic effect on this. The inclusion or exclusion of fines from stockpiles is also an issue here, since fines near the surface tend to starve the interior of oxygen due to their comparitively high reactivity; fines in the interior exacerbate combustion, also by virtue of their high reactivity. Although the exact effect of fines distributed within the stockpile is difficult to determine, as a result of computational complications, a general recommendation is to exclude fines from the interior of the pile, as much as is possible.

Note that the formation of large-scale inhomogeneity and the inclusion of fines is inherent in the usual method of stockpile construction (i.e. conveyor layering), and little can be done to prevent this , short of developing a new yet practical method of deposition. See Williams (1963), Shinohara, Shoji & Tanaka (1970), and Bicking (1967) for both theoretical and experimental studies of particle size segregation during laying of particulate materials.

The work of Bradshaw (1990) and others should be studied if some effort is to be made to choose an average particle size which would lessen likelihood of combustion.

All things considered, all efforts should be made during stockpile construction to prevent the unnecessary inclusion of inhomogeneities, particularly near the surface of the finished pile. If any such inhomogeneities are evident, either from visual examination or by any of the methods discussed above, these inhomogeneities should be covered over with a layer of material which would slow down the ingress of air.

6.4 Conclusion

The above outline of a formalism for monitoring coal stockpiles has been discussed in the interests of encouraging the application of scientific principles and methods in the management of resources. Although the thesis has generally concentrated on coal stockpiles, the principles described throughout can be applied to any resource stockpile that is prone to destruction by combustion. The applicability of some of the conclusions and techniques to physically different media (such as fibrous material) may require testing and verification, but the underlying methods are rigorously based and only the physically descriptive parameters eg. thermal conductivity, density etc. will require adjustment.

7. Conclusion

Reliable estimates of the parameters which characterise porous media are usually assumed to be available, although this is in fact seldom true, particularly in the case of large-scale stockpiles of coal. The extreme sensitivity of porous media to Rayleigh number has been demonstrated in several published studies (most notably that of Lapwood, 1948), thereby emphasising the need for a scientific approach to monitoring and analysing coal stockpiles.

In particular, practitioners need to know whether coal stockpiles are burning within (as certain types are prone to do), or whether they are likely to burn at some time in the future. As simple as these questions may seem, several workers have spent considerable time and effort in an attempt to answer them, and the work in this thesis has made a tangible contribution in this regard.

Classical two-dimensional conductive-convective models were applied to the analysis of four different, carefully controlled experimental coal beds; the best-fit permeability and surface heat-transfer coefficient were found by minimising the sum-of-squared temperature errors. Surface heat-transfer coefficient was shown to be of great importance in application to the coal stockpiling industry, though it is believed that a comprehensive study of this parameter is still required, particularly with regard to experimentation. No identifiable trend with particle size or energy flux could be identified, mainly due to inadequacies in design of experimental apparatus.

A simple one-dimensional model of conductive-convective heat transfer in a packed bed was developed and applied to the estimation of energy dissipation within coal beds. In particular, the model was applied to carefully controlled experimental situations, and it was shown that the heat transfer coefficient at the exposed surface of the bed is an extremely influential parameter, particularly since surface temperature is the only indication of combustion which is readily accessible to personnel monitoring stockpiles. It was shown that the amount of energy released within a bed can be estimated knowing only surface temperature and the heat-transfer coefficient at the surface. This is particularly useful in the field, where in general little or nothing is known about the internal structure of the bed, and aerial infra-red thermography is the only type of measurement that is feasible on a suitable scale

The model relates total energy flux (convective plus conductive) through the surface of the bed to the difference between ambient temperature and surface temperature, and is virtually independent of Rayleigh number for all cases of practical interest.

Total energy dissipation within a bed, obtained by integrating flux over the whole surface, can be used to grade combustion hazards, particularly if case-histories of a number of beds are maintained. The results can be used to compare behaviour of different stockpiles, or monitor the progress of a single stockpile over a period of time, as described in Chapter 6.

It is believed that this result makes a substantial contribution to knowledge in this field, since it is fundamentally based, is simple, and has been shown to accurately predict energy dissipation, subject to the availability of suitable estimates for surface heat-transfer coefficient.

The influential role played by the surface heat-transfer coefficient is clearly evident in the results of this model, particularly on examination of the surface temperature/energy flux curves contained in Chapter 5. An attempt (as mentioned above) was therefore made to investigate the role of particle size and temperature on the surface heat-transfer coefficient, with little success (due to inadequacies in experimental design). Briefly stated, inadequate confidence levels and scatter in the estimated coefficient prevented meaningful conclusions regarding this parameter from being reached. A number of possible reasons for this were identified, namely inaccurate temperature measurement, fundamental shortcomings of the classical conductive-convective model equations, and insufficient volume of collected data. It is, however, unlikely that increased accuracy of temperature measurement will significantly increase confidence in the estimated parameters.

Since scatter is worse at high temperatures, it is likely that improvements in model formulation will improve confidence levels of all parameter estimates. The major cause for unacceptable confidence interval width, however, is the fact that permeability affects the interior temperature profile quite drastically in comparison to the heat transfer coefficient, and since most of the temperature measurements were taken inside the bed, a change in permeability results in a larger variation in sum-of-squared errors than a similar change in surface heat-transfer coefficient. This explains the disproportionate effect of permeability on sum-of-squared errors.

Furthermore, since the spread of the confidence interval increases as the number of estimated parameters increases, and decreases as number of relevant experimental data points increases, it would make sense to either increase the number of experimental data points for each run, or to design an experiment in which a minimum number of unknown parameters exists. This would entail concentration of thermistors in a region near the surface of the experimental bed. Alternatively, a totally different type of apparatus is required, one in which the surface heat-transfer coefficient only is fitted. This would result in better estimates of the heat transfer coefficient, thus achieving the objective.

The work in this thesis played a role in drawing the attention of other researchers to the critical importance of the surface heat-transfer coefficient, see for example the publication by Glasser, Williams, Brooks, Burch and Humphries (1991). These researchers developed a single-parameter experimental apparatus, and report results which demonstrate a general downward trend in heat transfer coefficient with increasing convection velocity. Further work is required to elucidate this relationship, though results to date appear to be promising.

The main objective of this thesis has been the investigation of methods which allow the early identification and prevention of combustion hazards. It has been conclusively shown by Brooks and Glasser (1986) that convection within stockpiles is the mechanism which initiates and maintains the supply of oxygen, and that large-scale inhomogeneity within stockpiles (well documented, see Williams 1963, Shinohara, Shoji & Tanaka 1970, and Bicking 1967), results in localised flows of air which aggravate the problem of combustion.

It is therefore desirable to detect large-scale variations in permeability within a stockpile, and a method which gives indications of permeability and large-scale inhomogeneity has therefore been proposed and verified in the thesis. Although it has not yet been fully developed and tested on a large scale, it is believed that the method could be very useful in detecting local variations in permeability of large-scale stockpiles, a measurement which at present is not practically feasible.

The method is simple in concept, and uses pneumatic pulses and pressure measurement to 'probe' the bed. It has been demonstrated using a simple model that increased frequency of pulses resulted in smaller and smaller portions of the bed influencing the measured pressure at the surface. Application of the model to a bed with a less permeable layer at the bottom gave results noticably different to those for a simple homogeneous bed, thus demonstrating the feasibility of the method in principle.

Experimental measurements on inhomogeneous systems showed characteristics distinctly different from similar measurements on simple homogeneous systems, demonstrating that the concept has potential in practice as well as in theory. Measurements on layered beds, however, showed sharp increases in slope of the amplitude-frequency curve, whereas model results did not display any such characteristics. Investigations to date have not yet yielded any satisfactory explanation of the phenomenon, though it is believed that refinements to model geometry, and the relation between pressure gradient and flow would go a long way to resolving the issue.

Another issue which requires examination and improvement is the method used to introduce the pneumatic pulses into the bed. Of necessity, the apparatus used here makes contact with the bed, and precautions must be taken to prevent any significant disturbance in this region. One aspect which has not been addressed is the prevention of leaking (of the pulse) directly out of the bed, or a method of quantitatively analysing the results. These issues will need to be investigated if the technique is to be developed further.

However preliminary it may be at this stage it is believed that this technique is novel, and may in the future be applied to good affect if developed sufficiently.

Lastly, the preceding chapter outlines a formalism which could be applied in the management of coal stockpiles, particularly in the development and maintenance of a quantitative database of stockpile behaviour. Further development of the ideas in the preceding chapter would increase the reliability of the system described, particularly if combined with previous experience.

In summary, it is has been shown that surface-based measurements alone may be used to deduce substantially more information about coal stockpiles (and other porous media) than would at first appear possible. This thesis has therefore contributed to the state of knowledge in this field, by proposing and verifying two novel methods for monitoring and investigating stockpiles. It has also drawn attention to a parameter (surface heat transfer coefficient) whose importance far belies the level of exposure it has received in the relevant literature to date.

REFERENCES

Anderson P., Glasser D., 1990, Int.J.Heat.Mass 33(6) p1321

Audibert S., Gaudet J, 1987, Int.Chem.Eng., 27(1) p40.

Balakrishnan A., Pei D., 1979, I&E.C.Proc.Des.Dev. 18(1) p30.

Bejan A., 1978, J.F.Mech. 89(1) p97.

Bejan A., 1981, J.Heat.Trans. (Trans ASME) 103 p237

Benenati R., Brosilow C., 1962 A.I.Ch.E., 8(3) p359

Bertin H., Ozoe H., 1986, Int.J.Heat.Mass 29(3) p449

Beveridge G., Haughey D., 1971 Int.J.Heat.Mass 14 p1093

Bicking C., The Sampling of Bulk Materials, Materials Research & Standards, March 1967 .

Bird R., Stewart W., Lightfoot E., Transport Phenomena, Wiley, New York, 1976

Bradshaw S., Modelling the Spontaneous Combustion of Coal Stockpiles, Ph.D. Thesis, University of the Witwatersrand, Johannesburg, South Africa, 1989.

Brinkman H., 1947, Appl.Sci.Res., A1 p27

Brooks K., A Simplified Model for Spontaneous Combustion in Coal Stockpiles, Ph.D. Thesis, University of the Witwatersrand, Johannesburg, South Africa, 1986

Brooks K., Glasser D., 1986, Fuel, 65 p1035

Coulson J., Richardson J., (Eds. Backhurst J., Harker J.), Chemical Engineering, Vol. 1, Pergamon, Oxford, 1977.

Doi M., 1976, J.Phys.Soc.Jap., 40(2) p567

Flumerfelt R., Slattery J., 1969, A.I.Ch.E.J., 15(2) p291

Gray W., 1975, Chem.Eng.SCi., 30 p229

Glasser D., Williams D., Brooks K., Burch G., Humphries G., 1991, to be published.

Gresho P., Lee R., 1981, Comp. & Fluids 9 p223

Gunn D., 1970, Chem.Eng.Sci., 25 p53

Haughey D., Beveridge G., 1966, Chem.Eng.Sci., 21 p905

Havstad M., Burns P., 1982, Int.J.Heat.Trans. 25(11) p1755

Horne R., O'Sullivan M., 1978, J.Heat.Trans (Trans ASME), 100, p448

Hsu C., Cheng P., 1985, Int.J.Heat.Mass 28(3) p683

Hughes P., Klein S., Close D., 1976, J.Heat.Trans (Trans ASME), p336

Koch D., Brady J., 1986, A.I.Ch.E.J., 32(4) p575

Kreyszig E., Advanced Engineering Mathematics, John Wiley & Sons, New York, 1983

Kvernvold O., Tyvand P., 1979, J.F.Mech., 90(4) p609

Lapwood E., 1948, Proc.Camb.Phil.Soc. 44 p508

Levenspiel O., Chemical reaction Engineering, John Wiley & Sons, New York (1972)

Luyben W., Process Modelling, Simulation and Control for Chemical Engineers, McGraw-Hill, New York, 1973

Lebon G., Cloot A., 1986, Int.J.Heat.Mass., 29(3) p381

Martin H., 1978, Chem.Eng.Sci., 33 p913

McKibbin R., Tyvand P., 1982, J.F.Mech. 118 p315

Michelsen M., 1979, The Chem.Eng.J., 18 p67

Nag Software Library, Routine D03PGF, 1982.

Nemeth J., Virag T., 1989, Chem.Eng.Proc., 25 p47.

Roblee L., Baird R., Tierney J., 1958, A.I.Ch.E.J., 4(4) p460

Shinohara K., Shoji K., Tanaka T., 1970, I&EC Proc.Des.Dev., 9 p174

Slattery J., 1969, A.I.Ch.E.J., 15(6) p867

Tse F., Morse I., Hinkle R., Mechanical Vibrations: Theory and Applications, Allyn & Bacon Inc., 1978.

Vrettos N., Imakoma H., Okazaki M., 1989, ChemEng.Proc. 25 p35

Vrettos N., Imakoma H., Okazaki M., 1989, ChemEng.Proc. 26 p237

Weber J., 1974, Int.J.Heat.Mass, 17 p241

Whitaker S., 1966, Chem.Eng.Sci., 21 p291

Whitaker S. 1980, I&E.C.Fund. 19 p210

Williams J., 1963, Univ. of Sheffield Fuel Soc. 14

Yeh T., Gelhar L., Gutjahr A., 1985, Water Res.Research 21(4) p447

Young M., M.Sc. Thesis, University of the Witwatersrand, Johannesburg, South Africa, 1975

Young B., Williams D., Bryson A., 1986, Int.J.Heat.Mass, 29(2), p331

Zienkiewicz O., The Finite Element Method, McGraw-Hill, London, 1977

APPENDIX A Experimental Equipment

A.1 Heat Transfer Experimental Equipment

Young et al (1986) have published details of their experimental exuipment and procedures. These details are therefore not included here.

Benson-Armer & Leibowitz (unpublished) performed measurements similar to those described by Young et al (1986), but with a different energy-source arrangement, and slight modifications in thermistor positioning. Chapter 3 contains schematic diagrams of the bed and heater arrangement, and general equipment specifications are listed by Young et al.

Thermistor placement.

Thermistor placement is shown in Fig. 3.1.3. Thermistors were concentrated in the upper central region of the bed so as to maximise resolution of the temperature contours in this region (Refer Fig. 5.1.2).

Heater dimensions

The localised energy source was constructed as a 30mm diameter by 60mm long cylinder, inside which two 100 W halogen quartz light-bulbs were mounted (readily available, cost effective and reasonably compact 'heaters'). One of the bulbs acted as standby, in case the other bulb blew, which meant that the bed would not have to be unpacked merely to replace an exhausted bulb. Power input to the bulb was measured and controlled using a variac.

Procedures

Beds were hand-packed, a few particles at a time. This prevented the inclusion of large-scale inhomogeneities into the bed, and also prevented damage to the 'net' on which the thermistors were located.

After initial packing of the bed, the whole apparatus was flushed with nitrogen to exclude any possibility of combustion or 'self-heating' thereby introducing unknown factors into the experiments.

Once it had been packed with the particular size of particles under investigation, the bed was not disturbed at all between different runs, which were performed in order of increasing power input (thus minimising time taken to reach steady state). Using the electronic measurement circuit described by Young et al, the temperatures were monitored intermittently; steady state was generally attained within four to five days. At this stage, the temperatures at all points were measured and stored on magnetic tape.

A.2 Momentum transfer equipment

In order to facilitate measurements on the idealised system described in Chapter 5, a special system had to be designed. Before the final design was selected, a number of practical problems had to be addressed, namely:

1 - gas flows were to be restricted to the packed bed. If most of the gas were to flow through a free-surface of the bed, the object of the exercise would be defeated. It is accepted that this difficulty would apply equally, if not more, to a practical situation.

2 - The equipment had to be capable of simulating various bed depths, and changing this depth, or bed composition, had to be as quick and simple as possible.

3 - Approximate harmonic motion of the piston was required, to simplify analysis; fortunately this could be easily achieved to a degree adequate for the intended purpose.

After considerable thought and discussion, it was decided that the best method of ensuring that all gas flow had pass into the bed was to mount a disc around the 'mouth' of the compressor, and to ensure that this disc could be brought directly into contact with the bed surface. This would minimise gas bypassing, although some bypassing along the disc surface would still occur. Due to the anticipated size range of particles, (0.5mm to 2.0mm nominal diameter) and the final dimensions of the bed, the amount of bypassing may be neglected.

Due to the limited amount of space available, it was not practical to perform the measurements on a free pile of particles; a container was therefore provided to limit the lateral spread of the bed. The inside diameter of the container was made the same as the diameter of the disc, (thereby creating a seal) to facilitate lumped measurement of the beds (see Chapter 3). Note that it is not necessary to contain the bed, provided that the vertical scale of interest (layer depth, etc) is not much larger than the horizontal scale (disc radius). Should the vertical scale be much larger than the horizontal scale, the fraction of gas bypassing the bed-regions of interest would become unacceptably large, thereby distorting the results.

It is not known at this stage whether it is possible to develop a method of analysis which can account for gas bypassing the regions of interest, or which leaves the bed a short distance from the 'injection' point. Although such a methodology is essential to the practical application of the method being tested here, the limitations inherent in the equipment as designed are considered acceptable for primary development and testing of the concept.

Harmonic motion was achieved by mounting a disc acentrically on an axle. The angle-arm of the piston was connected to the eccentrically mounted disc, which was driven by a 2 kW Normand high torque motor. The design of the drive and linkage was such that the top link essentially followed the lowest point on the acentrically mounted disk. The vertical location of this point is sinusoidal, and with the dimensions shown (see Fig. 3.2.1) the piston moves 125mm on either side of the mean piston position. Piston volume varied approximately according to $V=0.442 + 0.246 \cdot \sin(\omega t)$, where V is in litres.

Fig. 3.2.1 shows a schematic diagram of the apparatus.

A.2.1 Pressure measurement

Due to the nature of the experiment, small transient differential pressures are to be expected. For this reason, a high precision, quality electronic pressure transducer was selected, namely a Data Instruments Model AB HP 0 to 6 psig. The transducer was connected to the 1/4" pressure tapping by means of a special low volume adapter. Note that the transducer provides accuracy of 0.25% of the full range pressure.

A data sheet for the range of transducers is attached.

A.2.2 Signal conditioning

The pressure transducer discussed above returns an analog voltage of 0 to 100 mV as pressure ranges from 0 to 6 psi. Since the analog- to-digital converter (see below) requires a 10V DC analog input to maximise resolution in the logged data, conditioning of the 0-100mV signal was required. Signal conditioning was carried out by a dedicated strain-gauge amplifier card (model PC-68) The adjustable amplifier was calibrated at a gain of 100 (to amplify 100mV to 10V), and the adjustable low-pass filter set to 100 Hz (since maximum signal frequency expected was 3Hz).

The signal conditioner also supplied a stable, filtered excitation voltage of 5V DC to the transducer.

A data sheet for the PC-68 is attached.

DATA INSTRUMENTS
4 Hartwell Place, Lexington, MA 02173 USA

Model AB

Pressure Transducer Instruction Sheet
Standard and High Performance

PHYSICAL

RANGES	0-5, 15, 25, 50 PSIG, 100, 200, 500, 1000, 2000, 3000, 5000, 10,000, 15,000 and 20,000 PSIS† (PSIA available - see Option 1).
OVERLOAD	2 times *(or 30K PSI max.)* rated pressure without damage; 5 times *(or 50K PSI max.)* rated pressure without bursting
CASE MATERIAL	316L stainless steel for ranges 50 PSI and under 15-5PH stainless steel for ranges 100 PSI and over
SHOCK & VIBRATION RESISTANCE	Undamaged by 50 G's. Meets MIL-STD-810 B, Fig. 514-4, curve AP, time schedule II

ELECTRICAL

SIGNAL OUTPUT	100 millivolts at rated pressure, ±1%, open circuit
EXCITATION VOLTAGE	5 Vdc or ac rms recommended; 6 V maximum.
ZERO BALANCE	Within ±5 mV at 70°F *(21.1°C)*
SENSITIVITY	*20 mV/V*
BRIDGE RESISTANCE	Input, 150 ohms ±50 ohms Output, 115 ohms *±25 ohms*
ELECTRICAL CONNECTION	4 conductor shielded cable, 3 feet *(0.9m)* long. *See OPTIONS*

PERFORMANCE

ACCURACY*	Within 1% F.S. from best fit straight line, including non-linearity, repeatability and hysteresis. See *OPTIONS*
RESOLUTION	Infinite
OPERATING TEMPERATURE RANGE	−65° to 200°F *(−53.9°C to 93.3°C)* Can be extended to 300°F *(149°C)* See OPTIONS
COMPENSATED TEMPERATURE RANGE	30°F to 130°F *(−1.1°C to 54.4°C)* standard *(30-160°F for AB High Performance)*
THERMAL EFFECT* ON ZERO	Less than 5% of full scale over compensated range. See OPTIONS
THERMAL EFFECT* SENSITIVITY	Less than 2% of reading over compensated range. See OPTIONS.

*Values here for AB Standard
See Options for AB High Performance

†Units 100 PSI and above have cases sealed from the surrounding atmosphere, providing maximum reliability in humid or corrosive environment (psis). Ranges below 100 PSI are vented to the atmosphere and read gage pressure independently of barometric pressure changes (psig).

OPTIONS

Various optional operating characteristics and mechanical features can be incorporated in standard Model AB transducers, at additional cost, for applications which require improved performance. These are designated by a numerical code:

Option 1 Absolute pressure version. Available in 15, 25 and 50 PSIA

The High Performance AB has accuracies of ±0.25% from best fit straight line for ranges 0-100 to 0-5000 PSIS. Higher or lower ranges, have accuracies of ±0.5%. All High Performance models have zero temperature compensation of less than ±1% of FSO/100°F (55°C) over compensated range and a span temperature compensation of *less than ±1% of reading per* 100°F (55°C) over compensated range.

Option 3 Barbed fitting for attaching protective hose around cable

Option 4 Install longer cable by splicing to existing 3 ft. cable

Option 5 Install longer continuous cable

Option 7 Extended Operating Temperature Range to 300°F *(148.9°C.)* 5 and 15 psi excluded. Includes Bendix PTIH-10-6P electrical connector with an extended case

Pin Code: A+ Excitation B+ Signal
C− Signal D− Excitation
E and F not used

General

The AB Standard and High Performance pressure transducer is a rugged, accurate and small pressure measuring instrument designed for industrial service. Its construction features simplicity, ruggedness, and absence of *moving* parts. Semiconductor strain gages mounted on a unique sensor *measure the deflection of the diaphragm* at its center. The strain gages are wired into a Wheatstone Bridge which is balanced at *no-load* conditions. Pressure on the diaphragm causes it to deflect, straining the gages, and changing their electrical resistance. When an excitation voltage is applied across two corners of the bridge, a signal voltage proportional to pressure is produced across the other two corners. The high sensitivity of the strain gage/sensor combination allows the diaphragm deflection to be as low as 0.002" (.05 mm). Thus, *the diaphragm stresses are* minimized insuring long life.

Data Instruments Inc. offers a wide range of signal conditioners, controllers and meter indicators for both bench and panel mount; and a calibrator for the Model AB.

These units supply the 5 volt excitation and signal amplification. Refer to catalog for details.

Application Information

The AB units are particularly suited for making measurements where shock and vibration are present. Because of low operating stresses, they may be used up to rated pressure range without any reduction in life expectancy.

All transducers measure gage pressure. On ranges of 100 psi and up, venting to atmospheric pressure is not necessary since normal barometric pressure changes will have negligible effect on accuracy. These units have been sealed to provide maximum reliability in the presence of moisture and corrosive atmospheres.

The 50 psi and lower range units have the internal cavity of the transducer vented to atmosphere. This is accomplished by means of a short tube which extends into the cable. Reference to atmospheric pressure is thus provided thru the cable jacket. It is important then not to pot the end of the cable nor to pinch it very tightly if clamping is required. The cable jacket should not be punctured, particularly in corrosive environments, and should be terminated in a clean, dry, environment.

AB pressure transducers may also be supplied to measure absolute pressures. These models in ranges of 15, 25, and 50 psia are evacuated and hermetically sealed. Their electrical balance is set to give minimum output at 0 psia.

Installation

The AB transducer may be easily mounted in the wall of a pressure vessel, pump housing, machine, etc. or it may be provided with an adapter to standard piping or tubing systems. Adapters for many different types of plumbing connections are available:

ADAPTERS

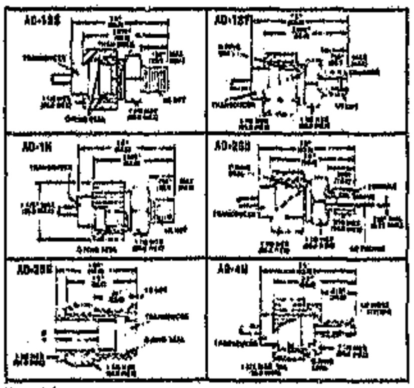

XX.XX = inches
(XX.XX) = mm

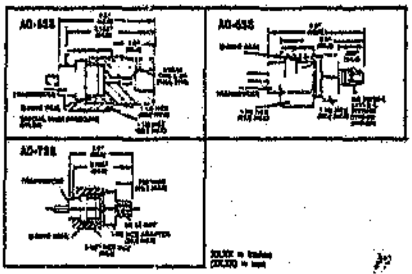

XX.XX = inches
(XX.XX) = mm

MODEL NO.	DESCRIPTION	MAXIMUM PRESSURE	BURST PRESSURE
AD-1SS	300 Series Stainless Steel, ¼" NPT male	10,000 PSI	20,000 PSI
AD-1SF	300 Series Stainless Steel, ¼" NPT male Snubber, 40 microns adapter	10,000 PSI	20,000 PSI
AD-1N	Nylon, ¼" NPT male	200 PSI	400 PSI
AD-2SS	300 Series Stainless Steel, ¼" tube fitting	3,000 PSI	6,000 PSI
AD-3SS	300 Series Stainless Steel, 1" NPT male flush mounting	10,000 PSI	20,000 PSI
AD-4N	Nylon, barbed fitting for ¼" ID hose	100 PSI	200 PSI
AD-6SS	410 Stainless Steel high pressure autoclave fitting, 9/16"-18 thread x ¼"	20,000 PSI	40,000 PSI
AD-8SS	300 Series Stainless Steel, MS-33656-4 male thread	10,000 PSI	20,000 PSI
AD-7SS	410 Stainless Steel, ¼" NPT male	20,000 PSI	40,000 PSI

The suggested mounting method shown below may be used for all pressure ranges. When using the suggested pressure mounting, care must be exercised not to damage the "O" ring

Suggested Mounting for All Pressure Ranges

during installation. Use of a lubricant is recommended. Hand tightening is usually sufficient to seal liquids up to 20,000 psi provided the "O" ring mounting surface finish is adequate (32 microinches or better).

Although the AB transducers are rugged, they should not be handled carelessly. Care should be taken to avoid undue force on the cable or bending it sharply where it is attached to the transducer. Avoid striking, scratching, or denting the diaphragm particularly on low range units. Also note that it is possible to apply enough pressure to the diaphragm with the thumb to overload low range units.

Protective Cap
Each transducer is shipped with a protective cap which should be removed before installation.

Maintenance

No maintenance is required with these transducers. The absence of moving parts and the solid state sensors make them trouble-free and reliable. Some precaution in handling the transducers is necessary, particularly in the low pressure ranges. Do not press on the diaphragm unless the unit is connected to a pressure readout to make sure the full scale rating is not exceeded. The diaphragm area should, of course, be protected from nicks, scratches and dents. The protective cap should remain on the unit until it is ready for installation.

It is important that the insulation resistance of the electrical circuit be maintained. Moisture, dirt or contaminated oils at the solder connections may be a source of trouble. It is important that the cable remains free from punctures and that it be protected from chemical attack. (Carefully read the installation section.) The cable supplied with the transducer has a tough PVC jacket. If the environmental conditions are severe, a protective sleeve may be inserted over the cable.

If malfunction of the transducer is suspected, the following electrical checks are recommended:

1. Input resistance (RED to BLACK) should be 160 ± 50 ohms.
2. Output resistance (GREEN to WHITE) should be 118 ± 25 ohms.
3. Resistance to ground between any lead and transducer case should be 500 megohms minimum. When making this measurement make sure that the megohmmeter is limited to 50 volts DC. Do not connect an insulation tester between two leads. The transducer will be permanently damaged.

CAUTION: 6 volts is the maximum voltage which can be safely applied to the transducer input or output terminals. If 6 volts is applied from the green to either the red or black terminals the unit may be permanently damaged.

If the transducer has been accidently overloaded, a permanent zero shift may occur. The transducer may still function properly however and a re-balancing with an external resistor as described in Section IV should be performed to verify the proper functioning of the unit.

Instrumentation and Operation Theory

The instrumentation for use with the AB transducers is very simple. Only a regulated constant voltage source and a meter recorder, oscilloscope or other readout instrument is required.

The AB transducer may be excited with either ac or dc voltage. For many temporary or test applications, a battery may be a suitable source. The recommended excitation is 5 V dc or ac rms. Do not exceed 6 V. The supply should be able to deliver a current of at least 50 mA at 5 V. Connect the excitation across the red and black leads. The green and white leads should be connected to the readout instrument.

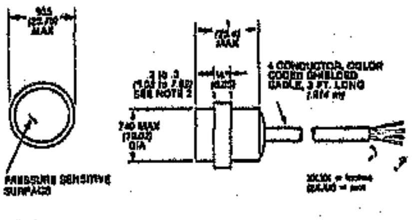

NOTES:
1. RECOMMENDED EXCITATION VOLTAGE: 5 VOLTS AC OR DC; 6 VOLTS MAXIMUM.

COLOR CODE:
RED (+) EXCITATION
GREEN (+) SIGNAL
WHITE (−) SIGNAL
BLACK (−) EXCITATION

2. DIMENSION OF LOCATING FLANGE VARIES DEPENDING ON RANGE.

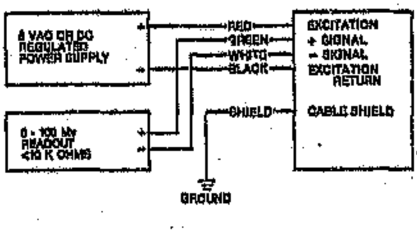

Circuit Diagram

Caution: Some power supplies exhibit an inductive kick or do not regulate properly the instant they are turned on. With such supplies a large transient voltage may be applied to the transducer resulting in possible electrical failure. With supplies of this type it is recommended that the transducer be energized only after the power supply has begun to regulate.

The bridge impedance of the AB transducers ranges from about 100 to about 200 ohms. This impedance increases approximately 6% per 100°F temperature rise. As a consequence, if series resistors are used to drop the excitation voltage to the recommended 5 volts, the voltage appearing at the transducer will increase with increasing temperature, thus producing a calibration or span error. This effect can easily be calculated. The maximum calibration error introduced by series input dropping resistors is + 6% per 100°F and occurs when the resistance becomes infinite. (Constant current supply.)

The signal voltage appearing across the output leads of the transducer is both a function of the applied pressure and the excitation voltage. The transducers have been calibrated to 100 mV ±1% full scale output with exactly 5.0 volts excitation. If, for example, 2.5 volts excitation is used, the output at full scale will be proportionally lower or 50 mV. At no load, a small residual output voltage will be present. This voltage (within 5% of the transducer's full scale output) can easily be nulled out by most read-out instruments. Nulling can also be achieved by placing a shunt resistor from the white lead to either red or black depending upon the polarity of the unbalance.

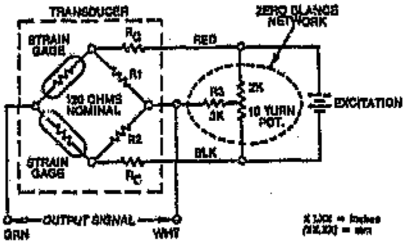

NOTES:

1. CIRCUIT PROVIDES APPROX. 60% FULL SCALE ZERO BALANCE RANGE.
2. "R_C" ARE CALIBRATION ADJUSTMENT RESISTORS INSIDE TRANSDUCER.

External Zero Balance Circuit

Circuitry used with the transducer can cause adverse changes in its temperature compensation. This problem can be avoided with an AB transducer by shunting only across the inactive resistors on the "White side" of the bridge. If for any reason the user feels he must shunt an active gage, the shunt should be kept as large as possible (20K Ω minimum) and an equal shunt on the other active gage will nullify the effect on temperature compensation. Shunting the active gages will also reduce the output signal somewhat: 20K Ω shunts will reduce the sensitivity by about 0.6%.

A wide variety of readily available meters make suitable readout devices for the AB transducers. When excited with about 6.6 V, the AB will drive a 100 microamp 1000 ohm meter full scale. It also has sufficient sensitivity for use with most digital panel meters.

Shunt calibration is a technique used with strain gage transducers to simulate the effect of applied pressure to produce an output signal. Shunting 1400 ohms across the black and white leads of the AB transducer produces a signal approximately equal to the transducer full scale. Similarly a 3000 ohm shunt will simulate a 60% output signal. These values are approximate and will vary from unit to unit. If shunt calibration is to be used, it is recommended that the actual transducer shunt output be determined by test and recorded.

Pressure Overloads

The AB transducers will withstand high overloads as tabulated in Table 1. *For overload ratings of adaptors, see page 2.*

If this overload rating is exceeded, electrical failure may occur. As a safety feature they have been designed to withstand much higher burst pressures than the pressure which will cause permanent damage.

Important: Both static and dynamic overloads must be considered when selecting a pressure transducer. In most systems, pressure fluctuations exist. These fluctuations can have very large and very fast peak pressures as in water hammer effects. If the transducer is connected to a slow responding instrument such pressure peaks may not be observed. Where pressure pulses are expected, the transducer rating should be high enough to prevent overload by the peak pressure. The life of the transducer will be reduced if the transducer is repeatedly operated in the overload range, particularly under dynamic conditions. An oscilloscope is a convenient tool for determining if high pressure transients exist in a system.

Table 1

Rated Pressure PSI	Maximum Pressure Without Damage PSI	Minimum Burst Pressure
20,000	30,000	50,000
15,000	25,000	50,000
10,000	20,000	50,000
5,000	10,000	25,000
3,000	6,000	15,000
2,000	4,000	10,000
1,000	2,000	5,000
500	1,000	2,500
200	400	1,000
100	200	500
50	100	500
25	50	250
15	30	150
5	12	50

MECHANICAL NATURAL FREQUENCY*

Range	Frequency (Hz)
5	2,500
15	3,000
25	4,000
50	6,000
100	8,000
200	10,000
500	16,000
1,000 & above	25,000

* Exclusive of Plumbing. Values listed are approximate.

DATA SHEET FOR PC-68

Specifications

Gain

Range: 2 to 5000 V/V
Temperature drift: 25ppm per degree C (max)
Nonlinearity: +/-0.005% max

Input bias current

Initial: +/-20nA max
Drift: +/-10pA per degree C max

Input impedance

Differential: 1 GOhm/100pF
Common mode: 1 GOhm/100pF

Input voltage

Linear differential: +/-5V
Max. common mode input: 10V (Gain = 1)

CMR, 1K source imbalance

G = 2, DC to 60Hz: 86dB min
G = 100 to 500, 1KHz bandwidth, DC to 60Hz: 110dB min
G = 100 to 500, 10Hz bandwidth, DC: 110dB min
G = 100 to 500, 10Hz bandwidth, 60Hz: 140dB min

Input noise (G = 1000)

Voltage, 0.1 - 10Hz: 0.3uV p-p
Voltage, 10 - 100Hz: 1uV p-p

Current, 0.1 - 10Hz: 60pA p-p
Current, 10 - 100Hz: 100pA p-p

Filter

Number of poles: 2
Roll-off: 40dB/decade

Bridge excitation

Output voltage range: +4 to +9 volts
Output current: 100mA
Input regulation: 0.05%/volt
Load regulation, 1mA - 50mA: 0.1%
Temperature stability: 0.004% per degree C
Output noise: 200uV p-p

Half-bridge completion

Resistor value: 20K +/-1%
Temperature tracking: +/-5ppm

Power supply

Voltage, rated performance: +/-15VDC
Voltage, operating: +/-12 to +/-18VDC
Supply current (including excitation supply): +/-10mA/channel

A.2.3 Data acquisition

Analog data from the transducer was fed into the A-D card (a PC-26 card, datasheet attached) in an IBM compatible XT computer, with a CPU frequency of 4.77 MHz. The A-D converter used is capable of converting analog data from one channel (as is the case here) at up to 16 000 Hz, clearly more than adequate for the purposes of this work. The converter has a digital resolution of 1 in 4095, i.e. 0.025% (again, adequate for this work). Data-logging software supplied with the A-D card calculated sampling frequency required to give samples at the required intervals, and took care of all the interfacing between the A-D card and the computer. Once sorted, data was stored on disc in ASCII format for later analysis.

A data sheet for the A-D converter is attached.

The above items, connected as shown in Fig. 3.2.2, constituted the measurement circuit.

Analogue to Digital Conversion Card Type PC-26

1 INTRODUCTION

The PC-26 card is a plug in data acquisition board for the IBM PC and compatible PC's. The PC-26 board includes the Analog Devices A/D converter AD 574 with a typical conversion time of 25 µs, and a 16 channel multiplexer. Typical conversion time for the whole system (Multiplexer, Sample & Hold, AD 574) is 40 µs.

The sample rate can be determined by software (using a software clock)or by the onboard programmable timer. The sampling software which is included with the PC-26 board allows the user to sample any of the 16 input channels with a sampling rate of 2000 Hz (Turbo Pascal) or 200 Hz (BASIC).

For full use of the PC-26 board an additional software package (written in TURBO PASCAL and ASSEMBLER) is available. With this software it is possible to program the onboard timer to provide a sampling frequency of between one sample every hour up to 9500 samples per second (using interrupt line IRQ 5). Using the software clock mode, sampling rates of up to 16 000 samples a second are possible. The sample data can be viewed on the screen (only with Graphics Monitor), and/or stored on disc for further analysis.

2. SPECIFICATIONS

A/D CONVERTER AD 574 JD (KD):

Resolution	:	12 bit
Conversion time	:	25 µs (AD 574)
	:	40 µs (Multiplexer, S&H, AD 574)
Input voltage	:	-5V to +5V
	:	-10V to +10V
	:	0V to +10V
Linearity	:	11 (12) bit, ie. 0.025% (0.012%)
Offset	:	adjustable to zero
Linearity drift	:	0.5/(0.5)/ppm/C
Offset drift)	:	10/(5)/ppm/C
Gain drift	:	50/(27)/ppm/C

SAMPLE & HOLD LF 398:

settling time	:	< 10 µs
Sample & Hold error	:	< 0.005%

MULTIPLEXER IH 6116

settling time	:	< 2 µs
input impedance	:	22 KΩ

APPENDIX B Experimental Results

B.1 Heat Transfer Experimental Results - Localised source

Benson-Armer & Leibowitz measured the steady-state temperature profiles in a bed heated by a centrally located cylindrical heater, as discussed in the paper by Anderson & Glasser (1990). Their results are as yet unpublished, and are therefore presented here in full.

A schematic sketch of the bed, showing heater placement, is contained in Fig. 5.1.1 in Chapter 5. Fig. 3.1.3 shows the placement of thermistors in the r-z plane of the cylindrical section. As discussed in Chapter 3, the experimental methods utilised are identical to those used by Young et al.

Benson-Armer & Leibowitz investigated three different beds, for three different levels of power input to the heater, as follows:

	Bed type		
	-5mm	10mm	20mm
	5 W	5 W	5 W
Power Input	7.5 W	10 W	7.5 W
	10 W	18 W	10 W

For each run, the average temperature of the temperature controlled room in which the experiments were conducted, is listed. The measured steady-state temperatures are listed below:

Q=5 W DP=-5MM

Tamb = 21.4

r	z	T
0.0	0.0	21.4
0.1	0.0	21.4
0.21	0.0	21.4
0.33	0.0	21.4
0.41	0.0	21.4
0.5	0.0	21.4
0.0	0.09	30.28
0.15	0.09	28.45
0.27	0.09	25.93
0.41	0.09	24.38
0.5	0.09	21.4
0.0	0.2	46.68
0.05	0.2	41.08
0.15	0.2	32.08
0.27	0.2	26.67
0.41	0.2	23.81
0.5	0.2	21.4
0.05	0.28	50.91
0.1	0.28	38.43
0.15	0.28	32.41
0.21	0.28	29.18
0.27	0.28	26.70
0.33	0.28	25.38
0.5	0.28	21.4
0.05	0.32	52.21
0.1	0.32	39.01
0.15	0.32	33.49
0.21	0.32	29.41
0.27	0.32	26.96
0.33	0.32	25.49
0.41	0.32	23.92
0.5	0.32	21.4
0.0	0.37	50.85

0.05	0.37	45.50
0.1	0.37	36.40
0.15	0.37	31.64
0.21	0.37	28.21
0.27	0.37	26.20
0.33	0.37	24.94
0.41	0.37	23.73
0.5	0.37	21.4
0.0	0.43	34.49
0.05	0.43	32.62
0.1	0.43	30.[illegible]7
0.15	0.43	28.29
0.21	0.43	26.09
0.27	0.43	25.02
0.33	0.43	24.12
0.5	0.43	21.4
0.0	0.5	26.87
0.05	0.5	26.65
0.1	0.5	26.24
0.15	0.5	24.94
0.21	0.5	24.08
0.27	0.5	23.44
0.33	0.5	23.01
0.41	0.5	22.22
0.5	0.5	21.4

Q=7,5 W   DP=-5MM

Tamb = 21.1

r	z	T
0.0	0.0	21.1
0.1	0.0	21.1
0.21	0.0	21.1
0.33	0.0	21.1
0.41	0.0	21.1
0.5	0.0	21.1
0.0	0.09	36.37
0.15	0.09	33.21
0.27	0.09	29.01
0.41	0.09	26.10
0.5	0.09	21.1
0.0	0.2	65.12
0.05	0.2	55.26
0.15	0.2	39.57
0.27	0.2	30.07
0.41	0.2	25.15
0.5	0.2	21.1
0.05	0.28	73.28
0.1	0.28	51.03
0.15	0.28	40.33
0.21	0.28	34.27
0.27	0.28	30.03
0.33	0.28	27.70
0.5	0.28	21.1
0.05	0.32	76.39
0.1	0.32	52.23
0.15	0.32	42.14
0.21	0.32	34.81
0.27	0.32	30.45
0.33	0.32	27.80
0.41	0.32	25.22
0.5	0.32	21.1
0.0	0.37	74.44

0.05	0.37	64.58
0.1	0.37	47.51
0.15	0.37	38.82
0.21	0.37	32.58
0.27	0.37	29.13
0.33	0.37	26.80
0.41	0.37	24.81
0.5	0.37	21.1
0.0	0.43	44.20
0.05	0.43	40.71
0.1	0.43	37.08
0.15	0.43	32.72
0.21	0.43	28.81
0.27	0.43	26.92
0.33	0.43	25.35
0.5	0.43	21.1
0.0	0.5	30.46
0.05	0.5	30.12
0.1	0.5	29.30
0.15	0.5	27.04
0.21	0.5	25.52
0.27	0.5	24.49
0.33	0.5	23.80
0.41	0.5	22.87
0.5	0.5	21.1

Q=10W   DP=-5MM
Tamb = 21.7

r	z	T
0.0	0.0	21.7
0.1	0.0	21.7
0.15	0.0	21.7
0.33	0.0	21.7
0.41	0.0	21.7
0.5	0.0	21.7
0.0	0.09	39.93
.15	0.09	35.98
[illegible]	0.09	30.84
0.41	0.09	27.14
0.5	0.09	21.7
0.0	0.2	75.12
0.05	0.2	63.05
0.15	0.2	43.84
0.27	0.2	32.07
0.41	0.2	25.83
0.5	0.2	21.7
0.05	0.28	85.15
0.1	0.28	57.93
0.15	0.28	44.80
0.21	0.28	37.20
0.27	0.28	31.98
0.33	0.28	29.07
0.5	0.28	21.7
0.05	0.32	89.09
0.1	0.32	59.42
0.15	0.32	46.99
0.21	0.32	37.90
0.27	0.32	32.49
0.33	0.32	29.17
0.41	0.32	25.90
0.5	0.32	21.7
0.0	0.37	86.81

0.05	0.37	74.65
0.1	0.37	53.58
0.15	0.37	42.85
0.21	0.37	35.07
0.27	0.37	30.84
0.33	0.37	27.91
0.41	0.37	25.36
0.5	0.37	21.7
0.0	0.43	49.47
0.05	0.43	45.14
0.1	0.43	40.63
0.15	0.43	35.18
0.21	0.43	30.30
0.27	0.43	27.96
0.33	0.43	25.99
0.5	0.43	21.7
0.0	0.5	32.18
0.05	0.5	31.79
0.1	0.5	30.76
0.15	0.5	27.90
0.21	0.5	26.02
0.27	0.5	24.73
0.33	0.5	23.87
0.41	0.5	22.57
0.5	0.5	21.7

Q=5W   DP=1CM

Tamb = 22.0

r	z	T
0.0	0.0	22.
0.1	0.0	22.
0.21	0.0	22.
0.33	0.0	22.
0.41	0.0	22.
0.5	0.0	22.
0.0	0.09	22.
0.15	0.09	23.63
0.27	0.09	22 86
0.41	0.09	22.85
0.5	.09	22.
0.0	0.2	28.15
0.05	0.2	27.39
0.15	0.2	25.07
0.27	0.2	23.48
0.41	0.2	22.94
0.5	0.2	22.
0.05	0.28	37.27
0.1	0.28	29.50
0.15	0.28	26.57
0.21	0.28	25.01
0.27	0.28	23.89
0.33	0.28	23.89
0.5	0.28	22.
0.05	0.32	42.22
0.1	0.32	30.74
0.15	0.32	27.29
0.21	0.32	25.35
0.27	0.32	24.
0.33	0.32	23.41
0.41	0.32	22.92
0.5	0.32	22.
0.0	0.37	51.09

0.05	0.37	40.89
0.1	0.37	32.31
0.15	0.37	27.60
0.21	0.37	25.1
0.27	0.37	23.83
0.33	0.37	23.34
0.41	0.37	22.87
0.5	0.37	22.
0.0	0.43	38.59
0.05	0.43	34.57
0.1	0.43	29.94
0.15	0.43	26.52
0.21	0.43	24.48
0.27	0.43	23.48
0.33	0.43	23.1
0.5	0.43	22.
0.0	0.5	28.75
0.05	0.5	28.45
0.1	0.5	26.27
0.15	0.5	24.3
0.21	0.5	23.17
0.27	0.5	22.67
0.33	0.5	22.49
0.41	0.5	22.35
0.5	0.5	22.

Q=10W DP=1CM

Tamb = 23.0

r	z	T
0.0	0.0	23.
0.1	0.0	23.
0.21	0.0	23.
0.33	0.0	23.
0.41	0.0	23.
0.5	0.0	23.
0.0	0.09	25.5
0.15	0.09	25.05
0.27	0.09	24.13
0.41	0.09	23.78
0.5	0.09	23.
0.0	0.2	31.20
0.05	0.2	30.13
0.15	0.2	27.09
0.27	0.2	24.94
0.41	0.2	23.91
0.5	0.2	23.
0.05	0.28	46.77
0.1	0.28	33.75
0.15	0.28	29.48
0.21	0.28	27.08
0.27	0.28	25.50
0.33	0.28	24.67
0.5	0.28	23.
0.05	0.32	57.01
0.1	0.32	36.54
0.15	0.32	30.85
0.21	0.32	27.67
0.27	0.32	25.5
0.33	0.32	24.63
0.41	0.32	23.80
0.5	0.32	23.
0.0	0.37	80.29

0.05	0.37	58.38
0.1	0.37	40.89
0.15	0.37	32.18
0.21	0.37	27.66
0.27	0.37	25.52
0.33	0.37	24.54
0.41	0.37	23.69
0.5	0.37	23.
0.0	0.43	59.56
0.05	0.43	49.69
0.1	0.43	38.38
0.15	0.43	31.17
0.21	0.43	26.89
0.27	0.43	24.92
0.33	0.43	24.15
0.5	0.43	23.
0.0	0.5	39.86
0.05	0.5	39.49
0.1	0.5	32.43
0.15	0.5	27.13
0.21	0.5	24.57
0.27	0.5	23.67
0.33	0.5	23.31
0.41	0.5	23.08
0.5	0.5	23.

Q=18W DP=1CM

Tamb = 21.0

r	z	T
0.0	0.0	21.
0.1	0.0	21.
0.21	0.0	21.
0.	0.0	21.
0.41	0.0	21.
0.5	0.0	21.
0.0	0.09	24.99
0.15	0.09	24.46
0.27	0.09	23.30
0.41	0.09	22.41
0.5	0.09	21.
0.0	0.2	33.06
0.05	0.2	30.67
0.15	0.2	27.03
0.27	0.2	24.33
0.41	0.2	22.66
0.5	0.2	21.
0.05	0.28	55.75
0.1	0.28	35.78
0.15	0.28	30.11
0.21	0.28	26.97
0.27	0.28	25.01
0.33	0.28	23.84
0.5	0.28	21.
0.05	0.32	73.38
0.1	0.32	40.35
0.15	0.32	32.13
0.21	0.32	27.92
0.27	0.32	25.28
0.33	0.32	23.74
0.41	0.32	22.50
0.5	0.32	21.
0.0	0.37	118.09

0.05	0.37	78.17
0.1	0.37	48.34
0.15	0.37	34.66
0.21	0.37	28.08
0.27	0.37	25.11
0.33	0.37	23.61
0.41	0.37	22.30
0.5	0.37	21.
0.0	0.43	85.89
0.05	0.43	67.41
0.1	0.43	46.21
0.15	0.43	34.21
0.21	0.43	27.30
0.27	0.43	24.23
0.33	0.43	23.02
0.5	0.43	21.
0.0	0.5	54.96
0.05	0.5	52.82
0.1	0.5	38.55
0.15	0.5	28.25
0.21	0.5	23.76
0.27	0.5	22.28
0.33	0.5	21.70
0.41	0.5	21.26
0.5	0.5	21.

Q=5W DP=2CM
Tamb = 20.0

r	z	T
0.0	0.0	20.
0.1	0.0	20.
0.21	0.0	20.
0.33	0.0	20.
0.41	0.0	20.
0.5	0.0	20.
0.0	0.09	21.24
0.15	0.09	21.15
0.27	0.09	20.68
0.41	0.09	20.59
0.5	0.09	20.
0.0	0.2	23.22
0.05	0.2	22.64
0.15	0.2	21.79
0.27	0.2	21.06
0.41	0.2	20.68
0.5	0.2	20.
0.05	0.28	26.92
0.1	0.28	23.94
0.15	0.28	22.46
0.21	0.28	21.88
0.27	0.28	21.22
0.33	0.28	20.93
0.5	0.28	20.
0.05	0.32	37.06
0.1	0.32	25.30
0.15	0.32	23.29
0.21	0.32	21.83
0.27	0.32	21.31
0.33	0.32	20.97
0.41	0.32	20.60
0.5	0.32	20.
0.0	0.37	48.72

0.05	0.37	33.55
0.1	0.37	26.55
0.15	0.37	23.80
0.21	0.37	22.02
0.27	0.37	21.18
0.33	0.37	20.92
0.41	0.37	20.53
0.5	0.37	20.
0.0	0.43	42.40
0.05	0.43	34.34
0.1	0.43	27.49
0.15	0.43	24.08
0.21	0.43	21.82
0.27	0.43	21.08
0.33	0.43	20.72
0.5	0.43	20.
0.0	0.5	36.06
0.05	0.5	30.17
0.1	0.5	24.17
0.15	0.5	22.15
0.21	0.5	20.88
0.27	0.5	20.56
0.33	0.5	20.40
0.41	0.5	20.38
0.5	0.5	20.

Q=7.5W DP=2CM

Tamb = 21.0

r	z	T
0.0	0.0	21.
0.1	0.0	21.
0.21	0.0	21.
0.33	0.0	21.
0.41	0.0	21.
0.5	0.0	21.
0.0	0.09	21.67
0.15	0.09	21.58
0.27	0.09	21.37
0.41	0.09	20.05
0.5	0.09	21.
0.0	0.2	23.76
0.05	0.2	23.13
0.15	0.2	22.20
0.27	0.2	21.48
0.41	0.2	21.33
0.5	0.2	21.
0.05	0.28	28.24
0.1	0.28	24.65
0.15	0.28	23.04
0.21	0.28	22.39
0.27	0.28	21.70
0.33	0.28	21.46
0.5	0.28	21.
0.05	0.32	41.38
0.1	0.32	26.38
0.15	0.32	24.04
0.21	0.32	22.41
0.27	0.32	21.86
0.33	0.32	21.56
0.41	0.32	21.33
0.5	0.32	21.
0.0	0.37	57.03

0.05	0.37	36.93
0.1	0.37	28.13
0.15	0.37	24.82
0.21	0.37	22.74
0.27	0.37	21.82
0.33	0.37	21.58
0.41	0.37	21.37
0.5	0.37	21.
0.0	0.43	51.46
0.05	0.43	39.30
0.1	0.43	29.94
0.15	0.43	25.49
0.21	0.43	22.75
0.27	0.43	21.91
0.33	0.43	21.56
0.5	0.43	21.
0.0	0.5	43.38
0.05	0.5	34.69
0.1	0.5	26.16
0.15	0.5	23.46
0.21	0.5	21.98
0.27	0.5	21.65
0.33	0.5	21.62
0.41	0.5	21.55
0.5	0.5	21.

Q=10 W DP=2CM

Tamb = 21.9

r	z	T
0.0	0.0	21.9
0.1	0.0	21.9
0.21	0.0	21.9
0.33	0.0	21.9
0.41	0.0	21.9
0.5	0.0	21.9
0.0	0.09	22.78
0.15	0.09	22.70
0.27	0.09	22.21
0.41	0.09	22.12
0.5	0.09	21.9
0.0	0.2	25.05
0.05	0.2	24.39
0.15	0.2	23.42
0.27	0.2	22.64
0.41	0.2	22.21
0.5	0.2	21.9
0.05	0.28	30.32
0.1	0.28	26.08
0.15	0.28	24.32
0.21	0.28	23.62
0.27	0.28	22.86
0.33	0.28	22.52
0.5	0.28	21.9
0.05	0.32	47.28
0.1	0.32	28.10
0.15	0.32	25.45
0.21	0.32	23.65
0.27	0.32	23.01
0.33	0.32	22.58
0.41	0.32	22.16
0.5	0.32	21.9
0.0	0.37	75.82

0.05	0.37	41.31
0.1	0.37	30.31
0.15	0.37	26.41
0.21	0.37	23.98
0.27	0.37	22.92
0.33	0.37	22.55
0.41	0.37	22.11
0.5	0.37	21.9
0.0	0.43	63.68
0.05	0.43	45.66
0.1	0.43	32.98
0.15	0.43	27.28
0.21	0.43	23.90
0.27	0.43	22.84
0.33	0.43	21.35
0.5	0.43	21.9
0.0	0.5	53.05
0.05	0.5	40.22
0.1	0.5	28.30
0.15	0.5	24.61
0.21	0.5	22.65
0.27	0.5	22.22
0.33	0.5	22.02
0.41	0.5	21.97
0.5	0.5	21.9

B.2 Momentum Transfer Experimental Results

As discussed in Chapters 3 and 4, measurements of the time-varying pressure at the surface of the beds were logged via an A-D converter by an IBM compatible XT computer. Measurements on eight different beds and three different orifice sizes were taken, at 7 or more different reciprocation frequencies. Since at least five hundred points were logged for each reciprocation frequency, this means that 3500 points were logged for each run, giving over 38 000 data points in total. It is clearly impractical to report each one of these points on paper, so the table below lists only amplitude and lag with respect to piston position. The table below summarises the runs which were performed; the results of each run are summarised in the pages which follow:

Table B.1 - Pneumatic Test Experimental Beds

Bed	Description
1	230 mm of 2 mm
2	340 mm of 2 mm
3	455 mm of 2 mm
4	350 mm of 0.5mm
5	70 mm of 2 mm on top of 350 mm of 0.5mm
6	130 mm of 2 mm on top of 240 mm of 0.5mm
7	200 mm of 2 mm on top of 240 mm of 0.5mm
8	200 mm of 2 mm on top of 240mm of 0.5mm (repeat 2 weeks later)
S	3 mm diam. orifice
M	6 mm diam. orifice
L	10 mm diam. orifice

230mm of 2mm

w (rad/s)	Amplitude (Pa)	Lag (s)
5.8	970	0.71
7.4	970	0.63
8.7	970	0.56
10.2	980	0.52
11.6	960	0.49
13.3	990	0.47
14.6	1010	0.45

340mm of 2mm

w (rad/s)	Amplitude (Pa)	Lag (s)
4.6	747	0.98
5.6	768	0.82
6.6	798	0.74
7.5	828	0.68
8.0	858	0.65
8.3	848	0.53
9.0	889	0.62
9.9	899	0.60
11.0	949	0.56
12.5	1020	0.52
13.8	1100	0.51

455mm 2mm

w (rad/s)	Amplitude (Pa)	Lag (s)
2.8	535	1.13
3.8	535	0.91
4.7	555	0.79
6.1	565	0.68
7.6	585	0.60
8.8	656	0.57
10.0	666	0.52
11.4	676	0.49
12.8	717	0.46
14.1	717	0.44
16.0	727	0.42
18.0	828	0.41

350mm of 0.5mm

w (rad/s)	Amplitude (Pa)	Lag (s)
2.8	727	1 56
3.7	797	1.19
4.5	838	1.02
5.4	878	0.88
6.2	929	0.77
7.2	989	0.72
8.1	1070	0.68
9.0	1161	0.67
9.9	1232	0.65
10.8	1272	0.61
12.0	1353	0.60
13.4	1464	0.55

70mm of 2mm on 350mm of 0.5mm

w (rad/s)	Amplitude (Pa)	Lag (s)
2.2	626	1.66
3.5	666	1.24
4.8	737	0.97
5.7	777	0.84
6.7	848	0.75
7.8	888	0.68
9.0	929	0.68
10.1	1070	0.68
11.7	1211	0.62
13.8	1525	0.57
15.8	2322	0.60
18.0	2979	0.54

130mm of 2mm on 200mm of 0.5mm

w (rad/s)	Amplitude (Pa)	Lag (s)
1.9	710	1.76
2.8	830	1.29
3.5	900	1.10
4.3	980	0.95
5.3	1160	0.85
6.2	1430	0.77
7.2	1600	0.70
7.9	1540	0.66
8.8	1630	0.60
9.9	2120	0.59
10.8	2630	0.54
11.9	3450	0.51
12.8	4490	0.49
14.6	5540	0.45

200mm of 2mm on 240mm of 0.5mm

w (rad/s)	Amplitude (Pa)	Lag (s)
3.6	525	1.20
4.3	555	1.06
5.3	606	0.91
6.4	646	0.80
7.1	677	0.74
8.2	717	0.66
8.9	737	0.65
9.9	788	0.71
11.3	858	0.61
12.2	990	0.64
13.4	1151	0.59

200mm of 2mm on 240mm of 0.5mm (repeat)

w (rad/s)	Amplitude (Pa)	Lag (s)
2.3	585	1.45
3.1	504	1.13
3.7	494	0.97
4.4	515	0.90
5.3	585	0.79
6.1	575	0.72
6.9	616	0.68
7.7	575	0.64
8.7	646	0.59
9.4	706	0.56
10.2	767	0.54
11.3	868	0.51
12.3	1040	0.49

3mm hole

w (rad/s)	Amplitude (Pa)	Lag (s)
2.1	6989	1.90
2.9	11866	1.46
3.7	16512	1.24
4.2	20148	1.13
5.0	25076	1.03
5.9	30702	0.90
7.2	37822	0.77
7.8	41357	0.69

6mm hole

w (rad/s)	Amplitude (Pa)	Lag (s)
2.8	1300	1.31
4.0	2300	1.05
4.6	2800	0.96
5.3	3500	0.88
5.8	4200	0.83
6.4	4900	0.78
7.1	5800	0.73
7.6	6600	0.71
8.9	8500	0.64
9.9	10000	0.61
10.6	11100	0.58
11.5	12600	0.56
12.7	14100	0.53

10mm hole

w (rad/s)	Amplitude (Pa)	Lag (s)
2.9	50	1.00
[illegible] 1	272	0.85
5.2	504	0.78
6.2	747	0.72
7.1	989	0.67
8.5	1444	0.63
9.2	1696	0.58
10.0	1939	0.55
11.0	2252	0.53
11.9	2565	0.51
12.9	2898	0.49

Appendix C Heat Transfer Modelling

C.1 Two dimensional modelling

The two-dimensional conductive convective model equations were so-ved using an iterative Galerkin finite element method, described in detail by Zienkiwicz (1977). Fig. C.1 shows the 15x15 graded mesh used; the shaded portion shows the position and extent of the heater.

The general program structure is described in the documents "DESCRIPTION OF FEPDE" and "PDFELM" which follow. Also contained in the document are a number of examples which were used to verify the validity of the code.

	r	z
1	0.00000	0.0000
2	0.00461	0.1210
3	0.01630	0.2186
4	0.03500	0.3026
5	0.07175	0.3800
6	0.11286	0.4554
7	0.16633	0.5400
8	0.23610	0.6095
9	0.32678	0.6600
10	0.44093	0.7668
11	0.57716	0.8405
12	0.72486	0.9052
13	0.86294	0.9561
14	0.96311	0.9887
15	1.0000	1.000

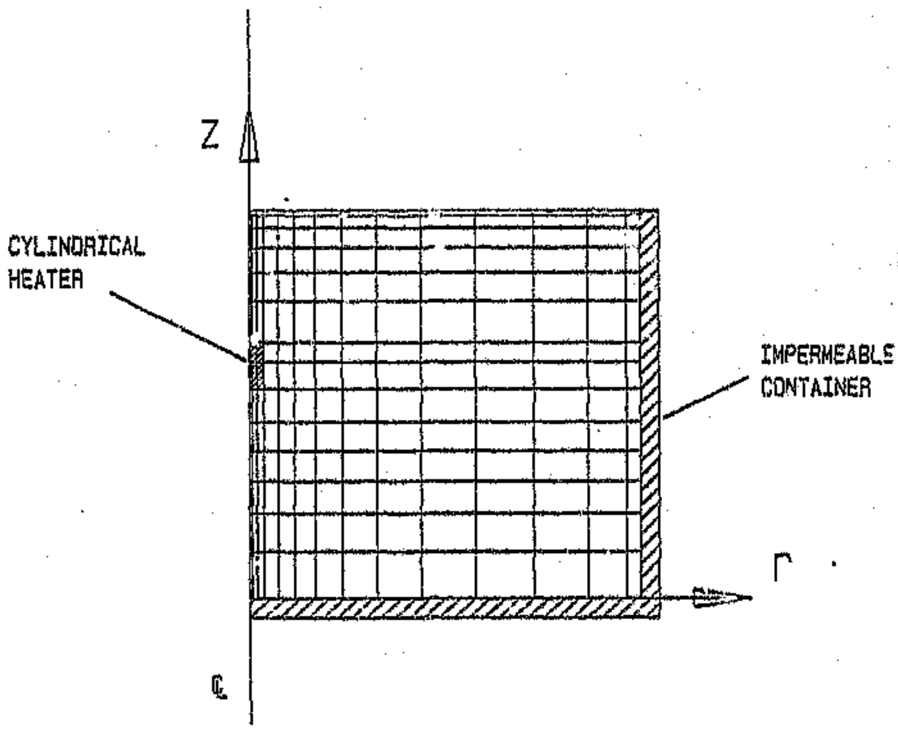

Fig. C.1 Finite Element Grid and Coordinates

Description of 'FEPDE' - a finite element code for the solution of systems of steady-state, two-dimensional non-linear partial differential equations

P. Anderson.

Department of Chemical Engineering
University of the Witwatersrand
1986

INTRODUCTION

'FEPDE' has been written to solve systems of nonlinear, linked partial differential equations using finite element methods. The finite element method was chosen for its versatility and ability to handle the complex form of equations and boundary conditions encountered in practice.

Knowledge of finite element theory is required to set up and solve a problem using 'FEPDE'. An adequate introduction to finite element theory may be found in the 'NAG Finite Element Library - Level 1' manual (1983). The data structure and coding of 'FEPDE' is based on the example program 'NAGFE3F2 FORTRAN', which may be found in the Level 1 manual, as well as on the 'ENGINEERING' disk on the Wits mainframe.

Overview of 'FEPDE'

The code may be divided into two 3 major sections:

1) Main section

This section sets up common blocks and reads in all the data required, eg. mesh geometry and topology, experimental measurements, output checking flags and so on. The nodal freedom array 'NF' (which is used in the assembly of element contributions into the final system matrix 'SYSK') is contructed from the user-supplied mesh and boundary condition data (see below). Any model parameters required are read in by the main program.

2) Subroutine 'FELMNT'

This is the section of program that actually calculates the 'element stiffness' matrices 'ELK', which are derived from the derivative terms in the equation(s), as well as the element vector 'XTVEC', which accounts for any other terms in the equation, such as energy generation ('heat source') terms or constants. The abovementioned vector and array are defined in user supplied subroutines (see below). These element contributions are assembled into the system matrix and vector 'SYSK' and 'RHS' by the routines 'ASUSM' and 'ASRHS' respectively, using the 'steering' vector 'NSTER' which is derived from element topology data by the subroutine 'DIRECT'.

Dirichlet and Cauchy boundary conditions are included by the Payne-Irons method, and a boundary integral, respectively.

3) Subroutines defining the equations and boundary conditions. These are divided as follows:

3.1) Subroutine 'EQNS'

This subroutine defines the equations resulting from the finite element analysis of the original partial differential equations. The contributions from each variable and each equation are calculated separately, and may depend on any variable dependent or independent), or the gradient of any dependent variable. See example below.

3.2) Subroutine 'SOURCT'

This subroutine calculates the contribution from source terms (which may be distributed or concentrated) or constants. The value returned by 'SOURCT' may depend on any variable (dependent or independent), or the gradient of any dependent variable.

3.3) Subroutine 'BFUNM'

This subroutine calculates the contributions of the dependent variables in the boundary conditions to the system matrix. Again, contributions from each variable and equation are calculated separately. The boundary condition terms may depend on any variable (dependent or independent), or the gradient of any dependent variable

3.4) Subroutine 'BFUNV'

This subroutine calculated the contributions of constants in the boundary conditions to the right-hand side matrix 'RHS'. Contributions from each equation are calculated separately. The boundary conditions may depend on any variable (dependent or independent), or the gradient of any dependent variable.

3.5) Function 'H'

This function calculates the dirichlet condition for the equations. The value may depend on any variable (dependent or independent) or the gradient of any dependant variable. Values for each equation are calculated separately.

3.6) Functions 'FXY' and 'DFXY'

'FXY' ['DFXY'] evaluates the value of [gradient of] any dependent variable given element number and position within the element [and direction in which gradient is required].

4) Service Subroutines

These are as follows:

4.1) Subroutines 'ASMAT' and 'ASVEC'

This assembles equation/variable matrix-contributions into the element matrix. This is best described by an example.

Eg. if the following equations are to be solved

$$P(\Phi) + Q(\Psi) = R(\underline{x})$$

$$S(\Phi) + T(\Psi) = U(\underline{x})$$

Where P, Q, S, and T are differential operators operating in R^2 (i.e. (x,y)).

Identify the contributions from P, Q, S, T with p, q, s, t respectively.

The element matrix contribution, e^1 from Φ in A may be written
as follows (assuming three noded triangular elements for example):

$$e_p = \begin{matrix} p & p & p \\ p & p & p \\ p & p & p \end{matrix} \qquad \text{similarly for } Q, S, T$$

Where the subscript P denotes contribution from that operator

e_P to e_T are then assembled into the overall element matrix as follows:

$$
E_{ele} = \left|\begin{array}{cccccccc}
\circ & q & \circ & q & \circ & q & \circ & q \\
s & t & s & t & s & t & s & t \\
\circ & q & \circ & q & \circ & q & \circ & q \\
s & t & s & t & s & t & s & t \\
\circ & q & \circ & q & \circ & q & \circ & q \\
s & t & s & t & s & t & s & t \\
\circ & q & \circ & q & \circ & d & \circ & q \\
s & t & s & t & s & & s & t
\end{array}\right|
$$

The 'p entries have been replaced with a $_\circ$ to clarify the assembly process. It is clear from the above demonstration that the matrices contributed by each variable are 'stretched' out and placed in a nNxnN matrix, where N is the number of variables, and n is the number of nodes per element. The above matrix is contructed by 'ASMAT', given e_P ... e_T.

Similarly the right hand side contributions are assembled by 'ASVEC' as follows:

$$
RHS_{ele} = \left|\begin{array}{c}
r \\ u \\ r \\ u \\ r \\ u \\ r \\ u
\end{array}\right|
$$

The boundary condition matrices and vectors as described in section 3 are subjected to the same assembly operations.

4.2) Subroutine 'SEPRT'

The solution of the system of linear equations defined by [SYSK|RHS] is in the form of a vector of length Nxtotal number of nodes. 'SEPRT' separates this lumped vector into arrays FVAL(i,j) where i denotes variable number, and j denotes node number. The value of any particular variable at any node are thus readily availableduring execution. This is useful and economical in cases where iteration is required.

<u>PDFELM</u>

A Finite Element Code for the Solution of

a General System of Steady or Unsteady

Nonlinear Partial Differential Equations

by:

P. Anderson (MSc(Eng))

and

S.M. Bradshaw (MSc(Eng))

Department of Chemical Engineering

University of the Witwatersrand

1987

CONTENTS

1 Introduction 182

1.1 General considerations and background 182

1.2 Who should use "PDFELM" ? 182

2 Brief Outline of Method of Solution 183

3 Applications 184

3.1 Simulation of rivulet flow - a single, linear partial differential equation 184

3.2 Simulation of steady thermal conduction in a composite medium - a single, nonlinear partial differential equation 186

3.3 Simulation of natural convection heat transfer in a porous annulus - two linked nonlinear partial differential equations 190 190

3.4 Fitting measured temperature data to a model - least-squares estimation of parameters 190

3.5 Summary 193

4 Operational Details 193

4.1 Data structure 193

4.2 General program structure 193

4.3 Format of the nodal data file 194

REFERENCES 198

1 Introduction

1.1 General considerations and background.

The general class of problem soluble by "PDFELM" is as follows:

$$M\ [\Phi_t, \Phi] = K\ [\Phi] \qquad (1/1)$$

Where M is an operator, operating linearly on the *first* time derivative of Φ. The l.h.s. of (1/1) takes the form of a linear sum of first order time-derivatives, whose individual coefficients may be nonlinear in spatial derivatives if necessary.

K is a general, nonlinear operator, operating on spatial derivatives of Φ of any order below that of the shape functions employed.

Note: Application of Green's theorem reduces the order of the spatial derivatives, thus expanding the applicability range of any given shape function.

The current "PDFELM" implementation uses the Galerkin weighted residual method, though only minor changes would be necessary to change this (to a collocation method, for example).

"PDFELM" 's predecessor ("FEPDE", Anderson, 1986), was designed to solve only the steady-state analogue of (1/1). It therefore a comparatively small task to extend the code and (structure to solve the unsteady-state problem as well.

The preliminary finite element analysis of the left and r.h. sides of (1/1) is discussed in detail in many texts, Norrie and de Vries (1973), for example. Assembly of r.h.s. contributions into a single matrix and a vector is discussed in detail by Anderson (1986). Assembly of l.h.s. contributions (into the matrix 'SYSM', the time-derivative multiplier) is done in a similar fashion.

1.2 Who should use "PDFELM" ? (or 'What is the purpose of this manual? ')

The mathematical sophistication required by finite-element methods exceeds that of the average user; moreover, some preliminary finite-element analysis on a problem is necessary before it can be submitted to "PDFELM". There are also various control options which must be correctly chosen if the program is to operate at maximum efficiency. As a result, this program is *not* a tool for beginners.

Therefore, the purpose of this manual is to:

a) inform those persons *au fait* with finite-element methods of the format of the program and required data, so that they may use it if necessary.

b) inform a wider audience of the type of problem soluble by the program, so that they may request instruction in the setting up of their particular problem, if applicable.

2 Brief Outline of Method of Solution

Finite-element analysis of equation (1/1) yields:

$$SYSM(\underline{\Phi}) \frac{\partial \underline{a}}{\partial t} = SYSK(\underline{\Phi})\underline{\Phi} + \underline{f}(\underline{x},\underline{\Phi}) \qquad (2/1)$$

Where SYSM and SYSK are matrices (both may depend on the dependent variable Φ as shown)

$\underline{a}$ is the time dependent part of Φ (where $\Phi = \underline{N} \cdot \underline{a}$)
$\underline{N}$ are the shape functions, dependent only on $\underline{x}$
$\underline{f}$ is a vector

Details of the composition of the above matrices and vectors are discussed in detail by Anderson (1986).

· for an unsteady-state solution, the system (2/1) is solved for $\partial \underline{a}/\partial t$ (r.h.s evaluated at the current time value) using supplied initial conditions. The solution is then advanced in time by a multistep method or by Gear's method.

· for a steady-state solution, the r.h.s. of (2/1) is equated to zero, and the resulting expression solved iteratively for Φ until successive values satisfy a user-specified convergence criterion.

Note: if the *coefficients* of the time derivatives do not depend on

Φ or t, (this can be seen by inspection) the user can set a flag which ensures that the matrix *'SYSM'* is assembled and decomposed (into upper and lower triangular matrices) only *once* during unsteady simulations, right at the start. This has a darmatic effect on run times, since solution of (2/1) during successive time-marching steps requires only 'back-substitution' into the triangular matrices. As the total number of degrees of freedom in a problem increases, reduction of 'SYSM' rapidly begins to dominate overall solution time.

3 Applications

Some sample problems (with solutions) which have been solved using the program are summarised below. Many of the results have been checked against published data; these checks are ommited here for the sake of brevity.

3.1 Simulation of Rivulet Flow - a single, linear partial differential equation.

The equation describing potential flow, in a wall-bound vertical rivulet, for example, is:

$$\frac{\partial v_z}{\partial t} = \frac{\mu}{\rho} \nabla^2 v_z - g_z$$

The boundary conditions are shown on fig. 1. Initial condition is $v_z = 0$ over the domain Ω.

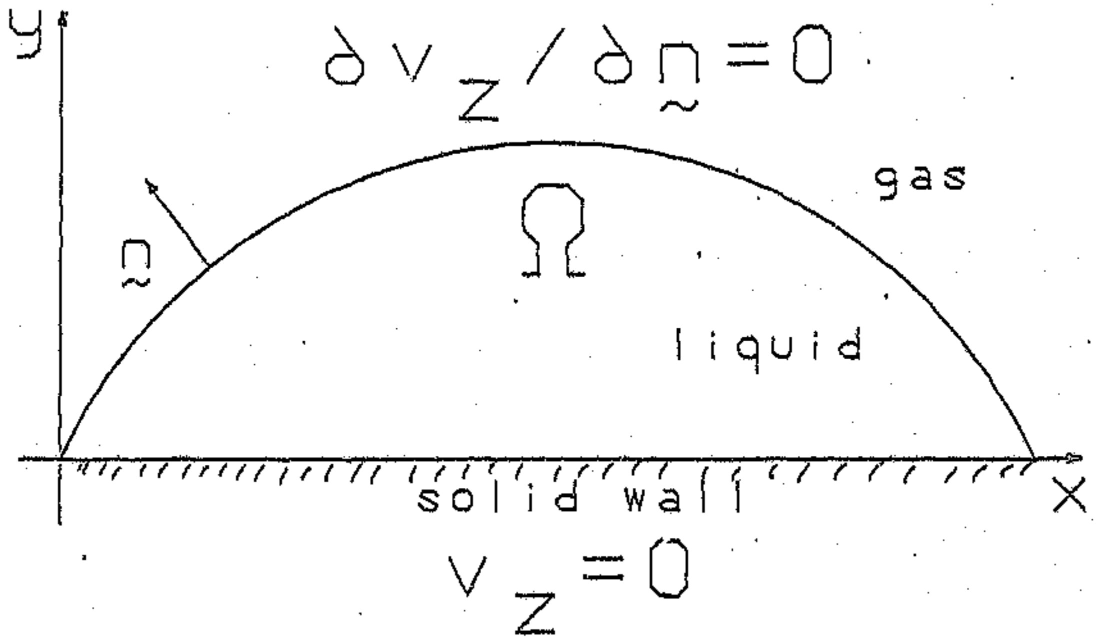

Fig. 1

Fig. 2 shows the steady-state velocity profile in a rivulet; note the maximum velocity at the furthermost edge of the rivulet (marked with a ·)

Fig. 3 shows the evolution of the maximum velocity with time.

This kind of analysis is relevant to the design of solid-fluidd chemical reactors, such as 'trickle-beds'.

3.2 Simulation of steady thermal conduction in a composite medium - a single nonlinear partial differential equation.

The equation describing steady thermal conduction in a composite medium whose conductivity depends on both position and temperature is as follows:

$$\nabla . \left[k(x,y,\theta) \nabla \theta \right] = 0$$

Boundary conditions are as shown in fig. 4; variation of thermal conductivity with position is also shown.

A temperature-position surface is shown in fig. 5 for the case where conductivity depends linearly on θ, $k(x,y,\theta) = k(x,y)[1+\theta]$. Fig. 6 shows the temperature along the vertical centreline, i.e. $x=0.5$. The 'step' resulting from the highly conductive core is clearly visible here.

Calculations of this sort are used to estimate thermal energy transfer in glass-fibre reinforced plastics and steel-concrete composites, for example.

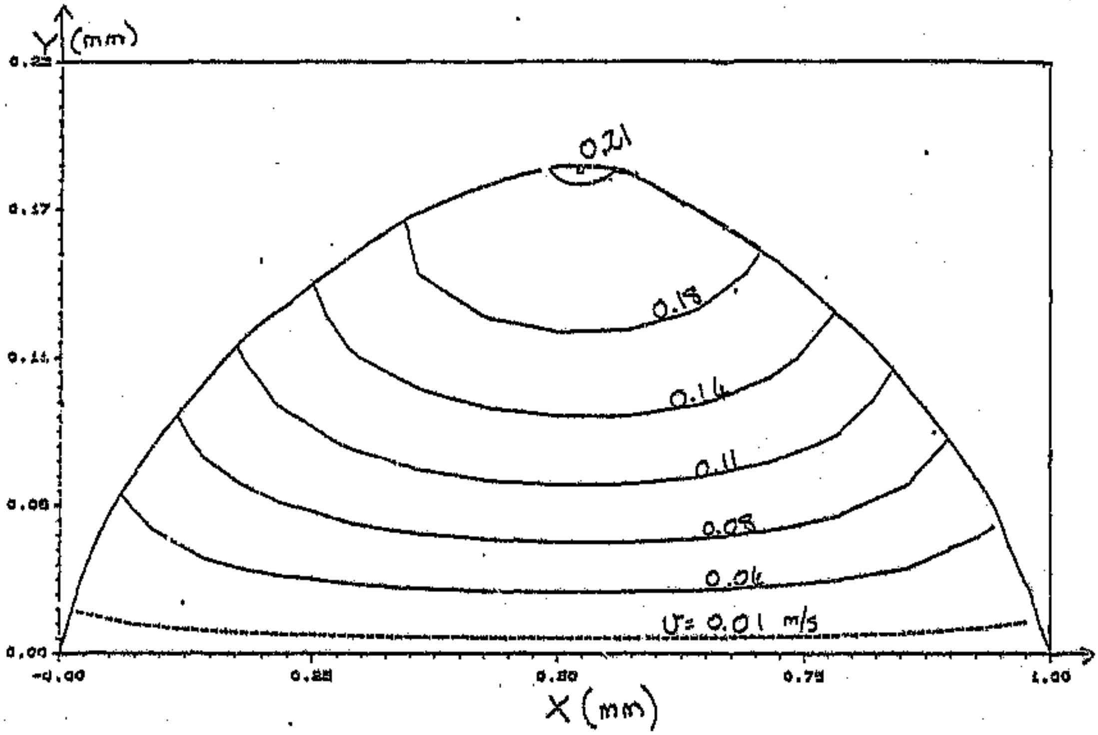

Fig. 2

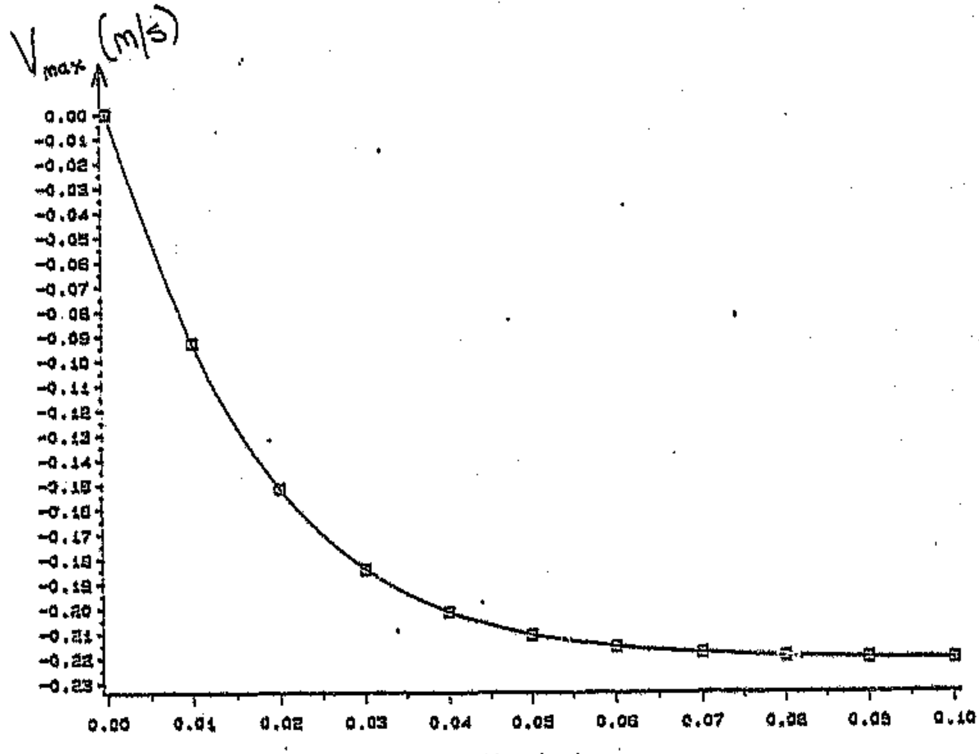

Fig. 3

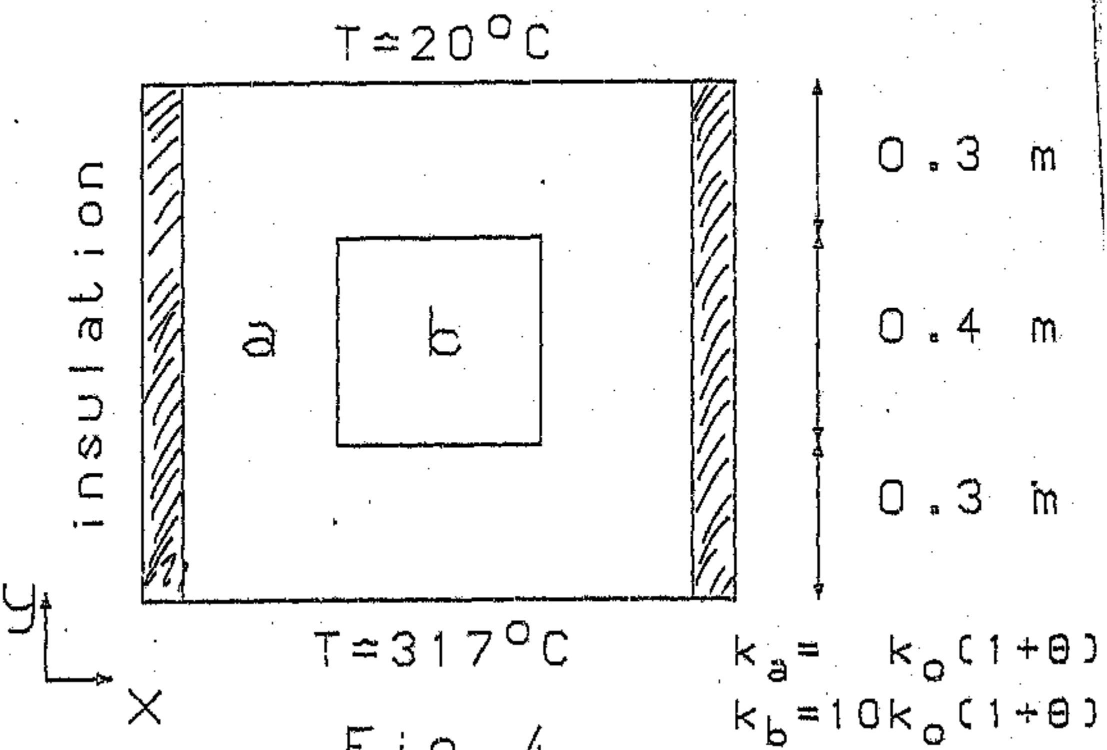

T ≈ 20°C
insulation
a
b
0.3 m
0.4 m
0.3 m
y
x
T ≈ 317°C
$k_a = k_o(1+\theta)$
$k_b = 10k_o(1+\theta)$

Fig. 4

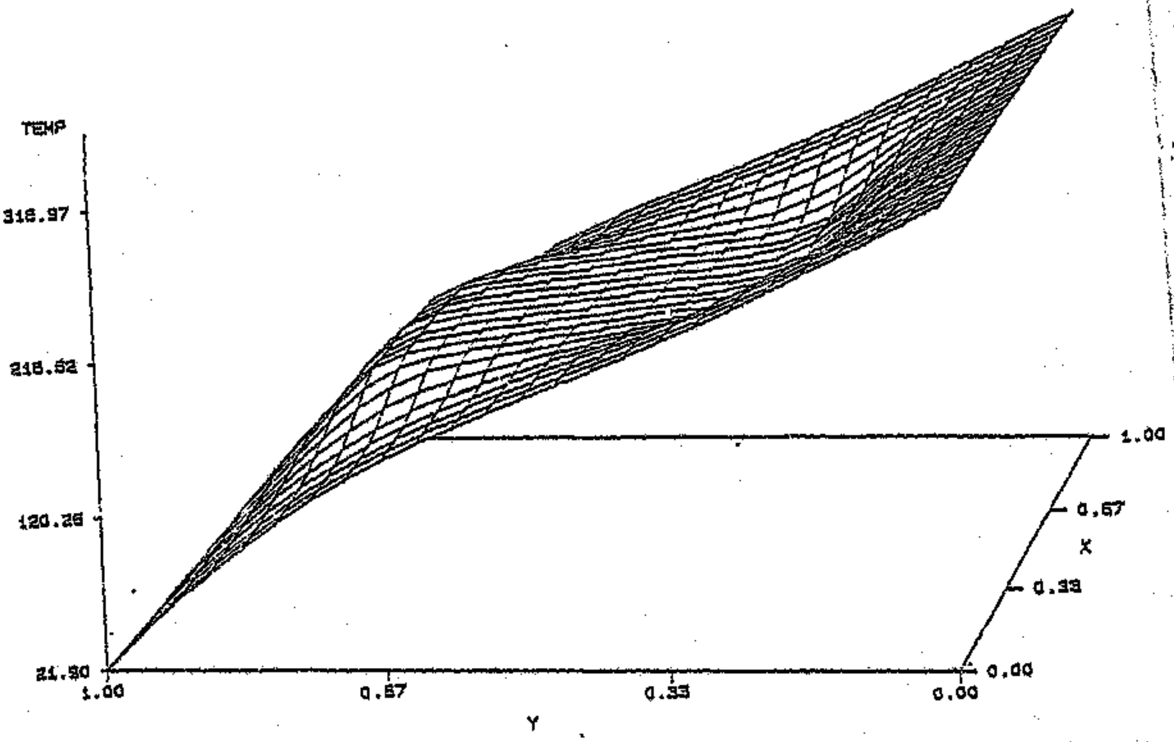
TEMP
316.97
216.62
120.26
21.90
1.00
0.67
0.33
0.00
Y
1.00
0.67
X
0.33
0.00

Fig. 5

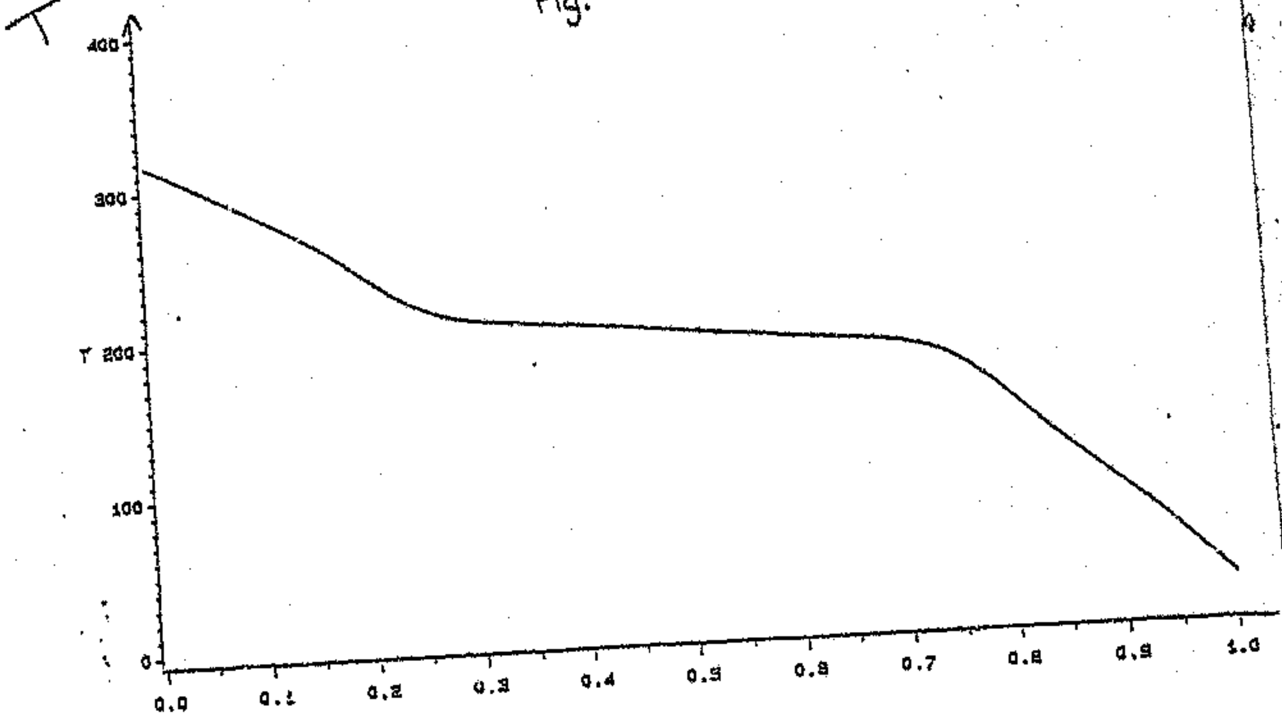
T
400
300
Y 200
100
0
0.0
0.1
0.2
0.3
0.4
0.5
0.6
0.7
0.8
0.9
1.0

Fig. 6

3.3 Simulation of natural convection heat transfer in porous annulus - two linked nonlinear partial differential equations

The equations describing free convection in this case are as follows:

$$\frac{\partial^2 \Psi}{\partial r^2} - \frac{1}{r}\frac{\partial \Psi}{\partial r} + \frac{\partial^2 \Psi}{\partial z^2} = r \, Ra \, \frac{\partial \theta}{\partial r}$$

$$\left[\frac{1}{r}\frac{\partial \Psi}{\partial z}\right]\frac{\partial \theta}{\partial r} - \left[\frac{1}{r}\frac{\partial \Psi}{\partial r}\right]\frac{\partial \theta}{\partial z} - \frac{\partial^2 \theta}{\partial r^2} - \frac{1}{r}\frac{\partial \theta}{\partial r} - \frac{\partial^2 \theta}{\partial z^2} = 0$$

Where the streamfunction, Boussinesq approximation and Darcy law have been used to simplify the full equations (see Bejan 1984 for details).

Appropriate boundary conditions and dimensions are shown in fig. 7.

Results for a Rayleigh number (Ra) of 300 are presented. Fig. 8 shows the streamlines, and fig. 9 shows the isotherms.

Such calculations are used to evaluate the average Nusselt number for heat transfer through layers of insulation around steam pipes, and heat-leaks into cryogenic installations, for example.

3.4 Fitting measured temperature data to a model - least-squares estimation of parameters.

The sum of squares of temperature prediction errors for some experimental measurements was minimised by variation of the Rayleigh number and a heat transfer coefficient. For experimental details and numerical results, see Anderson (1987). Fitted results predicted permeabilities (embedded in Ra) of the same order of magnitude as those estimated using known physical quantities (particle size, viscosity, etc.).

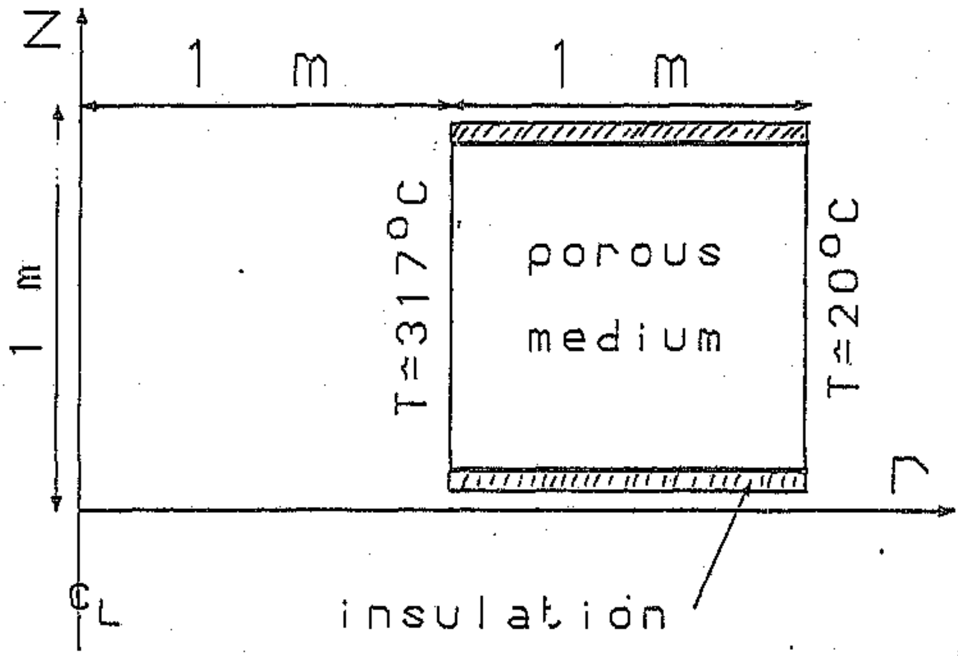

Fig. 7

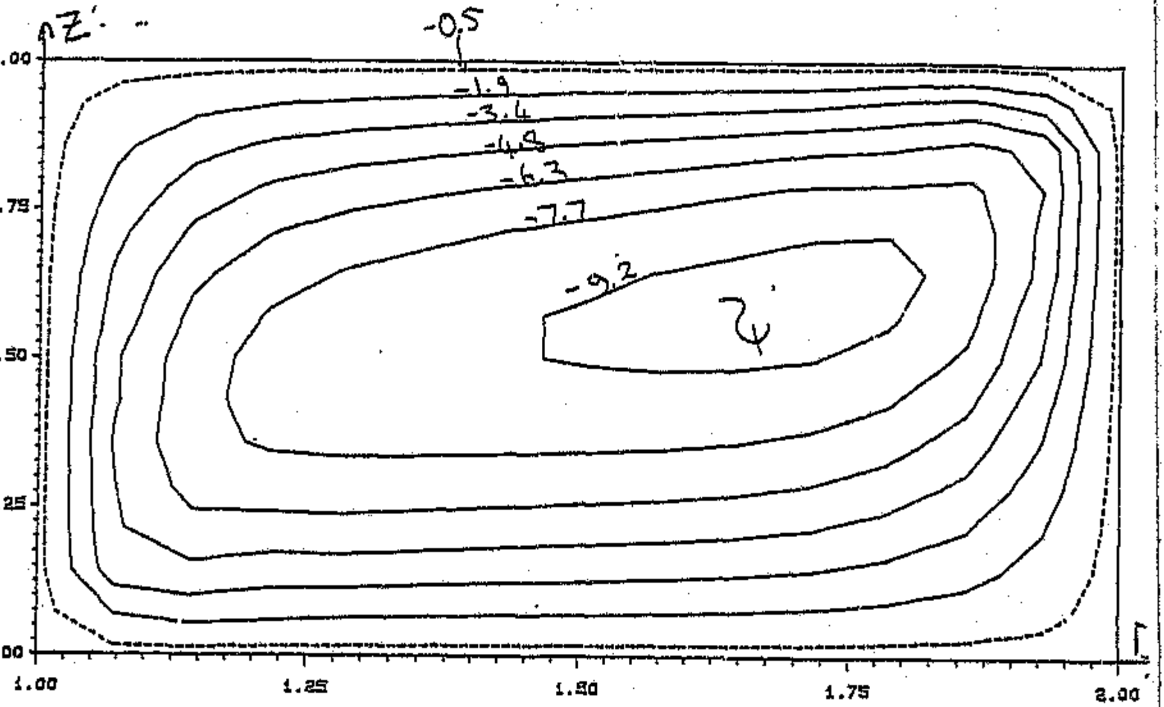
Z'
-0,5
-1.9
-3.4
-4.8
-6.3
-7.7
-9.2
Ψ
1.00
0.75
0.50
0.25
0.00
1.00
1.25
1.50
1.75
2.00
r

Fig. 8

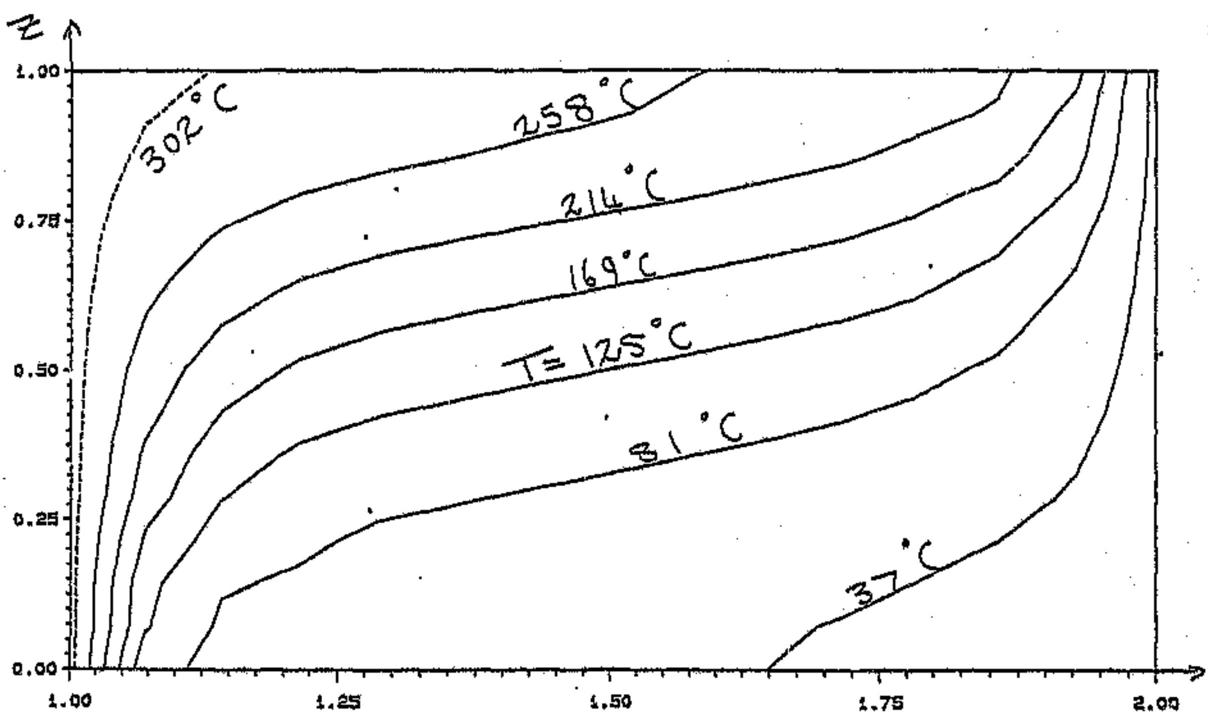
Z
302°C
258°C
214°C
169°C
T=125°C
81°C
37°C
1.00
0.75
0.50
0.25
0.00
1.00
1.25
1.50
1.75
2.00

Fig. 9

—

3.5 Summary

The four problem types described above are merely representative of the range of problems soluble by 'PDFELM'. A more general description of solvable equations is given in section 1.

4 Operational Details

4.1 Data structure

The data structure of 'PDFELM' has been built up (considerably) from that of a 'NAG' example program. Variable and common-block names are self explanatory, and far too numerous to list here. The significance and format of user supplied data (element geometry, topology etc.) are detailed in section 4.3, in order to assist the user to set up the required data file.

4.2 General program structure

Program, subprogram and function subprogram names are self explanatory. The main program and control subroutines are kept in a file called 'PDFELM FORTRAN', and the service and output control routines are kept in 'PDSUBS FORTRAN'. The reason for this is that normally only service routines (such as that which defines the equations to be solved, and boundary conditions) need to be edited and compiled by the user. This separation saves compilation time.

All subroutines of interest to the general user are listed and described in the 'FEPDE' manual (Anderson, 1986).

4.3 Format of the nodal data file

no. of nodes — spatial dimension — no. of equations

(*list of nodes - format as follows*)

node number — x-coord y-coord ...... as reqd.

element type — no. of elements — nodes per element

(*list of element topology - format as follows*)

element number — node1 node2 node3 node4 ....

no. of boundary condn. lists for variable 1 *

bndry. condn type	nodes per side	number of nodes in this list

list of bndry. nodes *in groups of ten*

inner bracket repeated - see *

outer bracket repeated (per variable as req'd)

no. of lists of 'extraction' nodes +

extrctn. var.	no. of extrcn. nodes	(list of nodes)

bracket repeated - see +

flag for manual check of convergence criteria

list of parameters req'd by problem.

ϵ_o	ϵ_{max}	no. of contin'n steps	flag for trace of convgnce.	flag for contin'n#	task flag

start. time	end time	no. of t steps

flag for SYSM characteristics (time or Φ dependent ?)

---

notes:

- 'Extraction' nodes. Although values at all nodes are printed at each step, it is often desirable to extract values at specific nodes (eg. centreline temperatures) and print them to a separate file. This facility allows such manipulations to be done conveniently

- #Continuation. The continuation method (see de Villiers, 1984) may be implemented if necessary. Parameters ϵ_0, ϵ_{max} and the number of continuation steps are essential data if this option is selected.

- flags set to zero cause bypass of feature

- task flag at present takes on values of 0,1,2,3,4.
  0 ⇒ single steady-state simulation
  1 ⇒ fit parameters to a model by minimization of sum of squared errors. This requires experimental data and means of interpolation.
  4 ⇒ unsteady state simulation.

For purposes of clarification, a sample nodal datafile is given below. This datafile is for (see fig. 10 for details):

- steady state solution (task flag=0) of a single equation over a domain of square cross section, using 9 quadrilateral elements of the 8 noded type.

- a Dirichlet (type 1) boundary condition is applied along the bottom edge (y=0); derivative (type 2) boundary conditions are applied along the remaining edges.

- Function values at the nodes on the positive-slope diagonal (bottom-left to top right) are extracted, hence '1' list.

- Convergence criteria checking is automatic.

- Convergence is traced by screen output.

- Continuation is employed, with ε advanced from 0 to 1 in 7 steps.

- Time stepping data and SYSM characteristics are irrelevant in this case.

SAMPLE DATA FILE

```
    9           2           1
    1           0.0         0.0
    2           0.166       0.0
    3           0.333       0.0
                .
                .
                .
   38           0.666       1.0
   39           0.833       1.0
   40           1.000       1.0

1       1    8    12   13   14    9    3    2
2       3    9    14   15   16   10    5    4
3       5   10    16   17   18   11    7    6
        .
        .
        .
9      27   32    38   39   40   33   29   28

2
2   3   19
             1   8   12   19   23   30   34   35   36   37
            38  39   40   33   29   22   18   11    7
1   3    5
             2   3    4    5    6
1
1   4        1  14   27   40
param1    param2    param3 .....
0
0       1.0  7   1   1   0
 (SYSM characteristics flag)
```

REFERENCES

Anderson P., 1986. *Description of 'FEPD[illegible]' - A User's Manual.* Dept. of Chemical Engineering, University of the Witwatersrand, Johannesburg.

Anderson P., 1987. *Anisotropic Transfer of Thermal Energy in Porous Media*, PhD progress report, Dept. Of Chemical Engineering, University of the Witwatersrand, Johannesburg.

Bejan A., 1984. *Convection Heat Transfer*, John Wiley & Sons, New York.

De Villiers N., 1984. *Continuation methods for the solution of nonlinear problems in engineering science*, PhD thesis, University of the Witwatersrand.

Norrie D., de Vries G. 1973. *The Finite Element Method*, Academic Press, New York.

C.2 One dimensional modelling

C.2.1 Derivation of the model equations

Application of an energy balance, the Boussinesq assumption (i.e. ρ_g constant except where it appears in buoyancy terms, implying that v_z is assumed constant) and the Darcy law to the one-dimensional geometry shown in Fig. 5.1.7 yields the following equations, in dimensionless form:

$$\frac{\partial^2\theta}{\partial\zeta^2} = v_z^* \frac{\partial\theta}{\partial\zeta} \tag{C.1}$$

At the bottom of the bed air flow is driven by the thermal convection induced by the power input q. It is is assumed that no energy is lost from this end, and so the boundary condition can be written:

$$-\left.\frac{\partial\theta}{\partial\zeta}\right|_{\zeta=0} + v_z^* \left.\theta\right|_{\zeta=0} = \frac{qL}{k_b T_0} \tag{C.2}$$

Heat transfer at the free surface can be modelled by a constant heat transfer coefficient and so this boundary condition is given by

$$-\left.\frac{\partial\theta}{\partial\zeta}\right|_{\zeta=1} = \mathrm{Bi}\left.\theta\right|_{\zeta=1} \tag{C.3}$$

The general solution to (C.1) is:

$$\theta(\zeta) = C_1 + C_2 \exp\left(\zeta v_z^*\right) \tag{C.4}$$

Insertion of the boundary conditions gives the equation of the temperature profile, equation (5.2). However, the velocity term in (5.2) is still unknown. This may be calculated by applying the Darcy law and Boussinesq assumption:

$$v_z = \frac{-K}{\mu}\left(\frac{\partial P}{\partial z} + \rho_g g\right) \quad \text{(Darcy law)} \tag{C.5}$$

Substituting for the pressure gradient using the Boussinesq approximation gives:

$$v_z = \frac{-K}{\mu}\left(-\rho_g^o\, g + \rho_g g\right)$$

$$= \frac{K\, g\, \rho_g^o}{\mu}\left(1 - \frac{T_o}{T}\right) \tag{C.6}$$

Nondimensionalising (C.6), and integrating both sides between $\zeta=0$ and $\zeta=1$ (remembering that v_z is constant under the Boussinesq assumption) gives equation (5.1), which is the desired result.

C.2.2 'LAYER', a FORTRAN 77 program to calculate internal energy dissipation within porous bodies from surface temperatures.

Listing of FORTRAN 77 program 'LAYER' follows. Program calculates surface temperature for various layer depths, surface heat- transfer coefficients, Rayleigh numbers, and energy inputs.

```
      IMPLICIT REAL*8 (A-H,O-Z)
      EXTERNAL FVQ
      COMMON /HTRANS/ BI, Q, XLEN, RA, KNTR
      DIMENSION RGUES(2), XH(3)
              XH(1)=3.0D0
              XH(2)=7.0D0
              XH(3)=11.0D0
      Y1=1.00D0
      V=1.10D0
      QA=1.00D0
      XLEN=1.00D0
          DO 999 NC=1,3
          HCOEF=XH(NC)
      DO 10 KNTR=4, 4004, 4000
        XLEN=KNTR/40.0D0
        DO 10 I=1,10
          QA=I/2.0D-1.0
          EPS=1.0D-9
          EPS2=1.0D-6
          ETA=4.0D0
          NSIG=5
          N=1
          ITMAX=1000
          TO=273.15D0+21.9E0
          TKB=0.16D0
          BI=HCOEF*XLEN/TKB
          Q=QA*XLEN/TKB/TO
          RGUES(1)=V
C               FIND ROOT OF EQUATION
```

```
         CALL ZREAL2(FVQ, EPS, EPS2, ETA, NSIG, N, RGUES, ITMAX, IER)
         V=RGUES(1)
         IF (IER.GT.0) THEN
            WRITE(4,*) 'IER = ',IER, XLEN, V
            STOP
         END IF
C                EVALUATE FUNCTION, VERIFY THAT A ROOT HAS BEEN FOUND
         FF=FVQ(V)
C                CALCULATE TEMPERATURE AT Y1 (Y=1)
         THT=THET(Y1,V)
         WRITE(4,*) TO*THT, QA
10    CONTINUE

999         CONTINUE
      STOP
      END

      DOUBLE PRECISION FUNCTION FVQ(VEL)
      IMPLICIT REAL*8 (A-H,O-Z)
      COMMON /HTRANS/ BI, Q, XLEN, RA, KNTR
C  FUNCTION  EVALUATES  TO  0  WHEN  CORRECT  VELOCITY
        IS SUBSTITUTED.  NUMERICAL OVERFLOW IS PREVENTED
      RA=400.0D0*XLEN
      V=VEL
      FVQ=0.00D0
      ANS3=0.00D0
      IF (V.LT.133.0) THEN
         ANS1=(-DEXP(V)*Q*V-DEXP(V)*V**2-DEXP(V)*V*BI)
         ANS2=(-DEXP(V)*Q*V-DEXP(V)*Q*BI-DEXP(V)*V**2-DEXP(V)*V*BI+Q*BI)
         ANS3=DLOG(ANS1/ANS2)
      END IF
      ANS=(RA*(ANS3+Q))/(Q+V)
      FVQ=V-ANS
      RETURN
      END
C
      DOUBLE PRECISION FUNCTION THET(Y,VEL)
      IMPLICIT REAL*8 (A-H,O-Z)
```

```
      COMMON /HTRANS/ BI, Q, XLEN, RA, KNTR
      V=ABS(VEL)
C     THET=(Q*(-EXP(V*Y)*BI+DEXP(v)*V+DEXP(V)*BI))/(DEXP(V)*V*(V+BI))
C           SIMPLE EXPRESSION, VALID FOR Y=1 ONLY
      THET=Q/(BI+V)
      RETURN
      END
```

C.3 Application of the layer model to realistic situations

Application of the model to estimation of energy dissipation from surface temperatures is described in detail in section 5.1.2. The listing of the program follows. Note that the program is suited to radially symmetrical temperature profiles, as measured in the laboratory. Extension to arbitrarily varying surface temperatures merely requires a two dimensional spline to interpolate measured temperatures instead of a one dimensional cubic spline as below.

Listing of FORTRAN 77 program 'SURFACE' follows. Program calculates total energy release by integrating the energy flux over the upper surface. Experimental temperature-coordinates are read in from a data file. Program is currently set up to deal with radially symmetric data, though extension to the general case is simple. The program was verified by comparing results to manual calculations on simple temperature profiles.

```
      EXTERNAL TRAD
      COMMON /SPLN/ J, X(30),Y(30), C(50,3), NPTS, IC, PI
      COMMON /FITP/ PAR(3)
      WRITE(4,*) 'POLAR COORDINATES'

        LISTING OF COEFFICIENTS FOR BEST FIT APPROXIMATION
        OF Q(ΔT) = PAR(1)*ΔT^PAR(2)
        PAR(1) & PAR(2) ARE DEPENDENT ON h AND TEMPERATURE
        RANGE AS SHOWN.

C                    h = 3   W/sq.m.K    0 < dT <  2.5
C     PAR(1)=3.891124
C     PAR(2)=1.153728
C                                        0 < dT < 10.0
C     PAR(1)=3.429993
C     PAR(2)=1.210146
C                    h = 7   W/sq.m.K    0 < dT <  2.5
C     PAR(1)=8.249110
C     PAR(2)=1.117403
```

```
C                                                    0 < dT < 10.0
C       PAR(1)=7.199935
C       PAR(2)=1.217635
C
C                    h =10.8 W/sq.m.K        0 < dT <  0.45
C       PAR(1)=11.80815
C       PAR(2)=1.028961
C                                                    0 < dT <  1.0
C       PAR(1)=12.31927
C       PAR(2)=1.04809
C                                                    0 < dT < 10.0
        PAR(1)=11.48116
        PAR(2)=1.154058
C
        PI=3.1415926
        IC=50
        J=0
        AERR=0.0
        RERR=1.0E-4
C READ IN NUMBER OF EXPERIMENTAL TEMPERATURE POINTS
        READ (1,*) NPTS
C  READ  TEMPERATURE  /  COORDINATES
        DO 10 I=1,NPTS
10  READ  (1,*)  Y(I),  X(I)
C                 APPLY ARTIFICIAL OFFSET TO TEMPERATURES
C                 TO PREVENT PROBLEMS WHEN RAISING
C                 VERY SMALL NUMBERS TO POWERS
        DO 11 I=1,NPTS
11      Y(I)=Y(I)-Y(NPTS)+0.001
        X0=0.00E0
        X1=X(NPTS)
C                 FIT CUBIC SPLINE TO SURFACE TEMPERATURE PROFILE
        CALL ICSCCU (X, Y, NPTS, C, IC, IER)
C                 INTEGRATE ENERGY FLUX OVER SURFACE,
C                 BY INTEGRATING Q(dT) OVER SURFACE
        XNTG=DCADRE (TRAD, X0, X1, AERR, RERR, ER, IER)
        WRITE(4,*) 'INTEGRAL = ',XNTG, Y(NPTS)
        WRITE(2,*) XNTG
```

```
      STOP
      END
C
      REAL FUNCTION TRAD (XX)
      COMMON /SPLN/ J, X(30),Y(30), C(50,3), NPTS, IC, PI
      REAL XNTRP(1), YNTRP(1)
        J=J+1
        NNTRP=1
        XNTRP(1)=XX
C               EVALUATE TEMPERATURE AT INTERMEDIATE POINT XX
        CALL ICSEVU (X, Y, NPTS, C, IC, XNTRP, YNTRP, NNTRP, IER)
C               CALCULATE ENERGY FLUX AT POINT XX
        DQA=QVST(DT)
C               MULTIPLY FLUX BY ANNULAR AREA BETWEEN R & R+dR
        TRAD=2.0*PI*XX*DQA
      RETURN
      END
C
      REAL FUNCTION QVST(DT)
C               FUNCTION CALCULATES ENERGY FLUX FROM SURFACE
                TEMPERATURE DIFFERENCE
      COMMON /FITP/ PAR(3)
      QVST=PAR(1)*(DT**PAR(2))
      RETURN
      END.
```

Appendix D Momentum transfer modelling

D.1 Derivation of unsteady model equations

The equations will be developed here for cartesian geometry for the sake of clarity. Assuming laminar flow, the Darcy law is used to describe velocity dependence on the local pressure gradient. A mole balance on the fluid is as follows:

$$(\rho vA)\Big|_x = (\rho vA)\Big|_{x+\Delta x} + A\epsilon\Delta x\,\frac{\partial\rho}{\partial t}$$

Substituting the Darcy law for v in the above equation and taking limits as $\Delta x \to 0$ gives:

$$\frac{\partial}{\partial x}\left(\rho\,\frac{K}{\mu}\,\frac{\partial P}{\partial x}\right) = \epsilon\,\frac{\partial\rho}{\partial t} \qquad \text{(D.1)}$$

Substituting the ideal-gas law in the above equation, and assuming:

i) isothermal operation
ii) μ independent of pressure

gives the desired result:

$$\frac{\partial}{\partial x}\left(KP\,\frac{\partial P}{\partial x}\right) = \epsilon\mu\,\frac{\partial P}{\partial t} \qquad \text{(D.2)}$$

The following initial and boundary conditions are common to all cases considered in this work:

$$P(x,0) = P_{amb} \quad \text{(D.3)} \qquad\qquad \frac{\partial P}{\partial x}\Big|_{x=L} = 0 \quad \text{(D.4)}$$

The first indicates that initially the porous layer is at ambient pressure, and the second imposes the no-flow condition at the solid wall or at any location L, where L is large enough that the pressure disturbance does not extend that far. Note that the larger the frequency of reciprocation (see below), the smaller L may be made in comparison to the true extent of the bed.

The boundary condition at x=0 is obtained via a material balance over a 'system' which includes the reciprocating device as well as the porous medium, and assumes ideal-gas behaviour:

$$\left[P_c(t)V_c(t) + \int_0^L P(x,t)\epsilon A dx\right]\Bigg|_{t=0} = P_c(t)V_c(t) + \int_0^L P(x,t)\epsilon A dx$$

Where $P_c(t)$ is the pressure inside the reciprocating chamber, and ϵ may be a function of x. Regarding geometry and the interpretation of A, the same argument as presented in D.1.2.1 applies.

The above equation may be solved for $P_c(t)$ to give:

$$P_c(t) = \frac{P_c(0)V_c(0) - \int_0^L \epsilon A\left[P(x,t) - P(x,0)\right]dx}{V_c(t)} \qquad \text{(D.5)}$$

Which is the desired result. A noteworthy feature of the above equation is that the instantaneous pressure profile P(x,t) is required in order to evaluate and apply the boundary condition.

$P_o(t)$ is the pressure imposed at the surface, which may, as indicated, be a function of time.

D.1.2 Simplification for incompressible fluids

D.1.2.1 Development of a semi-lumped parameter model

In reality, the resistance to flow of the gas is distributed over a region of the bed, radiating from the point of contact of the reciprocating device. Manipulation of the above solution which assumes incompressibility is difficult due to the transient nature of the equation. A lumped parameter model was therefore developed to make manipulation less complex. The system modelled is shown in Fig. D.4.1. The resistances are concentrated at the hole connecting one chamber to another.

The model is developed by performing a mole balance on the chambers:

For the first chamber, whose volume varies sinusoidally about a mean volume $V_{1,0}$:

$$\frac{dn_1}{dt} = \frac{P_1}{RT}\frac{dV_1}{dt} + \frac{V_1}{RT}\frac{dP_1}{dt} = v_1 A_1 \rho_{1m}$$

where ρ_{1m} is the molar density of the gas in chamber 1, and the ideal gas law is used to relate pressure, volume, and moles in each chamber. The above equation is solved for dP_1/dt:

$$\frac{dP_1}{dt} = \frac{v_1 A_1 \rho_{1m} RT}{V_1} - \frac{P_1}{V_1}\frac{dV_1}{dt} \qquad (D.6)$$

Coulson and Richardson (1977) present an equation expressing the flowrate of gas through an orifice for small pressure drops. This equation is restated as follows, to give molar flow:

$$v_1 \rho_{1m} A_1 = \frac{C_d \left(-2\Delta P \rho_1\right)^{1/2}}{M} = \text{molar flowrate through orifice 1}$$

here ρ is once again the mass density of the gas, and M is the molecular weight of the gas, and ΔP is the pressure difference across orifice 1, $= P_2 - P_1$

The above equation is substituted into (D.6), and linearised about some ΔP_o to give

$$\frac{dP_1}{dt} = \frac{\kappa_1 \left(P_2 - P_1\right)}{V_1} - \frac{P_1}{V_1}\frac{dV_1}{dt} \tag{D.7}$$

$$\text{where } \kappa_1 = \frac{C_d RT \left(\frac{-2\rho_1}{\Delta P_o}\right)^{1/2}}{M}$$

For relatively small deviations in P_1 and V_1, the above equation is linear. The same procedure is followed for each chamber, with the simplification that the term dV/dt is zero for all but the first chamber. For these other chambers, it is necessary to consider flow through both holes which connect to each chamber.

The general result is:

$$\frac{dP_n}{dt} = \frac{\kappa_{n-1}\left(P_{n-1} - P_n\right)}{V_n} + \frac{\kappa_n\left(P_{n+1} - P_n\right)}{V_n} \tag{D.8}$$

For chamber N, the result is simply obtained by setting $\kappa_N = 0$.

The resulting system of equations may be written as follows:

$$\frac{d\underset{\sim}{P}}{dt} = \underset{\approx}{K}\,\underset{\sim}{P} + \underset{\sim}{B} \tag{D.9}$$

Where the elements of the matrix K are as follows:

$$K_{ii} = \frac{-\kappa_{i-1} - \kappa_i}{V_i} \qquad K_{i,i-1} = \frac{\kappa_{i-1}}{V_i} \qquad K_{i,i+1} = \frac{\kappa_i}{V_i}$$

Note that $\kappa_0 = \kappa_N = 0$ in the above, and that all other terms of the matrix K are zero.

The initial conditions for the system of ODE's are:

$$P_i(t=0) = P_{amb} \quad i=1,..,N \qquad (D.10)$$

The only nonzero term of the vector B is the last member of the right hand side of equation (D.7), i.e. $-P_1/V_1\ dV_1/dt$. Recall that the term P_1/V_1 must be linearised if the equations are to be solved analytically. The term is therefore as follows, for the case of a sinusoidally varying volume:

$$\underset{\sim}{B}_1 = \frac{P_1^o}{V_1^o}\frac{dV_1}{dt} = \frac{P_1^o}{V_1^o}\Delta V.\omega.\cos(\omega t) \qquad (D.11)$$

Where ΔV is the maximum deviation of V_1 about the mean.

It may be justifiably argued that the above linearisation is inadequate in that κ approaches infinity as ΔP approaches zero. This is true, but since the flow will always be finite, and ω always approach zero as ΔP approaches zero, such a linearisation is considered sufficient for these purposes. Furthermore, the relative values of the κ are of interest, not the absolute values.

All other terms are zero. This is easily recognisable as the tridiagonal matrix common to all systems of serially connected bodies, see Tse, Morse and Hinkle (1978). Note that the system of equations (D.9) is soluble by analytical methods, such as decomposition using eigenvalues, see Kreyszig (1983).

NOTE

For the purposes of the derivation of the solution, it has been assumed here that all eigenvalues are real, and less than or independant. This validity of this assumption was verified for each of the calculation cases presented below:

According to this method, the solution is written as follows:

(For convenience, all of the above may be written in the deviation variable φ, where $\varphi_i = P_i - P_{amb}$.)

$$\underset{\sim}{\varphi} = \underset{\approx}{F}\,\underset{\sim}{G} \tag{D.12}$$

$$\varphi_i(t=0) = 0 \tag{D.13}$$

where F is the matrix of linearly independent eigenvectors correspc ding to the eigenvalues of the matrix K, and vector G is calculated as follows:

$$\dot{\underset{\sim}{G}} = \left\{ \underset{\approx}{F}^{-1}\underset{\approx}{K}\,\underset{\approx}{F} \right\} \underset{\sim}{G} + \underset{\approx}{F}^{-1}\underset{\sim}{B} \tag{D.14}$$

$$= \underset{\approx}{D}\,\underset{\sim}{G} + \underset{\sim}{E}$$

Since all the terms of B (except the first) are zero, the vector E is simply (refer equation D.10 for the expression for B_1):

$$E_i = F^{-1}_{i,1} \quad B_1 = F^{-1}_{i,1} \quad \frac{P_1^o}{V_1^o}\,\Delta V.\omega.\cos(\omega t) \tag{D.15}$$

It is a property of the matrices F and K that the term inside { } in (D.14) evaluates to a diagonal matrix, which we shall call matrix D, whose elements are the eigenvalues of matrix K (i.e. $K_{ii} = \lambda_i$). The individual, single variable first-order equations for G_i may be easily solved using any suitable method, to give:

$$G_i = \exp(-\lambda_i t)\cdot\left[\int \exp(-\lambda_i t)\ E_i(t)\ dt + C_i\right] \tag{D.16}$$

The arbitrary constants C_i are determined by applying the initial condition (D.13) and equation (D.12). Since $\varphi_i=0$ for all i at t=0, the same applies to $G_i(t=0)$. Substitution of (D.15) into (D.16), integrating as indicated, and substitution of t=0 gives $G_i(t=0) = C_i$. The arbitrary constants C_i are therefore all zero.

Equation (D.16) is therefore developed to give:

$$G_i = \left[\frac{-\lambda_i \cos(\omega t) + \omega \cdot \sin(\omega t) + \lambda_i \exp(-\lambda_i t)}{\omega^2 + \lambda_i^2} \right] \left(\frac{-P_i^o \omega \Delta V}{V_i^o} \right) \cdot F_{i,1}^{-1} \tag{D.17}$$

As expected, there is a transient period, which is of no interest here. Taking only large values of t simplifies the expression for G_i. The values of the actual pressure deviations in each compartment are determined according to (D.11); specifically, φ_1 is as follows:

$$\varphi_1 = \sum_{j=1}^{N} F_{1,j}\ G_j \tag{D.18}$$

Substituting (D.17) into D.18, and collecting coefficients of $\sin(\omega t)$ and $\cos(\omega t)$ gives:

$$\varphi_1 = \left[\frac{\sum_{j=1}^{N} F_{j,1}^{-1} F_{1,j} \omega^2}{\omega^2 + \lambda_j^2} \right] \cdot \sin(\omega t) - \left[\frac{\sum_{j=1}^{N} F_{j,1}^{-1} F_{1,j}\ \lambda_j\ \omega}{\omega^2 + \lambda_j^2} \right] \cdot \cos(\omega t) \tag{D.19}$$

which may be rewritten as $\varphi_1 = S_1 \cdot \sin(\omega t) - S_2 \cdot \cos(\omega t)$. Application of a standard trigonometry identity gives:

$$\varphi_1 = \left[S_1^2 + S_2^2\right]^{1/2} \cdot \sin\left(\omega t - \arctan(S_2/S_1)\right) \qquad (D.20)$$

which is the desired result.

D.1.2.2 Application of the model

The model was applied to the following cases, listed below. Also listed are the eigenvalues and corresponding eigenvectors. Note that eigenvalues are distinct and negative, or zero. For each case, the volumes of each chamber and the adjacent orifice 'permeabilities' are listed, followed by the corresponding Eigen matrix and eigenvalues. Following these is a table of calculated pressure in the first compartment and phase of this pressure with respect to the piston.

All of the results presented below have been calculated using $\Delta V = 0.025 m^3$. Notice that the low-frequency asymptote is

$$\lim_{\omega \to 0} P = P_{amb} \Delta V \cdot \left[\sum_{i=1}^{5} V_i\right]^{-1}$$

For the volumes as listed for the cases below, this limit is P=1.006 bar, i.e. $\varphi_1 = 0.006$ bar, as in the tables below.

The model results in the tables below have been plotted in Fig. 5.2.7, contained in Chapter 5. It will be seen that the amplitude-frequency behaviour is very similar to that for the distributed parameter numerically solved model. This lumped parameter model could be used to good effect in the development of an analytical procedure for the analysis of experimental data of this sort.

case a

κ_n	V_n
5.0	0.2
5.0	1.0
5.0	1.0
5.0	1.0
0.0	1.0

Matrix F - Eigen matrix

1.000	0.627	1.000	1.000	1.000
-0.250	0.209	0.624	0.893	1.000
0.062	-0.906	-0.925	0.307	1.000
-0.015	1.000	-0.735	-0.444	1.000
0.003	-0.428	0.836	-0.956	1.000

	λ_i
1	-31.250
2	-16.672
3	-9.398
4	-2.681
5	0.000

case a

w (rad/s)	φ_1 (bar)	lag (rad)	lag (s)
0.000	0.006	0.000	1.430
0.080	0.006	0.114	1.469
0.160	0.006	0.227	1.425
[illegible]	0.006	0.336	1.415
0.320	0.007	0.441	1.399
0.400	0.007	0.540	1.376
0.480	0.008	0.632	1.349
0.560	0.008	0.718	1.317
0.640	0.009	0.795	1.281
0.720	0.009	0.866	1.243
0.800	0.010	0.929	1.202
0.880	0.010	0.984	1.161
0.960	0.011	1.033	1.118
1.040	0.011	1.075	1.076
1.120	0.012	1.112	1.034
1.200	0.012	1.144	0.993
1.280	0.013	1.170	0.953
1.360	0.014	1.193	0.914
1.440	0.014	1.212	0.877
1.520	0.015	1.227	0.841

case b

κ_n	V_n
5.0	0.2
5.0	1.0
5.0	1.0
0.5	1.0
0.0	1.0

Matrix F - Eigen matrix

1.000	-0.729	1.000	-0.386	1.000
-0.250	-0.310	0.809	-0.376	1.000
0.062	1.000	-0.153	-0.321	1.000
-0.012	-0.565	-0.970	-0.226	1.000
0.000	0.020	0.114	1.000	1.000

	λ_i
1	-31.246
2	-14.373
3	-4.768
4	-0.613
5	0.000

case b

w (rad/s)	φ_1 (bar)	lag (rad)	lag (s)
0.000	0.006	0.000	1.858
0.080	0.006	0.146	1.885
0.160	0.006	0.280	1.828
0.240	0.007	0.394	1.749
0.320	0.007	0.486	1.639
0.400	0.008	0.560	1.517
0.480	0.008	0.620	1.399
0.560	0.009	0.670	1.291
0.640	0.009	0.714	1.197
0.720	0.010	0.754	1.116
0.800	0.010	0.791	1.047
0.880	0.011	0.825	0.988
0.960	0.011	0.857	0.937
1.040	0.012	0.888	0.893
1.120	0.012	0.918	0.854
1.200	0.013	0.946	0.819
1.280	0.013	0.973	0.788
1.360	0.014	0.998	0.760
1.440	0.014	1.022	0.734
1.[illegible]20	0.014	1.045	0.710

case c

κ_n	V_n
5.0	0.2
5.0	1.0
0.5	1.0
0.5	1.0
0.0	1.0

Matrix F - Eigen matrix

1.000	1.000	-0.237	-0.632	1.000
-0.247	0.636	-0.224	-0.624	1.000
0.048	-0.887	-0.150	-0.573	1.000
-0.001	0.055	1.000	0.323	1.000
0.000	-0.003	-0.579	1.000	1.000

	λ_i
1	-31.185
2	-9.112
3	-1.364
4	-0.339
5	0.000

case c

w (rad/s)	φ_1 (bar)	lag (rad)	
0.000	0.006	0.000	3.572
0.080	0.006	0.262	3.513
0.160	0.008	0.425	3.276
0.240	0.009	0.496	2.655
0.320	0.010	0.522	2.067
0.400	0.010	0.532	1.631
0.480	0.011	0.538	1.329
0.560	0.011	0.545	1.120
0.640	0.012	0.555	0.974
0.720	0.012	0.567	0.867
0.800	0.013	0.581	0.787
0.880	0.013	0.597	0.726
0.960	0.013	0.614	0.678
1.040	0.013	0.632	0.639
1.120	0.014	0.650	0.607
1.200	0.014	0.669	0.581
1.280	0.014	0.689	0.552
1.360	0.015	0.708	0.538
1.440	0.015	0.728	0.521
1.520	0.015	0.747	0.505

case d

κ_n	V_n
5.0	0.2
0.5	1.0
0.5	1.0
0.5	1.0
0.0	1.0

Matrix F - Eigen matrix

1.000	0.330	-0.792	-0.950	1.000
-0.203	0.307	-0.762	-0.940	1.000
0.003	-0.952	1.000	-0.329	1.000
0.000	1.000	0.848	0.460	1.000
0.000	-0.421	-0.927	1.000	1.000

	λ_i
1	-30.086
2	-1.687
3	-0.957
4	-0.270
5	0.000

case d

W (rad/s)	φ_1 (bar)	lag (rad)	lag (s)
0.000	0.006	0.001	7.429
0.080	0.008	0.490	6.945
0.160	0.010	0.654	6.122
0.240	0.012	0.654	4.086
0.320	0.014	0.619	2.723
0.400	0.015	0.585	1.932
0.480	0.016	0.558	1.461
0.560	0.017	0.539	1.163
0.640	0.018	0.524	0.962
0.720	0.018	0.513	0.819
0.800	0.019	0.506	0.713
0.880	0.019	0.50	0.632
0.960	0.020	0.49	0.568
1.040	0.020	0.493	0.516
1.120	0.020	0.492	0.474
1.200	0.021	0.491	0.439
1.280	0.021	0.491	0.409
1.360	0.021	0.492	0.384
1.440	0.021	0.494	0.362
1.520	0.022	0.497	0.343

D.2 PERIODIC - A FORTRAN 77 program which rigorously solves the one dimensional compressible model equations

A listing of program PERIODIC follows. Periodic solves the rigorous one dimensional compressible fluid model equations. Periodic uses NAG routine D03PGF to solve the partial differential equation (D.2); the boundary condition at x=0 is implemented by subroutine BNDY, and subroutine PRESXO. Subroutine PRESXO evaluates equation (D.5) by integrating the pressure profile.

The time step TSTP is selected initially so that D03PGF is called 4 000 times during each cycle of the piston (whose volume is calculated in subroutine VOLFT). If D03PGF does not require such small time steps, it merely interpolates backwards to determine the solution at the required time. This is repeated until sufficient points of the solution have been generated. Printed out solution is limited to maximum pressure and time lag.

```
PROGRAM PERIODIC
IMPLICIT REAL*8 (A-H, O-Z)
COMMON /DSCRET/ U(1,80), X(80)
DIMENSION WK(30000)
EXTERNAL BNDY, MONT, PDEF
EXTERNAL FCN, FCNJ
REAL*8 Y(1), YP(1), WARAY(5)
COMMON /BND/ U0, U1
COMMON /VEL/ VEL, COUNT
COMMON /PARAMS/ VO,DV, [illegible] A, XMU, TOL, H, TOLD, VFBED, SPHRC,
* PO,POLD, PHIO, ROO, DPART, PI, PI2, WRK(35), DTCOEF,ADJ,XDSC
* ,DPDX, XMOLW, BCONT, M, NDE, METH, MITER, INDEX, IWRK, NPTS

COMMON /IO/ ITERM, NOUT
REAL SDUMMY
COMMON /GEAR/ DUMMY(48), SDUMMY(4), IDUMMY(38)
COMMON /DBAND/ NLC, NUC
DATA IERR / 7/, IPAR /8/, LAG /9/, IPMX /16/
  ITERM=4
 READ (IPAR,*) PHIO
 READ (IPAR,*) DPART
 READ (IPAR,*) SPHRC
 READ (IPAR,*) VO
 READ (IPAR,*) DV
 READ (IPAR,*) XLEN
 READ (IPAR,*) WHZO
 READ (IPAR,*) WHZF
 READ (IPAR,*) ADJ
 PI=3.141592654D0
    WO=WHZO*(2.0D0*PI)
    WF=WHZF*(2.0D0*PI)
    WSTP=(WF-WO)/6.01
    WSTP=(WF-WO)/6.01
  A=PI*0.2D0**2/4.0D0
  RO=0.0D0
    PPRV=0.0D0
  DO 1103 XDSC=0.20,1.0000,0.1999
   WRITE(LAG,*)'DISCONTINUITY AT X = ',XDSC
```

```
        WRITE(IPMX,*)'DISCONTINUITY AT X = ',XDSC
      DO 789 W=W0, WF, WSTP
        TMAX =4.50D0*PI/W
        TSTEP=PI/4000.0D0/W
C           NOTE: ALL PRESSURES ARE REDUCED I.E. P=PRESSURE/PATM
        P0=1.0D0
        DVTPRV=-1.0D0
C
C  SET  PARAMETERS  FOR  SOLUTION  OF  O.D.E  DESCRIBING  B.C.
C           INITIAL CONDITION P* = 1.00E0
        INDEX=1
        IPRT=0
        NPMX=150
C
C           WRITE(LAG,*)'  FREQUENCY = ',W
            WRITE(4,*)' FREQUENCY = ',W
C           WRITE(IPMX,*)'FREQUENCY = ',W
            TOLD=0.00D0
            XMU=1.8D-5
            NDE=1
            TOL=1.0D-4
            H=1.0D-5
            NOUT=3
            DELT=0.02
            ABSER=1.0D-3
            RELERR=0.000D0
            INORM=0
            IWK=30000
            IWRK=35
            NPDE=1
            IU=1
            M=0
            IBAND=1
            IMON=0
            NPTS=80
            HX=1.0/FLOAT(NPTS-1)
            X(1)=0.00D0
            TS=0.0
```

```
            DO 20 I=2,NPTS
               X(I)=X(I-1)+DELT
               DELT=DELT*1.01D0
20          CONTINUE
            DO 30 I=1,NPTS
               U(1,I)=0.0D0
            X(I)=X(I)/X(NPTS)*XLEN
30          X(I)=(1.00D0-R0/XLEN)*X(I)+R0
C  INTEGRATE  FREE  VOLUME  IN  BED
            VFBED=0.0D0
            NN=NPTS-1
            DO 99 N=1,NN
              TMP1=PHI(X(N))
              TMP2=PHI(X(N+1))
              VFBED=VFBED+A*(TMP1+TMP2)/2.0D0*(X(N+1)-X(N))
99          CONTINUE
      WRITE(ITERM,*)' FREE BED VOLUME = ',VFBED
            IND = 0
            TOUT = 0.0D0
            NSTPS=TMAX/TSTEP
            NPMX=NSTPS/NPMX
            NSTPS=INT(TMAX/TSTEP)
            TOLD=0.00E0
            ICOUNT=0
           POLD=0.00D0
       WRITE(ITERM,*) 'INTERNAL PRESSURES PRINTED AT X= ',X(30)
       DO 100 XI = 1.0D-5, TMAX, TSTEP
           ICOUNT=ICOUNT+1
           TOUT = XI
           IFAIL = 0
       CALL D03PGF (NPDE, M, PDEF, BNDY, TS, TOUT, U, IU,NPTS,X,RELERR,
     *              ABSER,INORM, MONT, IMON, IBAND, WK, IWK,IND,IFAIL)
           IF (IFAIL.NE.0) WRITE(ITERM,*)'FAILURE OF D03PGF'
           IF (IFAIL.NE.0) WRITE(NOUT,*) 'FAILURE OF D03PGF'
           IF (IFAIL.NE.0) WRITE(LAG,*) 'FAILURE OF D03PGF'
           IF (IFAIL.NE.0) WRITE(IPMX,*) 'FAILURE OF D03PGF'
           IND = 1
C               CALCULATE INTERNAL PISTON PRESSURE MASS BALANCE
```

```
C  CALCULATE  INTERNAL  PISTON-PRESSURE  AT  1)K  2)K=INF. 3)K=0
           CALL PRESX0(TOUT, VOLM, POLD, PKINF, PK0)
           DVT=POLD-U(1,1)
C                 IF P IS LOCAL MAXIMUM, WRITE PMAX
           IF ((DVTPRV.GT.0.0).AND.(DVT.LT.0.0)) THEN
              DO 901 NLG=1,8
                 ILG=NLG-1
                 XLGT=(4.0*NLG+1.0)*PI/2.0/W
                 IF (XLGT.GT.TOUT) GO TO 902
901           CONTINUE
902           DUMY=(2.0*(ILG-1)+1.0)*PI/W
              WRITE(LAG,13) XLGT-TOUT, POLD, W
              WRITE(IPMX,13) POLD, PKINF, W
13                     FORMAT (3X,F8.5,3X,F8.5,3X,F7.4)
               WRITE(ITERM,*) U(1,1)-U(1,50)
           END IF
C                 IF P-P0=0, CALCULATE PHASE LAG
           DVTPRV=DVT
           PPRV=POLD
           ITEST=MOD(ICOUNT,NPMX)
           IF (ITEST.EQ.0) THEN
              IPRT=IPRT+1
              CALL VOLFT(VOLUME, TOUT)
              TRLIM=POLD
C             IF (TRLIM.LT.0.0D0) TRLIM=0.0D0
C             WRITE(NOUT,909)  TOUT, POLD, PK0
            END IF
           IF (IFAIL.NE.0) WRITE(ITERM,*)'ERROR - IFAIL = ',IFAIL
           COUNT=COUNT+1.0
100     CONTINUE
            WRITE(NOUT,*)' FREQUENCY = ',W
         IF (ABS(W-WF).LT.(0.8*WSTP)) THEN
            DO 567 JJ=1,NPTS
567          WRITE (NOUT,*) U(JJ,1), X(JJ)
         END IF
789   CONTINUE
1103     CONTINUE
900   CONTINUE
```

```
909  FORMAT  (3X,F10.4,3X,5(F10.7,2X))
      STOP
      END
C
      SUBROUTINE BNDY(NPDE, T, UX, IBND, P, Q, R)
      IMPLICIT REAL*8 (A-H, O-Z)
      REAL*8 P(NPDE), Q(NPDE), R(NPDE), UX(NPDE)
      COMMON /PARAMS/ VO,DV, W, A, XMU, TOL, H, TOLD, VFBED, SPHRC,
     * PO,POLD, PHIO, ROO, DPART, PI, PI2, WRK(35), DTCOEF,ADJ,XDSC
     * ,DPDX, XMOLW, BCONT, M, NDE, METH, MITER, INDEX, IWRK, NPTS
      COMMON /DBAND/ NLC, NUC
      REAL SDUMMY
      COMMON /GEAR/ DUMMY(48), SDUMMY(4), IDUMMY(38)
      EXTERNAL FCN, FCNJ
      IF (IBND.EQ.0) THEN
         P(1)=1.00D0
         Q(1)=0.00D0
         R(1)=POLD
C
         RETURN
      END IF
      IF (IBND.EQ.1) THEN
         P(1)=0.00D0
         Q(1)=1.00D0
         R(1)=0.00D0
         RETURN
      END IF
      RETURN
      END
C
      SUBROUTINE MONT(NPDE, X, NPTS, T, TLAST, U, IU, TOUT, DT)
      IMPLICIT REAL*8 (A-H, O-Z)
      COMMON /IO/ ITERM, NOUT
      DIMENSION U(IU,NPTS), X(NPTS)
        UV=0.0D0
      RETURN
      END
```

```
      SUBROUTINE PRESXO (TIME, VOLUME, PSURF, PKINF, PKEQO)
      IMPLICIT REAL*8 (A-H, O-Z)
      EXTERNAL PHI
      COMMON /DSCRET/ U(1,80), X(80)
      COMMON /PARAMS/ VO,DV, W, A, XMU, TOL, H, TOLD, VFBED, SPHRC,
     * PO,POLD, PHIO, ROO, DPART, PI, PI2, WRK(35), DTCOEF,ADJ,XDSC
     * ,DPDX, XMOLW, BCONT, M, NDE, METH, MITER, INDEX, IWRK, NPTS
        XNT=0.00D0
        NN=NPTS-1
        DO 99 N=1,NN
          TMP1=PHI(X(N))   *U(1,N)
          TMP2=PHI(X(N+1))*U(1,N+1)
          XNT=XNT+(TMP1+TMP2)/2.0D0*(X(N+1)-X(N))
99      CONTINUE
        CALL VOLFT(VOLUME, TIME)
        BCONT=XNT
C                PISTON PRESSURE FOR ACTUAL K
        PSURF=(VO-XNT*A)/VOLUME-1.0D0
C                PISTON PRESSURE FOR INFINITE K
        PKINF=PO*(VO+VFBED)/(VOLUME+VFBED)
C                PISTON PRESSURE FOR ZERO K
        PKEQ0=VO/VOLUME-1.0D0
        RETURN
        END

      SUBROUTINE PDEF (NPDE, X, T, UX, DUX, F, G, C)
      IMPLICIT REAL*8 (A-H, O-Z)
      COMMON /DBAND/ NLC, NUC
      REAL SDUMMY
      COMMON /GEAR/ DUMMY(48), SDUMMY(4), IDUMMY(38)
      COMMON /VEL/ VEL, COUNT
      COMMON /IO/ ITERM, NOUT
      REAL*8 C(NPDE),DUX(NPDE),F(NPDE),G(NPDE,NPDE),UX(NPDE),X,T
      COMMON /PARAMS/ VO,DV, W, A, XMU, TOL, H, TOLD, VFBED, SPHRC,
     * PO,POLD, PHIO, ROO, DPART, PI, PI2, WRK(35), DTCOEF,ADJ,XDSC
     * ,DPDX, XMOLW, BCONT, M, NDE, METH, MITER, INDEX, IWRK, NPTS
       PFX=1.0D0
C            CALCULATE DISTANCE DEPENDENT VOIDAGE (HENCE PERMEABILITY)
```

```
      PHIX=PHI(X)
      PDIAM=DPRT(X)
      PRM=PHIX**3*(SPHRC*PDIAM)**2/(1.0D0-PHIX)**2/150.0D0*ADJ
      COEF=XMU/(101.325D3*PRM)
      C(1) = PHIX
      G(1,1) = (1.0D0+UX(1))/COEF
      F(1)=0.00D0
      RETURN
      END
C
      SUBROUTINE VOLFT(PSTVOL, T)
      IMPLICIT REAL*8 (A-H, O-Z)
      COMMON /PARAMS/ V0,DV, W, A, XMU, TOL, H, TOLD, VFBED, SPHRC,
     * P0,POLD, PHI0, RO0, DPART, PI, PI2, WRK(35), DTCOEF,ADJ,XDSC
     * ,DPDX, XMOLW, BCONT, M, NDE, METH, MITER, INDEX, IWRK, NPTS
      PSTVOL=V0-DV*DSIN(W*T)
      RETURN
      END
C
        DOUBLE PRECISION FUNCTION PHI(XDIST)
        IMPLICIT REAL 8 (A-H, O-Z)
      COMMON /PARAMS/ V0,DV, W, A, XMU, TOL, H, TOLD, VFBED, SPHRC,
     * P0,POLD, PHI0, RO0, DPART, PI, PI2, WRK(35), DTCOEF,ADJ,XDSC
     * ,D DX, XMOLW, BCONT, M, NDE, METH, MITER, INDEX, IWRK, NPTS
      COMMON /DSCRET/ U(1,80), X(80)
      PHI=PHI0
      EPS=XDIST/X(NPTS)
C  IF  (EPS.GT.0.3)  PHI=1.5D0*PHI0
      RETURN
      END
C
        DOUBLE PRECISION FUNCTION DPRT(XDIST)
        IMPLICIT REAL*8 (A-H, O-Z)
      COMMON /PARAMS/ V0,DV, W, A, XMU, TOL, H, TOLD, VFBED, SPHRC,
     * P0,POLD, PHI0, RO0, DPART, PI, PI2, WRK(35), DTCOEF,ADJ,XDSC
     * ,DPDX, XMOLW, BCONT, M, NDE. METH, MITER, INDEX, IWRK, NPTS
      COMMON /DSCRET/ U(1,80), X(80)
      EPS=XDIST/X(NPTS)
```

```
DPRT=DPART
IF (EPS.GT.XDSC) DPRT=DPART/3.0
RETURN
END
```